

Biochemical Characterization of Fluorophore-Binding Nucleic Acids

by

Alexandra Tormann

A thesis

presented to the University of Waterloo

in fulfillment of the

thesis requirement for the degree of

Master of Science

in

Chemistry

Waterloo, Ontario, Canada, 2022

© Alexandra Tormann 2022

Author's Declaration

I hereby declare that I am the sole author of this thesis. This is a true copy of the thesis, including any required final revisions, as accepted by my examiners.

I understand that my thesis may be made electronically available to the public.

Abstract

Aptamers, single stranded RNA or DNA that bind to target ligands with high affinity and specificity, have a wide range of applications, from therapeutics to biosensing, which makes biochemical characterization of the utmost importance. This research aimed to implement various analytical instrumentation methods for the biochemical characterization of DNA Mango aptamers sequences 2a, 4a, and 6b, to TO1-3PEG.

In Chapter 3, fluorescence spectroscopy titrations were conducted. An equilibrium dissociation constant of 160.6 nM was calculated for the 4a aptamer sequence in sodium phosphate buffer. The increase in fluorescence enhancement was weaker than anticipated; therefore, further investigation is required.

Isothermal titration calorimetry experiments were also conducted, summarized in Chapter 4. The binding affinity for the DNA Mango aptamer sequences was determined. It was concluded that no binding interactions between the 2a or 6b aptamer sequences and the target ligand were observed. The 4a sequence was found to bind weakly to the target ligand in both a sodium phosphate and a HEPES buffer.

Native PAGE studies were also completed, outlined in Chapter 5. The native PAGE experiments indicated the presence of multimeric structures with structural heterogeneity in both the 4a and 6b sequences. A monomeric structure was also observed in the 4a aptamer.

Chapter 6 investigated the binding affinity of two DNA Mango aptamer sequences, 4a and 6b, to the target ligand via Surface Plasmon Resonance. Numerous experimental conditions were explored, but binding interactions were not detected for the explored aptamers, therefore either eluding to a weak binding interaction, or the absence of binding altogether.

Acknowledgements

First and foremost, I would like to thank my graduate supervisor, Dr. Dieckmann. Dr. Dieckmann, as I am sure you know, this has not been an easy journey for me, but your unwavering support and guidance truly made it an enjoyable experience. Thank you for agreeing to take me on as a graduate student and thank you for being a wonderful mentor. In addition, I would like to thank the members of Dr. Dieckmann's research group, Kyle, Kyla, and Natasha.

I would also like to thank the members of my committee, Dr. Maheshwari and Dr. Liu. I consider myself extremely lucky to have had the opportunity to complete my graduate studies at the University of Waterloo, a world-renowned institution with brilliant faculty members, such as those of you who agreed to sit on my committee. Thank you for your time and your effort. A special thanks to Dr. Dara Gilbert.

Finally, I would like to thank my family and friends. To my mother, father, and sister, Cynthia, Wolf, and Rachel – thank you for your overwhelming love and encouragement. For those of you who do not know, both of my parents and my sister have degrees in music performance – quite a contrasting discipline of study to chemistry, which often made discussions about my research difficult or strained. This, however, never impacted the support they provided me, and I could not be more grateful to have such an amazing family. To my friends: this degree would not have been possible without you all. Lastly, to my boyfriend: having completed your PhD. in organic chemistry from the University of Waterloo not too long ago, you know firsthand the struggles and hardships of graduate studies. You have been

nothing but supportive and loving, always offering advice and suggestions, and I could not have done this without you.

In dedication to my grandmother, Hilda Szabo.

Table of Contents

Author's Declaration	ii
Abstract.....	iii
Acknowledgements.....	iv
Dedication.....	vi
List of Figures.....	x
List of Tables	xii
List of Abbreviations.....	xiii
Chapter 1 - Introduction to Aptamers and Analytical Instrumentation	1
1.1 - History of Functional Nucleic Acids.....	2
1.2 - Aptamers.....	4
1.3 - Fluorescent Aptamers.....	5
1.4 - Fluorophore-Binding Aptamers.....	7
1.4.1 - Spinach Aptamer.....	8
1.4.2 - Broccoli Aptamer.....	9
1.4.3 - Corn Aptamer.....	9
1.4.4 - Malachite Green.....	10
1.4.5 - Mango Aptamer.....	12
1.4.5.1 - RNA Mango Aptamer Properties.....	14
1.5 - Surface Plasmon Resonance.....	15
1.5.1 - SPR in Literature.....	19
1.6 - Fluorescence Spectroscopy.....	22
1.7 - Isothermal Titration Calorimetry.....	23
1.7.1 - ITC in Literature.....	26
1.8 - Research Objectives.....	30
Chapter 2 - Materials and Methods.....	32
2.1 - DNA Purification.....	32
2.1.1 - Anion Exchange Chromatography.....	37
2.1.2 - Size Exclusion Chromatography.....	38
2.2 - RNA Transcription.....	39

2.3 - Buffer Preparation.....	39
2.4 - Streptavidin Sensor Preparation for SPR.....	40
2.5 - SPR Sample Preparation.....	41
2.6 - SPR Validation Protocol.....	41
2.7 - ITC Sample Preparation.....	42
2.8 - Native PAGE.....	42
Chapter 3 - Fluorescence Spectroscopy Titrations.....	45
3.1 - Previous Fluorescence Research.....	45
3.2 - Fluorescence Titration Investigation.....	45
Chapter 4 - Isothermal Titration Calorimetry.....	48
4.1 - ITC Investigation on 4a DNA Mango Aptamer Sequence.....	48
4.1.1 - Fluorescence Investigation on Effect of DMF on Binding Interactions.....	52
4.1.2 - Implementation of HEPES Buffer.....	54
4.2 - ITC Investigation on 6b DNA Mango Aptamer Sequence.....	58
4.3 - ITC Investigation on 2a DNA Mango Aptamer Sequence	60
4.4 - ITC Conclusions.....	61
Chapter 5 - Native PAGE.....	63
5.1 - 4a DNA Aptamer Investigation.....	63
5.1.1 - Exploration of Annealing Methods.....	65
5.2 - 6b DNA Aptamer Investigation.....	67
5.3 - Native PAGE Conclusions.....	69
Chapter 6 - Surface Plasmon Resonance.....	71
6.1 - Non-Specific Binding Experiments.....	71
6.1.1 - 6b DNA Mango Non-Specific Binding Experiment.....	73
6.1.2 - Hoechst DNA.....	80
6.1.3 - RNA Mango Aptamer.....	84
6.2 - Concentration Dependence Investigation.....	86
6.2.1 - 4a DNA Mango Concentration Dependence.....	86
6.2.2 - 6b DNA Mango Concentration Dependence.....	87
6.2.3 - RNA Mango Concentration Dependence.....	89

6.3 - SPR Conclusions.....	90
Chapter 7 - Conclusions.....	92
References.....	95

List of Figures

Figure 1.1 – Structure of DNA.....	3
Figure 1.2 – Structure of GFP.....	6
Figure 1.3 – Chemical Structure of Spinach Aptamer and DFHBI Ligand.....	8
Figure 1.4 – Chemical Structure of Corn Aptamer and DFHO Ligand.....	10
Figure 1.5 – Chemical Structure of Malachite Green Aptamer and Malachite Green.....	11
Figure 1.6 – Chemical Structure of Mango Aptamer and TO1-3PEG.....	12
Figure 1.7 – Chemical Structure of Mango II Aptamer with TO1-3PEG-biotin.....	14
Figure 1.8 – Surface Plasmon Resonance Schematic.....	17
Figure 1.9 – Surface Plasmon Resonance Sensorgram.....	18
Figure 1.10 – Structure of SRB-2.....	20
Figure 1.11 – Chemical Structure of AR101-B and B-TMR.....	21
Figure 1.12 – Jablonski Diagram.....	23
Figure 1.13 – Example of Raw, Real-Time ITC Experimental Data.....	24
Figure 1.14 – Extraction of Thermodynamic Properties from ITC Titration Curve.....	25
Figure 1.15 – Chemical Structure of DHMBI and DMHBI+.....	27
Figure 1.16 – Chemical Structure of ThT and DFHO.....	28
Figure 1.17 – Chemical Structure of SR, SR101, and RB.....	29
Figure 2.1 – Structures of Utilized DNA Sequences.....	33
Figure 3.1 – Fluorescence Titration Curve Pertaining to DNA Mango 4a for KD Determination.....	46
Figure 4.1 – Normalized Injection Heats from ITC Experiment with 4a DNA Mango.....	49
Figure 4.2 – Isotherm of 4a DNA Mango TO1-3PEG in Sodium Phosphate Buffer.....	50
Figure 4.3 – Normalized Injection Heats of DMF Titration.....	52
Figure 4.4 – Fluorescence Investigation to Determine the Effect of DMF on Binding Interactions Between 4a DNA Mango and TO1-3PEG.....	53
Figure 4.5 – ITC Isotherm of 4a DNA Mango-TO1-3PEG in HEPES Buffer.....	55

Figure 4.6 – Isotherm of Repeated 4a DNA Mango-TO1-3PEG in HEPES Buffer.....	56
Figure 4.7 – Normalized Injection Heats of TO1-3PEG ITC Titration.....	58
Figure 4.8 – Normalized Injection Heats of 6b DNA Mango Titration.....	59
Figure 4.9 – Isotherm for 6b DNA Mango Titration.....	60
Figure 5.1 – SYBR Stained Native PAGE for 4a DNA Mango Visualization.....	64
Figure 5.2 – SYBR Safe Stained Native PAGE for 4a DNA Mango Visualization.....	66
Figure 5.3 – SYBR Safe Stained Native PAGE for 6b DNA Mango Visualization.....	68
Figure 6.1 – Response to Streptavidin Aliquot Injection.....	73
Figure 6.2 – Response of Channel 1 and Channel 2 to TO1-3PEG Injection.....	74
Figure 6.3 – Response of Channel 1 and Channel 2 to 6b DNA Mango Injection.....	75
Figure 6.4 – Corrected Response to 6b DNA Mango Injection.....	77
Figure 6.5 – Response of Channel 1 and Channel 2 to 6b DNA Mango Injection in High Salt Buffer.....	78
Figure 6.6 – Response of Channel 1 and Channel 2 to Various 6b DNA Mango Injections.....	79
Figure 6.7 – Channel 1, Channel 2, and Corrected Signal for Hoechst DNA Injections.....	82
Figure 6.8 – Response to Biotinylated Hoechst DNA and Hoechst Hairpin DNA Injections...	83
Figure 6.9 – Responses of Channel 1 and Channel 2 to RNA Mango Injections.....	84
Figure 6.10 – Responses of Channel 1 and Channel 2 to Various RNA Mango Injections.....	85
Figure 6.11 – Corrected Response to Various Concentrations of 4a DNA Mango.....	87
Figure 6.12 – Corrected Response to Ranging Concentrations of 6b DNA Mango.....	88
Figure 6.13 – Corrected Response to Various Concentrations of RNA Mango.....	89

List of Tables

Table 1.1 – GFP Derivatives and Respective Modifications.....	7
Table 1.2 – Summary of Equilibrium Dissociation Constants Obtained from Different Analytical Approaches.....	30
Table 2.1 – Utilized DNA and RNA Sequences.....	32
Table 2.2 – Required Acrylamide Content in PAGE for Optimal Separation.....	35
Table 2.3 – Contents of a 10% PAGE Solution.....	35
Table 2.4 – Utilized Buffers.....	40
Table 2.5 – Well Contents of Native PAGE.....	43
Table 3.1 – Determined Binding Affinities of DNA Mango Aptamers to TO1-3PEG by Fluorescence Spectroscopy.....	45
Table 4.1 – Samples Analyzed in Fluorescence Titration Investigation of Effect of DMF.....	53
Table 4.2 – ITC Determined Equilibrium Dissociation Constants and Parameters.....	61
Table 5.1 – Well Contents of Native PAGE for Optimal Annealing Method Determination...	65

List of Abbreviations

AEC	Anion Exchange Chromatography
AR101-B	Atto Rhodamine Biotin
bp	Base pair
B-TMR	5/6-biocytyl Tetramethylrhodamine
BSA	Bovine Serum Albumin
cDNA	Complementary DNA
DEAE	Diethylaminomethyl
DFHBI	3,5-difluoro-4-hydroxybenzylidene imidazolinone
DFHO	3,5-difluoro-4-hydroxybenzylidene-imidazolinone-2-oxime
DI	Deionized
DMF	Dimethylformamide
DMHBI	3,5-dimethoxy-4-hydroxybenzylidene imidazolinone
DNA	Deoxyribonucleic acid
eGFP	Enhanced Green Fluorescent Protein
ESPT	Excited State Protein transfer
F _{max}	Maximum Fluorescence
FPLC	Fast Protein Liquid Chromatography
GFP	Green Fluorescent Protein
HBI	Hydroxybenzylidene Imidazolinone
HPLC	High Protein Liquid Chromatography
HSA	Human Serum Albumin
IDT	Integrated DNA Technologies
IPA	Isopropanol
ITC	Isothermal Calorimetry
K _a	Association Constant
K _D	Equilibrium Dissociation Constant
LMW	Low Molecular Weight
LSPR	Localized Surface Plasmon Resonance
mRNA	Messenger Ribonucleic Acid
NMR	Nuclear Magnetic Resonance Spectroscopy
NSB	Nonspecific Binding
nt	Nucleotide
PAGE	Polyacrylamide Gel Electrophoresis
PCR	Polymerase Chain Reaction
PEG	Polyethylene Glycol
RB	Running Buffer
RB	Rhodamine B
RFU	Relative Fluorescence Units
RNA	Ribonucleic Acid
rRNA	Ribosomal Ribonucleic Acid
SEC	Size Exclusion Chromatography

SELEX	Systematic Evolution of Ligands by Exponential Enrichment
siRNA	Small Interfering Ribonucleic Acid
snRNA	Small Nuclear Ribonucleic Acid
SPR	Surface Plasmon Resonance
SR	Sulforhodamine
SR101	Sulforhodamine 101
TEMED	Tetramethylethylenediamine
ThT	Thioflavin T, 4-(3,6-dimethyl-1,3-benzothiazol-3-ium-2-yl)-N,N-dimethylaniline
tRNA	Transfer RNA

Chapter 1

Introduction to Aptamers and Analytical Instrumentation

Aptamers are small (20-60 nucleotides), single-stranded RNA or DNA that bind to target ligands (metal ions, protein biomarkers, a cell), with both high affinity and specificity.^{1,2} With recent advances in the use of aptamers as therapeutic agents for human diseases and other degenerative disorders, characterization of binding affinities is of the utmost importance. Factors that make aptamers advantageous in comparison to antibodies for such purposes include easy modification, increased stability, quick tissue uptake and elimination, *in vitro* production, and reduced variation from batch-to-batch.² By further studying these molecules, our understanding of the structure and kinetics of nucleic-acid binding can be advanced. To do so, analytical instrumentation methods can be employed.

Analytical instrumentation can be utilized to separate, identify, and quantify chemical components of materials of interest. Two forms of analysis can be performed with the use of analytical instrumentation, qualitative and quantitative analysis, for the determination of the identity and the abundance of a chemical species, respectively.^{3,4} More specifically, analytical instruments can be employed to obtain information regarding the chemical or thermodynamic properties of a system, structural information, or kinetic information. Such instruments are implemented in a variety of fields such as biology, medicine, and green energy, for applications such as drug delivery, environmental pollution monitoring, or analyzing protein function.³

In the 21st century, a diverse range of analytical methods exist, each having their own advantageous properties – while some instruments are employed for their capability of high sensitivity measurements, other instruments may be exploited for their cost efficiency, or for their superior performance with certain sample types. Such methods include, but are not limited to, Surface Plasmon Resonance (SPR), Fluorescence Titration, and Isothermal Calorimetry (ITC).

1.1 History of Functional Nucleic Acids

Watson and Crick, perhaps two of the most famous names in scientific history, discovered the structure of DNA in 1953. Watson and Crick determined that DNA was comprised of two chains of nucleotide pairs, encoding genetic information for all living things, and were awarded the Nobel Prize in 1962, along with Wilkins.⁵⁻⁸ Three years prior to this discovery Ochoa and Kornberg investigated the mechanisms of biological synthesis of nucleic acids, RNA and DNA, and were awarded the Nobel Prize in 1959.⁹ These two discoveries made possible a new era of biology, leading to fields such as biotechnology and molecular biology. The realm of biology was advanced further in the 1968 when the field of molecular biology emerged after genetic coding was cracked. This advancement is credited to three researchers: Robert Holley, Har Khorana, and Marshall Nirenberg, who classified the function of DNA in protein synthesis. While Holley discovered and characterized the function of transfer RNA (tRNA), Khorana and Nirenberg determined the genetic code.¹⁰⁻¹² They were awarded the Nobel Prize in 1968.¹³ In 1978, the Nobel Prize was awarded to Werner Arber, Hamilton Smith, and Daniel Nathans for the discovery of restriction enzymes, restriction endonucleases, and their use in creating genetic maps, respectively.¹⁴⁻¹⁶ Just two years later, in 1980, Paul Berg, Walter Gilbert, and Fredrick Sanger were awarded the Nobel Prize – Gilbert and Sanger were together recognized for their development of DNA sequencing methods.^{17,18} Berg, on the other hand, was granted the award for his work pertaining to the mechanisms of DNA recombination in viruses.¹⁹ Since these major advancements, DNA has likely become the most recognizable structure (Figure 1.1) and name in biology and has opened many doors to the understanding of genetic information.

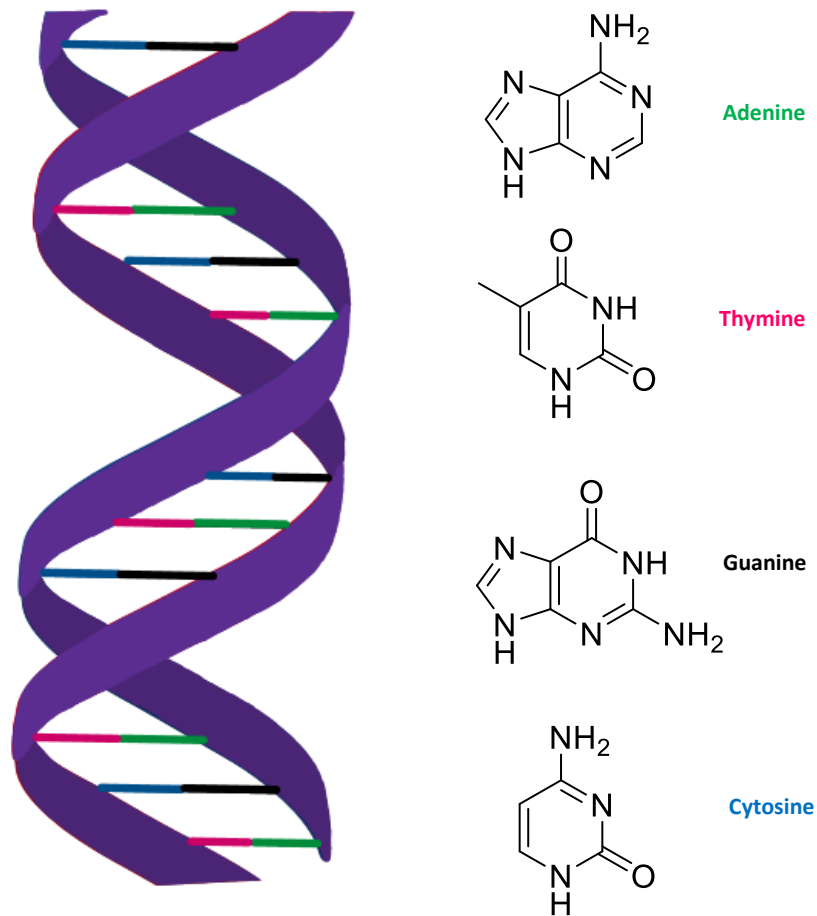


Figure 1.1 - Structure of DNA. DNA strands (purple) are comprised of alternating deoxyribose and phosphate groups that make up the DNA backbone, a double helix. Attached to each sugar are one of four bases: cystine (blue), adenine (green), thymine (pink), and guanine (black).

But to fully understand human genes, a shift in research from DNA to the “central dogma” known as ribonucleic acid (RNA), a messenger molecule, was required.²⁰ Up until the late 1980s, the functions and roles of RNA outside of messenger RNA (mRNA), transfer RNA (tRNA), ribosomal RNA (rRNA) and small nuclear ribonucleoproteins (snRNPs), was not heavily considered.²¹ In 1989, however, another radical, discovery was made – Thomas Cech and Sidney Altman independently discovered that RNA had a function other than carrying instructions from DNA. Specifically, they discovered that RNA not only genetically carries both physical and mental characteristics, but it also functions as a biocatalyst.^{22,23} Having self-catalytic abilities suggested

that life possibly started as RNA.^{24,25} Despite the fact that this may now be commonly known, at the time of the discovery, many fundamental aspects of the molecular basis of life were deeply impacted. This is now deemed the RNA world hypothesis.

In short, this was a major advancement in the realm of biology, seeing as RNA could have roles in molecular biology beyond the expression of genetic code. These catalytic RNA molecules were dubbed ribozymes, and since their discovery, several other types of functional nucleic acids have been investigated and researched such as nucleic acid enzymes and aptamers.

1.2 Aptamers

Aptamers are small (20-60 nucleotides), single-stranded RNA or DNA that bind to target ligands (metal ions, protein biomarkers, a cell), with both high affinity and specificity.^{1,2} The discovery of aptamers was made by two independent research groups, Jack W. Szostak's at Harvard University and Larry Gold at the University of Colorado Boulder. Szostak's group termed the selection of RNA that is able to bind to a target ligand "*in vitro* selection", whereas Gold's group used the term *Systematic Evolution of Ligands by Exponential Enrichment*, or SELEX.^{26,27} Briefly, the process of SELEX for an RNA aptamer begins by screening a sequence library, typically between 10^{14} to 10^{15} sequences, for sequences that bind to a selected target.²⁷⁻²⁹ The selection rounds initiate by exposing the sequences to the immobilized target, to which some sequences will bind, and others will not. Nonbinding oligonucleotides are washed away, while the bound molecules are recovered and converted to complementary DNA (cDNA).^{26,27} The cDNA sequences are then amplified by polymerase chain reaction (PCR), after which they are converted back to RNA sequences via *in vitro* transcription for further rounds of selection, with each subsequent round of selection imposing more stringent conditions on binding to isolate sequences

that have the highest affinity for the target. After the selection process, the highest binding affinity aptamer is sequences and used for additional studies.

With recent advances in the use of aptamers as therapeutic agents for human diseases and other degenerative disorders, characterization of binding affinities is of the utmost importance. Factors that make aptamers advantageous in comparison to antibodies for such purposes include easy modification, increased stability, quick tissue uptake and elimination, *in vitro* production, and reduced variation from batch-to-batch.² By further studying these molecules, our understanding of the structure and kinetics of nucleic-acid binding can be advanced.

1.3 Fluorescence

Fluorescent molecules are classified as molecules containing extended conjugated double bond sequences and are considered advantageous for imaging and spectroscopy techniques given their ease of detection and safety, as well as the ability to examine multiple tags in a single experiment. The first discovery of fluorescence was made by Sir Frederik William Herschel in 1845, who noted that a quinine solution “though perfectly transparent and colourless when held between the eye and the light, or a white object, it yet exhibits in certain aspects, and under certain incidences of light, an extremely vivid and beautiful celestial blue colour”.^{30,31} Decades later, in fluorescent antibody labeling was discovered by Coons *et al.*^{32,33} Then, in 1962, Shimomura and colleagues discovered the green fluorescent protein (GFP) during the purification of a bioluminescent protein aequorin from the jellyfish *Aequorea Victoria*.³⁴ The structure of GFP was generated in Chimera and is illustrated in Figure 1.2.

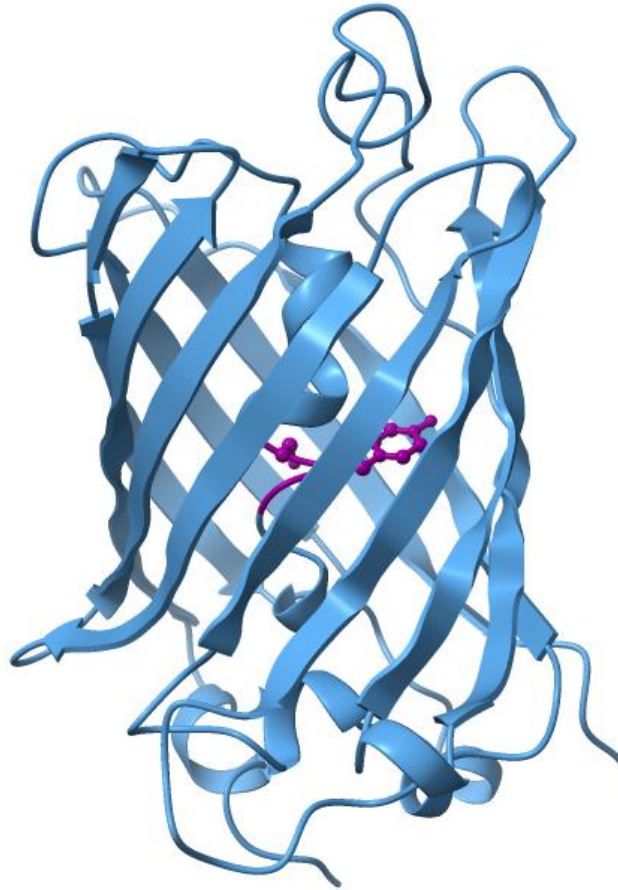


Figure 1.2 - Structure of GFP. The structure of Green Fluorescent Protein (GFP, PDB ID: 1GFL) is a beta barrel consisting of 11 beta strands. These strands enclose an alpha helix, which contains the chromophore, 4-hydroxybenzilidene (HBI). Ligand illustrated as a ball and stick model in purple.

In the mid-1970s, GFP was shown to emit a green light after energy transfer from aequorin. The discovery was made by Morise and colleagues and provided further insight into the fluorescent properties of GFP.³⁵ Other considerable advancements involving GFP include the GFP gene clone, discovered by Prasher *et al.* in 1992, or the expression of the GFP gene in eukaryotic and prokaryotic cells, *Caenorhabditis elegans* and *Escherichia coli*, respectively, by Chalfie *et al.* in 1994.^{36,37} This development demonstrated that GFP could be utilized as a fluorescent marker for both protein localization and expression. Since these discoveries, GFP has become a commonly used biological marker due to its stability, and the unique property that a cofactor is not required

in the spontaneous cyclization that forms its chromophore.³⁸ GFP has since been modified and engineered to provide a wide range of variants that produce blue, cyan, and yellow fluorescent proteins, providing numerous biomedical and biotechnology applications, such as cell visualization and genetically encoded sensors. The ability for such modifications and applications can be attributed to the Phillips group and the Remington group, who disclosed the tertiary structure of both the wild type GFP and the mutant GFP (S65T).³⁹⁻⁴¹

Inspired by GFP, various compounds, including GFP chromophore analogs, were developed with similar fluorescent properties, but improved upon the limitations seen with GFP. For example, GFP has been reported to have pH and chloride ion sensitivity, as well as substandard photostability. To improve upon these limitations, several variables were adjusted, such as increasing the quantum yield, photostability, and molar extinction coefficient, or by implementing site-directed mutations. Table 1.1 summarizes GFP derivatives and their modifications.⁴²⁻⁴⁵

Table 1.1 - GFP Derivatives and Respective Modifications

Green Fluorescent Protein Derivatives	Properties
Enhanced GFP (eGFP)	Improved brightness
F64 L (GFP2)	Enhanced temperature sensitivity
Blue Fluorescent Protein (BFP)	Substitution of Tyr66 with histidine, sensitivity to photobleaching
Cyan Fluorescent Protein (CFP)	Increased photostability, intermediate spectral characteristics
Yellow Fluorescent Protein (YFP)	Mutagenesis on the residue structurally adjacent to Y66
Enhanced YFP (EYFP)	High pKa, less sensitivity to halide ions

1.4 Fluorophore-binding Aptamers

Fluorophore-binding aptamers, or fluorescent light-up aptamers, are a subclass of aptamers that target fluorescent molecules and enhance fluorescence upon binding.⁴⁶⁻⁵⁰ Currently, several fluorophore binding aptamers have solved structures, including the spinach aptamer, broccoli

aptamer, corn aptamer, malachite green, and tetramethylrhodamine aptamer 3. Another fluorophore-binding aptamer with a determined structure is the mango aptamer⁶¹.

1.4.1 Spinach Aptamer

Coined the “spinach” aptamer due to the green fluorescence, this 98 nucleotide (nt) aptamer was selected to bind 3,5-difluoro-4-hydroxybenzylidene imidazolinone, or DFHBI.⁵¹ DFHBI was first reported by Jaffrey and coworkers in 2011 as one of the first GFP-derived fluorogens, DMHBI.⁵¹ Figure 1.3 illustrates the structure of the spinach aptamer and its respective ligand, DFHBI.

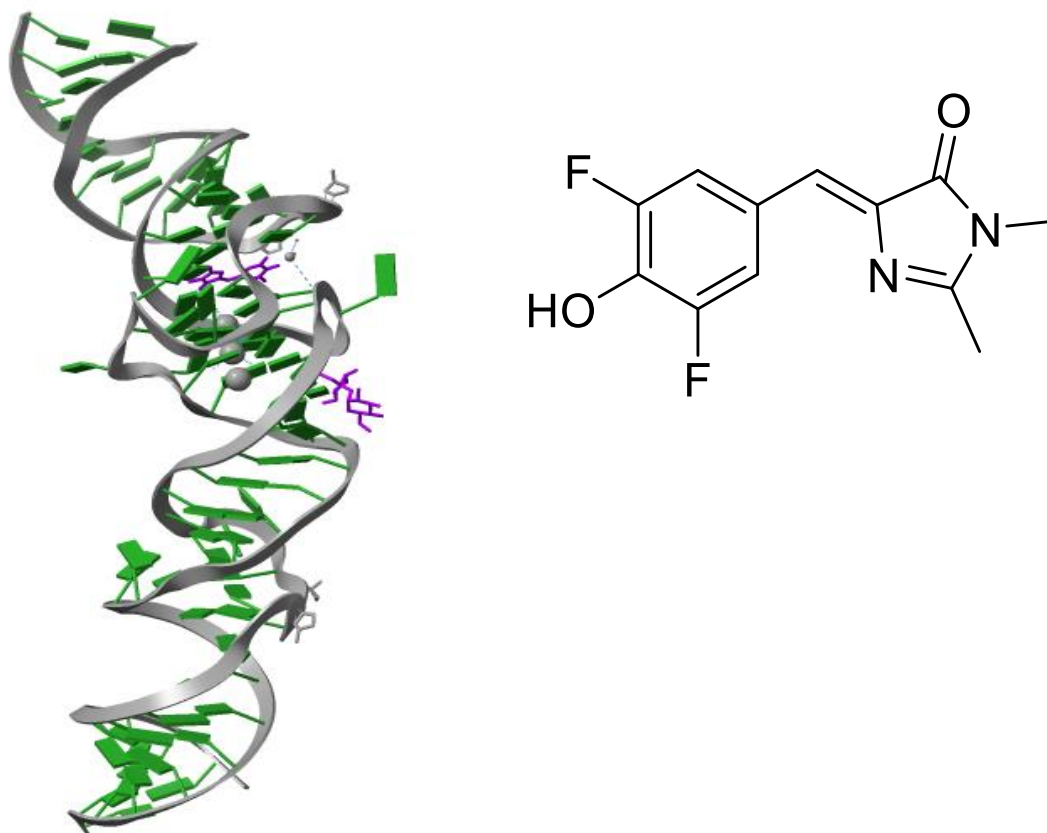


Figure 1.3 - Chemical Structure of Spinach Aptamer and DFHBI Ligand. A) The structure of the spinach aptamer with bound DFHBI (purple). Nucleotides shown in green. Image generated in Chimera (PDB ID: 4TS2). B) Chemical structure of DFHBI.

The RNA-fluorophore complex exhibits parallels to enhanced GFP (eGFP). More specifically, the spinach-DFHBI complex was found to exhibit a molar brightness that was 53% of eGFP but was declared brighter than most other aptamer-fluorophore complexes. Differing from GFP, however, is the insensitivity of Spinach to photobleaching and the immediate fluorescence after transcription in cells. Further research with the Spinach aptamer led to various other derivatives, such as Spinach2 (96 nt), Baby Spinach (51 nt), and iSpinach (69 nt).⁵²⁻⁵⁴ The variant, iSpinach, short for “improved Spinach aptamer”, was optimized by Ryckelynck and coworkers in 2016, and improved factors such as brightness, thermal stability, and salt sensitivity.⁵²

1.4.2 Broccoli Aptamer

The Broccoli aptamer (49 nt) was first selected for in 2014 by Jaffrey and coworkers, by including fluorescence enhancement in their selection process.⁵⁵ Broccoli demonstrated superior properties for application-based research. Furthermore, the aptamer exhibited 84% of eGFP brightness.⁵⁴ To further improve these results, dimeric Broccoli (dBroccoli) was developed by fusing together two Broccoli sequences. This derivative yielded an almost 2-fold improvement in brightness.⁵⁴

1.4.3 Corn Aptamer

The most recently discovered fluorescent light-up aptamer is known as the Corn aptamer, and was selected in 2017, again by Jaffrey and coworkers.⁵⁶ The fluorophore to which it binds is DFHO, as shown in Figure 1.4.

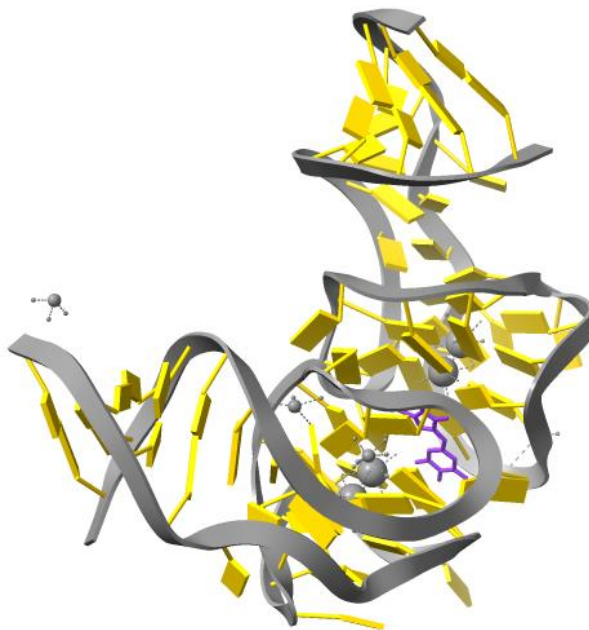


Figure 1.4 - Chemical Structure of Corn Aptamer. The structure of the Corn aptamer with bound DFHO (purple). Nucleotides shown in yellow. Image generated in Chimera (PDB ID: 5BJO). Chemical structure of DFHO shown on p.28.

It was hypothesized by Jaffrey and coworkers that the N-hydroxyl imine substituent at the 2-position would prohibit the potential for photobleaching, and while the complex did demonstrate improved photostability, Corn-DFHO exhibited only 22% eGFP brightness.⁵⁴

1.4.4 Malachite Green

In 1999, Grate et al. utilized SELEX to select for an RNA aptamer for malachite green (MG, Figure 1.5).⁵⁷

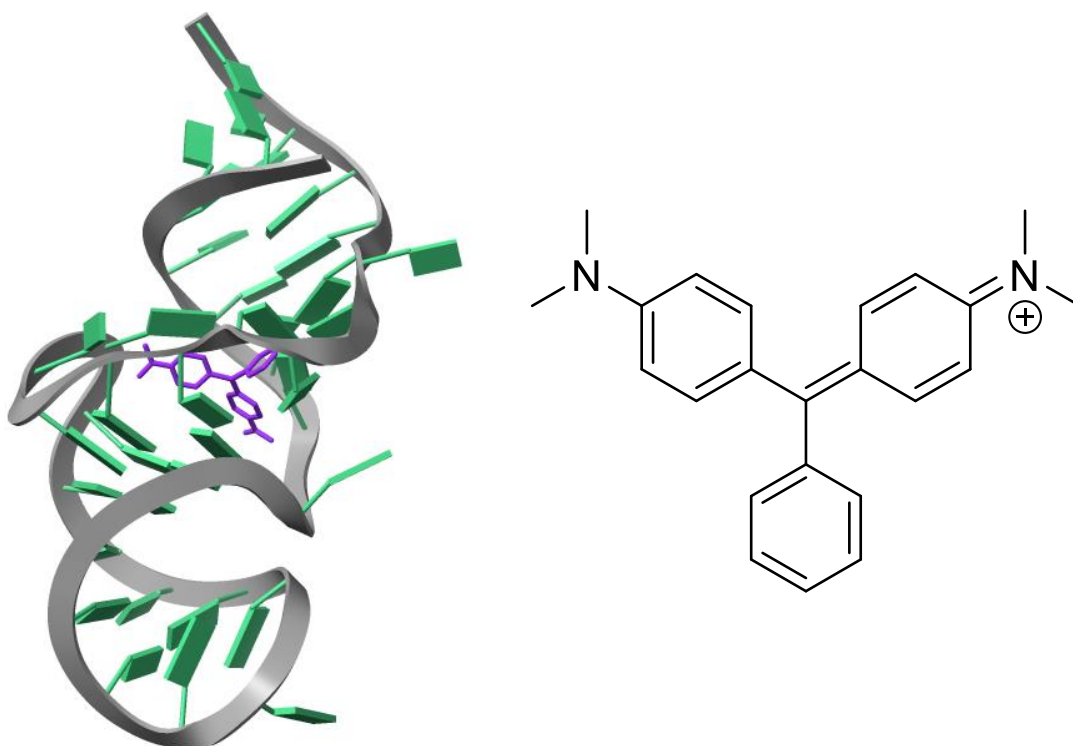


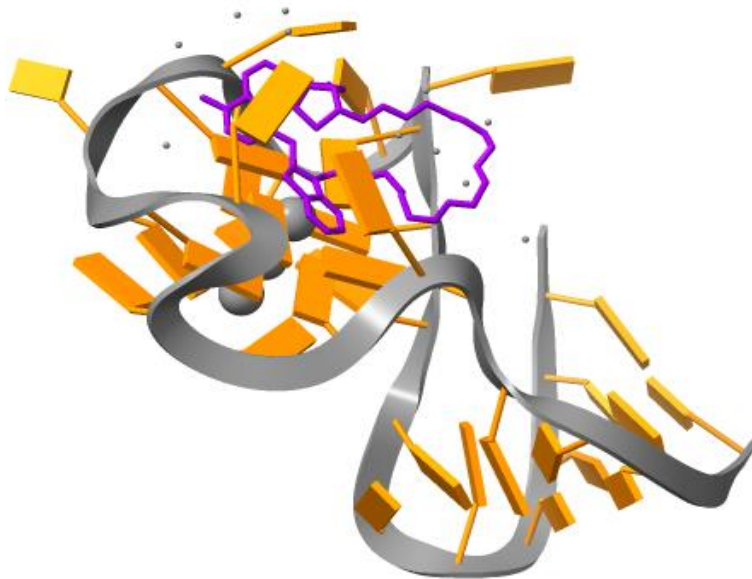
Figure 1.5 - Chemical Structure of Malachite Green Aptamer and Malachite Green. A) The structure of the malachite green aptamer with bound malachite green (purple) and nucleotides shown in seafoam green. Image generated in Chimera (PDB ID: 1Q8N). B) Chemical structure of malachite green.

MG in solution produces little to no fluorescence; however, four years after the selection of the aptamer, Babendure et al. demonstrated that the MG-bound aptamer (MGA) increases the fluorescence of MG by ~2300-fold.^{54,58} Furthermore, the research group described the goal for the selection of an aptamer for MG: to utilize the illumination of the organic dye to generate reactive oxygen species, which would, in turn, deactivate an attached messenger RNA.⁵⁸ In 2004, a research group from Columbia University, Stojanovic *et al.* utilized this immense fluorescence intensity increase to construct label-free fluorescent sensors.⁵⁸ Specifically, the MG aptamer was employed as a sensing domain and another aptamer as a target recognition domain.⁵³ While it was reported that a communication module was designed in order to ensure that binding occurred between the MG aptamer and MG, the researchers claimed the trial-and-error process of the communication

module was a significant limitation. Despite the limitation, this was considered a widely successful advancement, allowing for new avenues to be explored in constructing molecular sensors.^{54,59}

1.4.5 Mango Aptamer

One of the most prominent additions to the fluorescent light-up aptamer family is the RNA Mango aptamer (29 nt). First selected for in 2014 by Dolgosheina *et al.* against a biotinylated thiazole orange derivative (TO1-2PEG-biotin), the aptamer combined both high affinity and intense brightness.⁶⁰ The aptamer was also found to bind to TO3-biotin, in which the methylcholine and benzothiazole aromatic rings are connected by three carbon links as opposed to one. The Mango aptamer was found to bind to each ligand with affinity in the nanomolar range.⁶⁰ Specifically, the Mango aptamer had an equilibrium dissociation constant of 3.2 nM and 7 nM to the TO1-biotin and TO3-biotin, respectively. Figure 1.6 illustrates the structure of the Mango aptamer with the bound TO1-3PEG, as well as the chemical structure of the ligand itself.



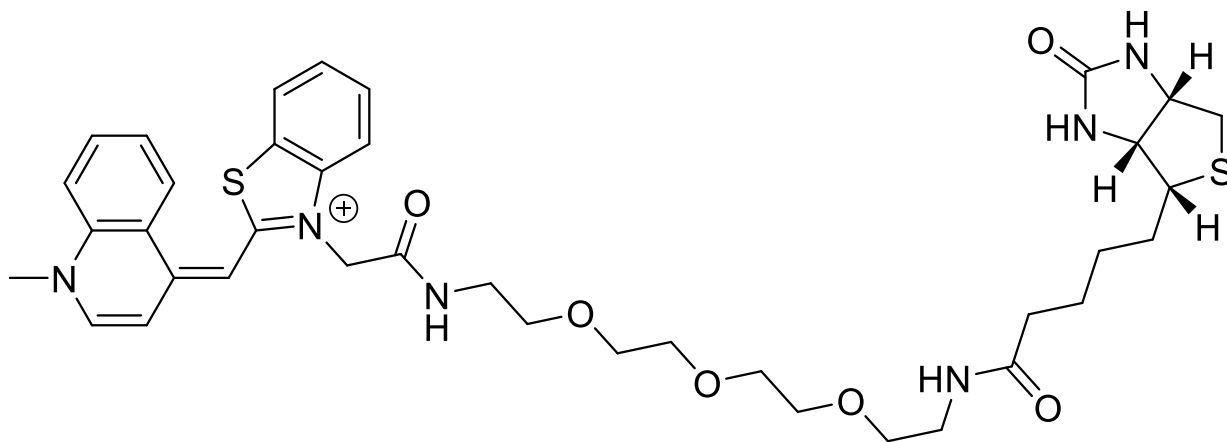


Figure 1.6 – Chemical Structure of Mango Aptamer and TO1-3PEG. A) The structure of the Mango aptamer with bound TO1-3PEG-biotin (purple). Nucleotides shown in orange. Image generated in Chimera (PDB ID: 5V3F). B) Chemical structure of TO1-3PEG-biotin.

Additionally, it was reported that the Mango aptamer had similar fluorescent enhancement to the Spinach system, which they concluded made it an attractive and advantageous option for fluorescently monitoring RNA complexes while utilizing the fluorophore as a tag for purification.⁶⁰

In 2018, Trachman *et al.* reported a higher affinity RNA Mango aptamer, Mango-II (Figure 1.7).⁶¹

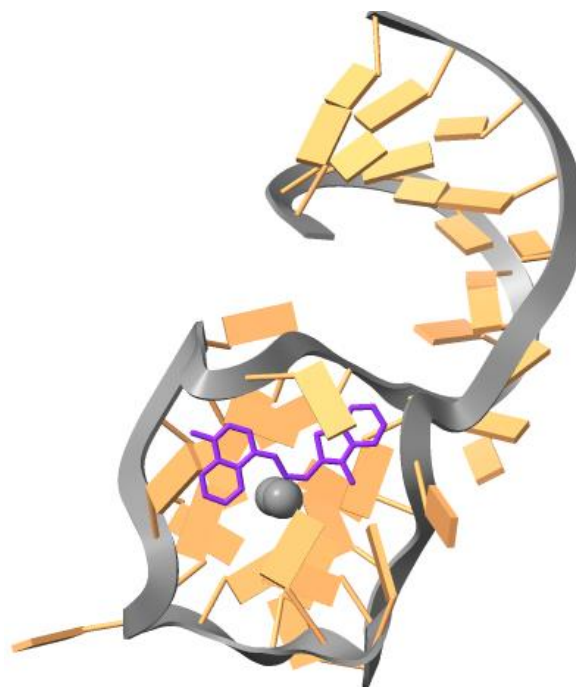


Figure 1.7 – Structure of Mango II Aptamer with TO1-3PEG-Biotin. Ligand shown in purple; nucleotides shown in peach. Image generated in Chimera (PDB ID: 6C64).

Not only did the researchers observe an increased brightness (RFU) in comparison to the original Mango aptamer, but also reported a higher affinity for both TO1- and TO3-Biotin – 1.1 and 1.4 nM, respectively.⁶¹ Furthermore, the researchers noted improved stability and increased resistance to formaldehyde. Trachman *et al.* noted three structural differences for which these improvements can be attributed, which are discussed in the following section.

1.4.5.1 RNA Mango Aptamer Properties

The RNA Mango aptamer employs thiazole orange-derived fluorophores, and therefore exhibits red-shifted emission. Its crystal structure was solved and was found to contain an additional four base pair (bp) duplex stem, which aids in sequence stabilization.⁵⁴ While it crystallized with two molecules per unit, it demonstrated monomeric structures in solution. The

fluorophore-binding location is a G-quadruplex, which consists of three tiers connected by six loops of 1-2 nt; therefore minimizing the functional size of the aptamer to 23 nt.⁵⁴

The biotinylated thiazole orange binds on top of the G-quadruplex, and with three nucleotides forming a “lid-like structure”, the fluorophore binding is assisted.⁵⁴ Specifically, each of the lid bases has been determined to stabilize a different TO1-biotin moiety – A20 stabilizes the methylcholine, A26 stabilizes the benzothiazole of TO1-biotin, and the U15 stabilizes the biotin moiety.⁵⁴ This individual base stabilization is contrasting to the stabilization of the lid bases of the Spinach aptamer, in which one entity is formed through hydrogen-bonding.

In contrast to the RNA Mango aptamer, the Mango-II aptamer has a 4-fold rotational symmetry that is lacked by the original Mango aptamer.⁶¹ Specifically, the guanines of the T2 and the T3 G-quartets of the Mango-II aptamer are segregated by propeller loops containing adenine, whereas in the original Mango aptamer, one T3 guanine collapses out of the plane of the other guanines by 30 degrees.⁶¹ Additionally, it was noted that at the GAA^A intersection between the quadruplex and the P1 duplex contain significantly increased hydrogen bonding interactions.⁶¹ Another difference between these two aptamers occurs within the T1 G-quadruplex – this region of the Mango-II aptamer was reported to be “augmented into a hexad by two adenines”, specifically A14 and A25, whereas the original Mango aptamer is only augmented by one adenine; therefore forming a pentad.⁶¹

1.5 Surface Plasmon Resonance

Surface plasmon resonance (SPR) is an optical technique that is utilized to measure the binding affinity of molecular interactions in real time.^{62,63} It is a label-free interaction analysis method that has a wide variety of applications from drug discovery and development to quality control, diagnostic assays, and basic research such as disease mechanisms and protein function

characterization.^{64,65} Specifically, the technique can be used for kinetic studies, affinity characterization, target identification, and concentration determination. Not only does SPR provide detailed insight into the binding strength and stability of a molecular interaction, but it also has numerous advantages. For example, SPR is a reliable, accurate, and quantitative technique with high sensitivity. Additionally, the instrument only requires small sample volumes, saving on cost, and reducing the time needed for both expression and purification, and implements regenerable sensor chips.^{64,65}

The optical system of an SPR instrument consists of a light source, a detector, and a sensor chip (Figure 1.1). The sensor chip is a glass substrate, on which a gold film is coated, which can be chemically modified to allow for easier immobilization of one of the binding partners to the sensor surface.⁶⁶ The light source, often monochromatic, illuminates the gold film. The detector measures the unique optical spectrum produced by surface plasmon resonance phenomenon.⁶⁴ Surface plasmons (electrical oscillations) occur when the light source that shines through a prism beneath the sensor chip generates a total internal reflection condition (i.e., the light source shines incident light at an angle greater than the critical angle).^{65,66} When this phenomenon occurs, a plasmonic wave is generated on the surface of the gold nanoparticles of the sensor chip. The electric field of the plasmonic wave extends hundreds of nanometers into the solution flowing through the microfluidic system above the surface of the sensor. The reflected light will have a significant decrease in intensity at a certain angle, which is measured at the detector. The incident angle of light that causes this phenomenon to occur is known as the resonance angle.^{62,63} Upon the binding of a molecule to the surface of the sensor chip, the refractive index of the space through which the plasmonic wave propagates changes, therefore shifting the reflectance angle measured by the detector.⁶³ The amount by which the reflectance angle shifts depends on the quantity of

material that binds to the sensor surface. Figure 1.8 demonstrates the traditional set up of an SPR instrument.^{62,67}

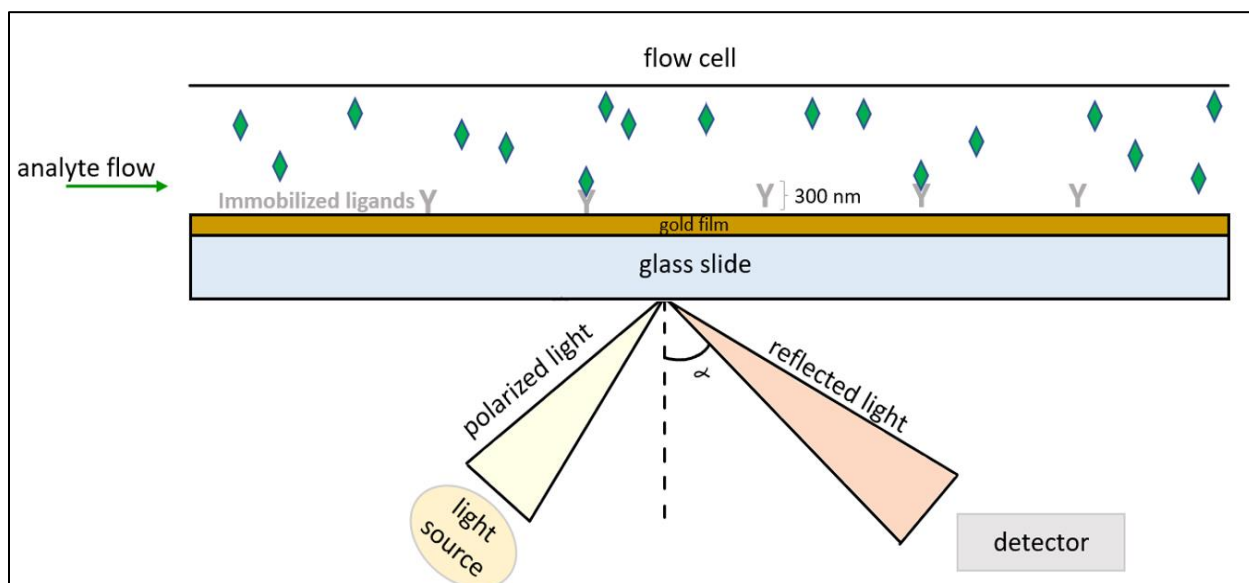


Figure 1.8 - Surface Plasmon Resonance Schematic. Target ligands (grey) are immobilized on the gold film of the glass substrate, extending 300 nm into solution. Analyte (green diamonds) flows through the microfluidic system over the immobilized ligands. Some analyte binds to the immobilized ligand. Analyte that does not bind continues to flow through the microfluidic system.

SPR data is outputted and displayed in a sensorgram – a plot of response versus time, thus illustrating the progress of the reaction over time.⁶³ In SPR analysis, the response is response units (RUs). Figure 1.9 illustrates a typical response of an interaction during an SPR experiment.⁶⁷

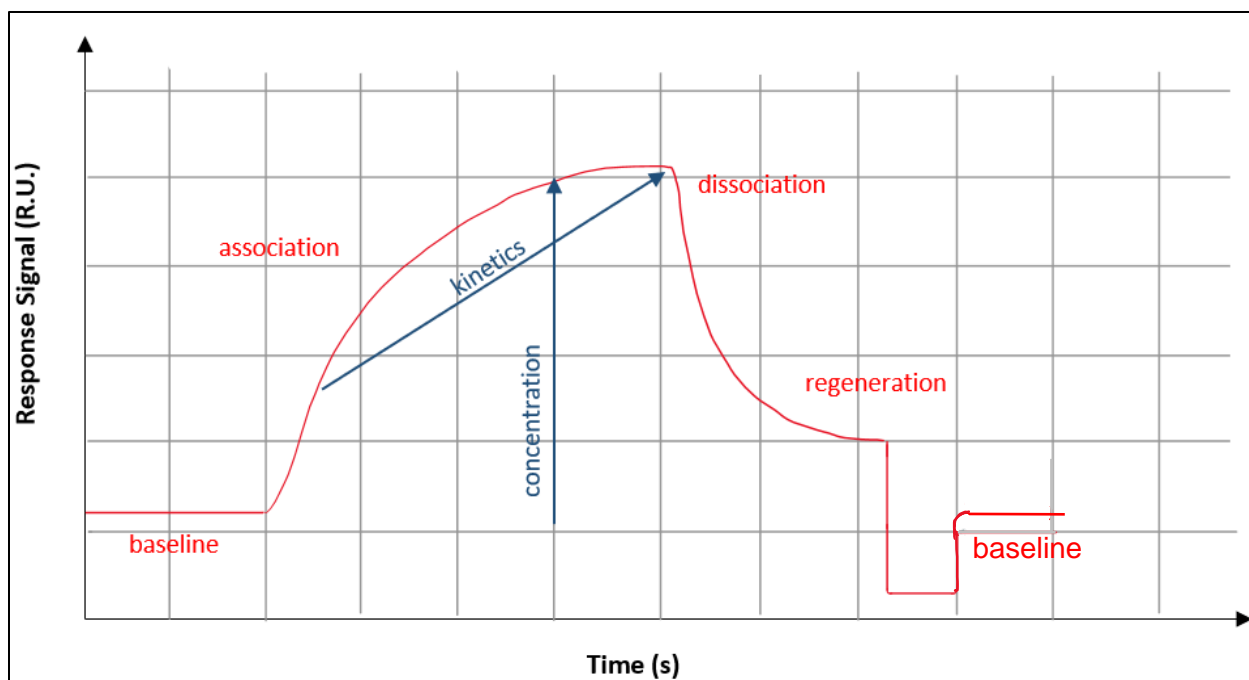


Figure 1.9 – Surface Plasmon Resonance Sensorgram. A stable baseline is obtained prior to injecting the aptamer. The aptamer is then injected. Upon binding of the aptamer to the ligand, an association is observed as an increase in the response. Once the analyte passes through the microfluidic system and is replaced by buffer, the analyte will dissociate from the ligand, generating a decrease in response signal. If the analyte binds tightly to the immobilized ligand, a regeneration solution is injected to break the complex, returning the signal back to baseline.

Firstly, a stable baseline is obtained. Then, a ligand is injected and immobilized on the sensor surface. An analyte is then injected, which results in an increase in the response signal (association).^{66,67} This is indicative of the analyte interacting with the immobilized ligand on the sensor surface. Analyte molecules that do not bind or interact with the target continue to flow through the microfluidic tubing, passing over the sensor surface. Some time after the remaining analyte has passed over the sensor surface, the analyte bound to the immobilized ligand will begin to dissociate from the target. This is made evident by a decrease in the response signal. Lastly, a regeneration solution is injected into the instrument to remove any remaining analyte bound to the immobilized target and to return the response signal back to a stable baseline reading. The

regeneration solution allows for the sensor chips to be reused for multiple analysis cycles, permitting the surface of the sensor does not degrade.⁶⁵

For the purpose of kinetic studies, the data from the sensorgram allows for the determination of both the association and dissociation constant, k_a and k_d , respectively, which in turn leads to the equilibrium dissociation constant, K_D ($K_D = k_d/k_a$), a measure of the strength of a binding interaction. Considering that the equilibrium dissociation constant is a ratio of the association and dissociation rates, it can be evaluated that a smaller K_D is generally indicative of a higher binding affinity. Determining the equilibrium dissociation constant is of great importance for identifying the number of binding sites and understanding the binding kinetics of an analyte-ligand pair.

1.5.1 SPR in Literature

Most recently, Nicoya's OpenSPR system was employed as an analytical instrument for the detection of non-delta SARS-CoV-2 variants.⁶⁸ Specifically, in 2021, Puligedda *et al.* utilized Nicoya's two channel system to measure the binding kinetics between 2E8 IgG monoclonal antibody (mAb) and the SARS-CoV-2 S1 protein (Wuhan-Wu-1 strain).⁶⁸ An equilibrium dissociation constant of 7.38 +/- 0.58 nM was reported, with a k_{on} of $1.4 \times 10^5 \text{ M}^{-1}\text{s}^{-1}$ and a k_{off} of $9.4 \times 10^{-4} \text{ s}^{-1}$. It was remarked that the binding affinity of the 2E8 IgG mAb was approximately 1.5-fold lower than the CA1 mAb and 3-fold lower than the CB6 mAb – binding affinities also measured via SPR by Shi *et al.* in 2020.^{68,69}

Another interesting advancement was made by Singh *et al.*, who employed SPR for binding affinity measurements during research regarding engineered Ras effector protein RASSF5 (NORE1A) variants for promoting anticancer activities in lung adenocarcinoma.⁷⁰ In this research, Singh *et al.* used various computational designs and *in vivo* evolution to engineer a high-affinity

Ras-binding protein, which was not only found to inhibit procancer pathways, but also encourage anticancer pathways. The binding affinities of RASSF5 mutants with Ras-GTP (an active GTP-bound state) and Ras-GDP (an inactive GDP bound state), and all ranged in the low μM or high nM affinity.⁷⁻⁷² Additionally, all mutants showed preferential affinity for the Ras-GTP than the Ras-GDP.

The last notable exploitation of SPR in binding affinity investigations, was conducted by Dr. Kyle Piccolo, a former graduate student in Dr. Dieckmann's research group. Piccolo *et al.* explored and categorized potential ligands for the sulforhodamine B binding RNA aptamer (SRB-2).⁷³ Figure 1.10 illustrates the SRB-2 sequence, generated by *UNAFold*.

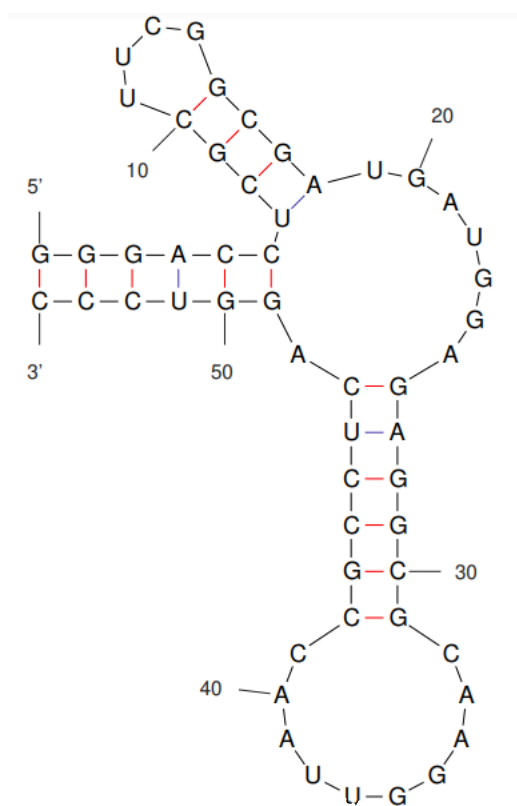


Figure 1.10 - Structure of SRB-2

LSPR was employed, along with ITC and NMR spectroscopy, to screen for binding affinities. The LSPR investigation explored two ligands, Atto rhodamine 101 biotin (AR101-B) and 5/6-biocytn

tetramethylrhodamine (B-TMR), yielding equilibrium dissociation constants of 4.66 μM for binding to AR101-B and 1.37 μM for binding to B-TMR.⁷³ The structures for the two researched ligands are shown below in Figure 1.11a and 1.11b, respectively.

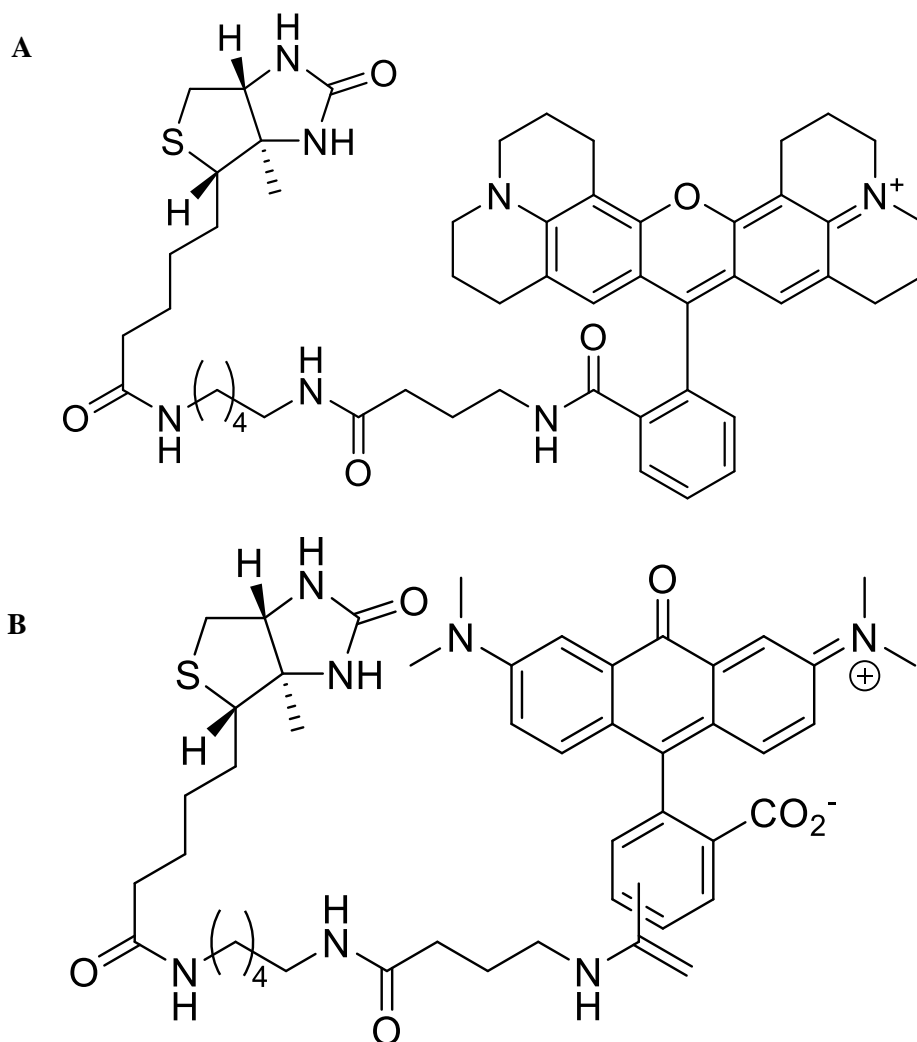


Figure 1.11 - Chemical Structure of AR101-B and B-TMR

Given these constants, indicative of a relatively weak binding affinity, the research concluded that rhodamine B, another investigated dye was the ideal ligand, both structurally and electrostatically, for high affinity binding of the SRB-2 aptamer.

1.6 Fluorescence Spectroscopy

Fluorescence spectroscopy, also known as spectrofluorometry or fluorimetry, can be employed to investigate the conformation or dynamics of a system.⁷⁴ Additionally, the technique is alternative method by which the equilibrium dissociation constant of a binding interaction can be determined, provided that the fluorescence properties change upon binding. Specifically, by measuring the fluorescent intensity of sample, the equilibrium dissociation constant can be evaluated via the following equation:

$$\% F_{max} = F_{max} * \frac{[Nucleic Acid]}{K_D + [Nucleic Acid]}$$

where F_{max} is the maximum fluorescence and K_D is the equilibrium dissociation constant.⁷⁵

Fluorescence can occur when electromagnetic radiation at a particular wavelength is absorbed by a molecule. The energy of the photon of light that is absorbed by the molecule is transferred to an electron in the ground state.⁷⁶ This results in the electron being promoted to an excited electronic state. After some time, the electron will release some thermal energy, and will relax to a lesser excited state. Finally, through collisions with other molecules, the electron will release energy as a photon of light at a different, longer wavelength than that which was absorbed. Upon the release of the photon of light, the electron returns to the ground state, and the emitted light can be detected.⁷⁶ There are several routes by which the electron can return to the ground state – either through fluorescence, the emission of a photon occurring from a transition between states of the same multiplicity, or phosphorescence, the emission of light during a transition between states of different spin multiplicity. Figure 1.12 is known as a Jablonski diagram, and illustrates the process of absorption, fluorescence and phosphorescence.^{76,77}

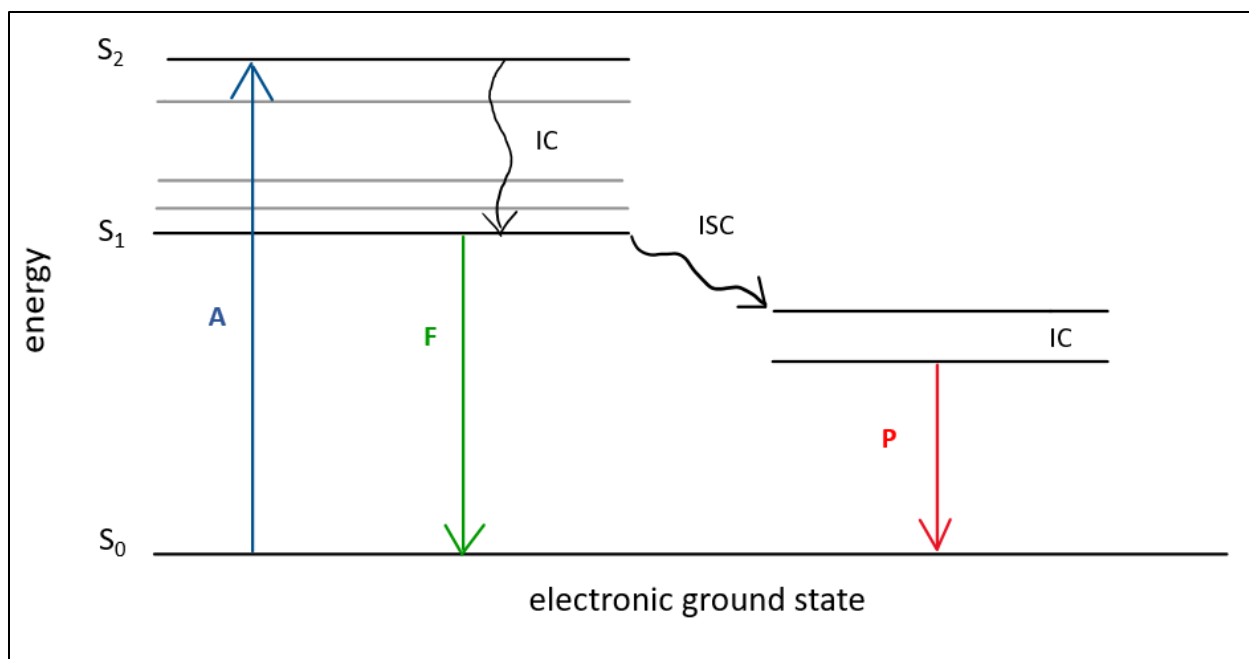


Figure 1.12 - Jablonski Diagram. An electron absorbs a photon of light and gets promoted to an excited state. Through loss of heat and collisions with other molecules, the electron releases the absorbed energy as a photon of light and relaxes back to the ground state via two pathways: IC: Internal Conversion (fluorescence); ISC: Intersystem Crossing (phosphorescence).

1.7 Isothermal Titration Calorimetry

Isothermal titration calorimetry (ITC) is an analytical technique that can be used to determine the thermodynamic properties of binding interactions in solution.^{78,79} Specifically, ITC can determine the change in enthalpy (ΔH) and entropy (ΔS) of a reaction, the stoichiometry of a reaction (n), the Gibbs free energy (ΔG), and the binding affinity (K_a). The enthalpy provides information regarding the magnitude to which H-bonding and electrostatic interactions impact binding, whereas the entropy arises as a result of hydrophobic interactions and conformational changes (i.e. restriction or freedom of backbones or sidechains).⁸⁰ From the binding affinity, the equilibrium dissociation constant (K_D) can be calculated, a value that provides the propensity for the bound aptamer to dissociate from the target ligand. To determine the aforementioned variables, ITC first calculates the power required to keep the sample cell at the same temperature as the reference cell. The power required to maintain zero temperature difference between the sample

cell and reference cell is monitored as a function of time, and plotted as the raw data output, as illustrated in Figure 1.13 below.

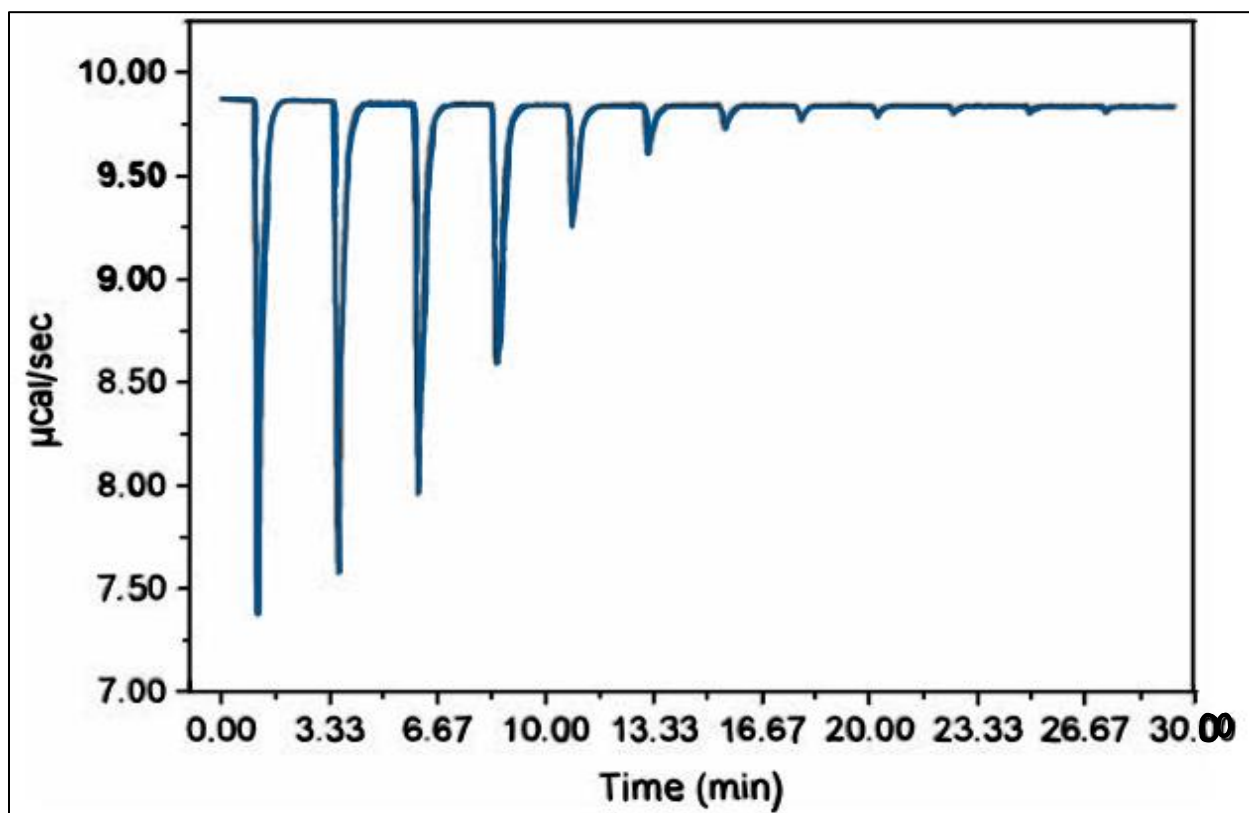


Figure 1.13 - Example of Raw, Real-Time ITC Experimental Data. Individual injection heats produced as a result of titrating a ligand into a nucleic acid.

The raw data is then integrated in order to calculate the individual injection heats. The individual injection heats are then plotted as a function of molar ratio of titrant to material in the sample cell and normalized by the amount of titrant injected. Figure 1.14 highlights an integrated and normalized data set and displays the variables that can be extracted.

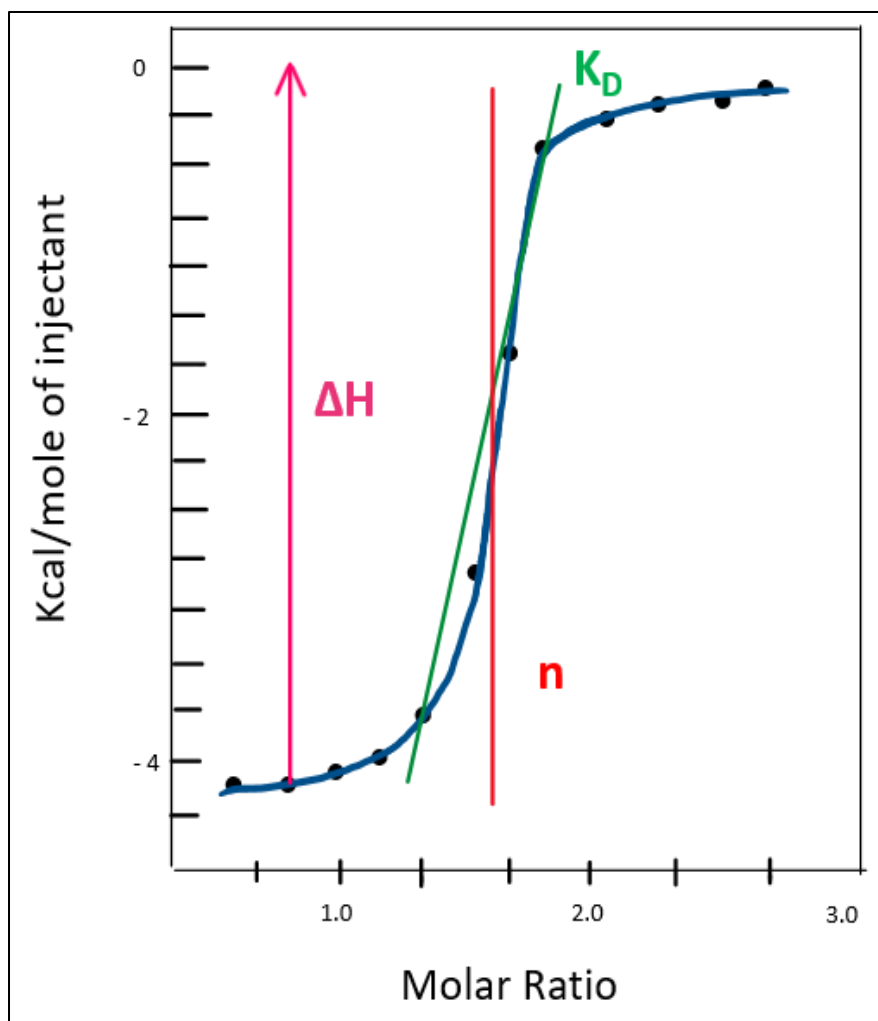


Figure 1.14 - Extraction of Thermodynamic Properties from ITC Titration Curve. The change in enthalpy (ΔH , pink), can be extracted as the magnitude of the largest, normalized injection heat (100% binding). The stoichiometry (n , red) can be obtained as the midpoint of the titration. The equilibrium dissociation constant (K_D , green) is obtained as the slope of the titration curve.

More specifically, in a 1:1 binding experiment, the stoichiometry (n) is the midpoint of the titration – i.e. between 100% binding and 0% binding. The enthalpy can be measured as the magnitude of heat at 100% binding. Lastly, the steepness of the slope is directly related to sample concentration and the binding affinity.

1.7.1 ITC in Literature

In 2020, Bottari *et al.* investigated the reported high affinity of three aptamers for ampicillin.⁸¹ Ampicillin is an antibiotic that binds to RNA, including several aptamers with affinities in the nanomolar range. Specifically, in 2012, Song *et al.* selected for three aptamer sequences to bind to ampicillin, AMP4, AMP17, and AMP18, and found their binding affinities to be 9.4, 13.4, and 9.8 nM, respectively.^{81,82} The researchers used several instruments to measure binding affinities, such as ITC, native nano-electrospray ionization, and proton nuclear magnetic resonance spectroscopy (¹H NMR) and concluded that none of the aptamers showed a high affinity for ampicillin. Specifically, the previously documented equilibrium dissociation constant of the AMP17 aptamer was 13.4 nM; however, Bottari *et al.* were unable to detect any heat exchange during the titration that could be linked to specific binding. After exploring other experimental conditions, such as aptamer changes, pH alterations, different buffers, and varying ionic strength through salt substitutions, a binding response was still not observed, and concluded that the only heat exchange was a result of the injection heat.⁸¹

To further prove the lack of binding, Bottari *et al.* tested a positive control, specifically the MN4 cocaine-binding aptamer. Since the MN4 cocaine-binding aptamer also binds strongly to quinine with a nanomolar affinity (100 nM), this system was subjected to ITC analysis.⁸¹ The binding affinity for the MN4 aptamer to quinine was determined to be 171 nM, and while Bottari *et al.* claims this value to be consistent with that determined by Neves *et al.*, their investigation reported binding affinities ranging from 300 nM – 35 μ M.⁸³

Taking it one step further, the researchers investigated one more binding system with an affinity in the micromolar range, to ensure that the ITC could detect this level on binding. Specifically, the ITC analysis was employed to determine the equilibrium dissociation constant of the L-argininamide to its aptamer.^{81,84} The results yielded a binding affinity of 176 μ M, well on

par with the literature reported 165 μM . With two positive controls, one with a binding affinity in the nM range and one in the μM range, Bottari *et al.* concluded that ITC had the capability of determining aptamer-ligand interactions over a wide range, and furthermore, that the binding interactions of the ampicillin-binding aptamers was not well understood, and hastily reported without multi-faceted investigation.

In 2019, Steinmetzger *et al.* reported that the binding affinity between the Chili aptamer and two targets, 3,5-dimethoxy-4-hydroxybenzylidene imidazolinone (DMHBI, Figure 1.15a) and DMHBI⁺, an analog of DMHBI with a positively charged side chain (Figure 1.15b) were successfully measured via ITC.⁸⁵

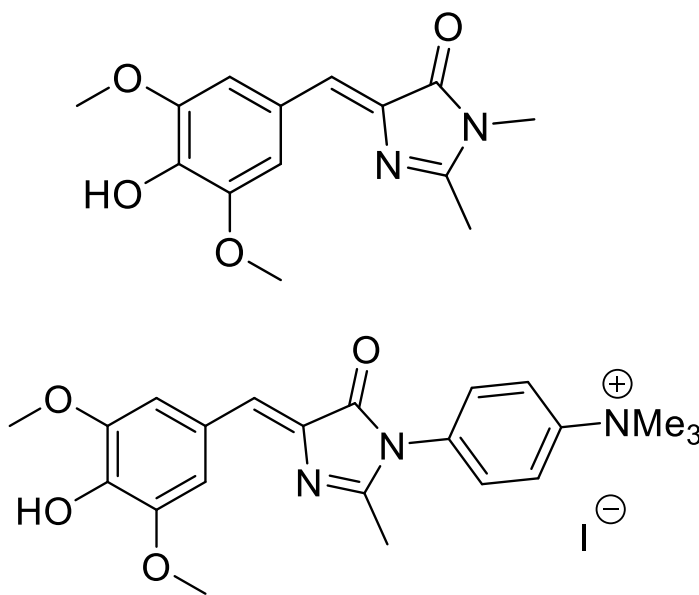


Figure 1.15 - Chemical Structure of DMHBI and DMHBI⁺

The researchers confirmed a binding affinity in the nanomolar range for both targets but reported that stronger binding was observed for the analog. Specifically, an equilibrium dissociation constant of 371 \pm 55 nM was determined for the Chili-DMHBI complex, in

comparison to 21.4 +/- 5.6 nM for the Chili-DMHBI⁺ complex – roughly a tenfold stronger binding than that observed with the neutral ligand.

In 2019, another study conducted by Sjekloća and Ferré-D'Amaré determined the binding affinity of a two-site binding system, 4-(3,6-dimethyl-1,3-benzothiazol-3-ium-2-yl)-N,N-dimethylaniline (Thioflavin T, ThT, Figure 1.16a)-Corn aptamer complex.⁸⁶ The Corn aptamer was originally selected for 3,5-difluoro-4-hydroxybenzylidene-imidazolinone-2-oxime (DFHO), the structure of which is shown in Figure 1.16b.

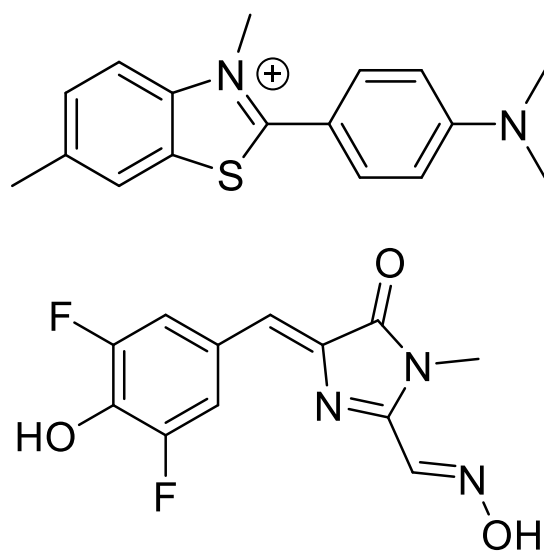


Figure 1.16 - Chemical Structure of ThT and DFHO.

The Corn-DFHO complex demonstrated the capability of increasing fluorescence by 600-fold, but it was recently discovered that ThT could bind to RNA and DNA G-quadruplexes with equilibrium dissociation constants in the micromolar range, so this ligand was explored by Sjekloća and Ferré-D'Amaré.⁸⁶⁻⁹⁰ Dissociation constants of 2 μ M and 11 μ M for the Corn-ThT complex were determined. The binding interactions of the aptamer to a target were further investigated with thiazole orange (TO); but according to the authors, poor solubility of TO in aqueous solutions containing potassium prohibited ITC analysis.⁸⁶

Lastly, Dr. Piccolo's PhD. thesis implemented ITC to determine the binding affinity of several ligands to SRB-2.⁹¹ Specifically, Dr. Piccolo investigated 3 ligands, sulforhodamine B (SR), sulforhodamine 101 (SR 101), and rhodamine B (RB), and found the equilibrium dissociation constants of these RNA-ligand complexes to be 1.45 +/- 0.09 μM , 4.7 +/- 0.70 μM , and 0.447 +/- 0.08 μM , respectively. Figure 1.17 illustrates the chemical structures of the ligands, where 1.10a: SR; 1.10b: SR101, and 1.10c: RB.

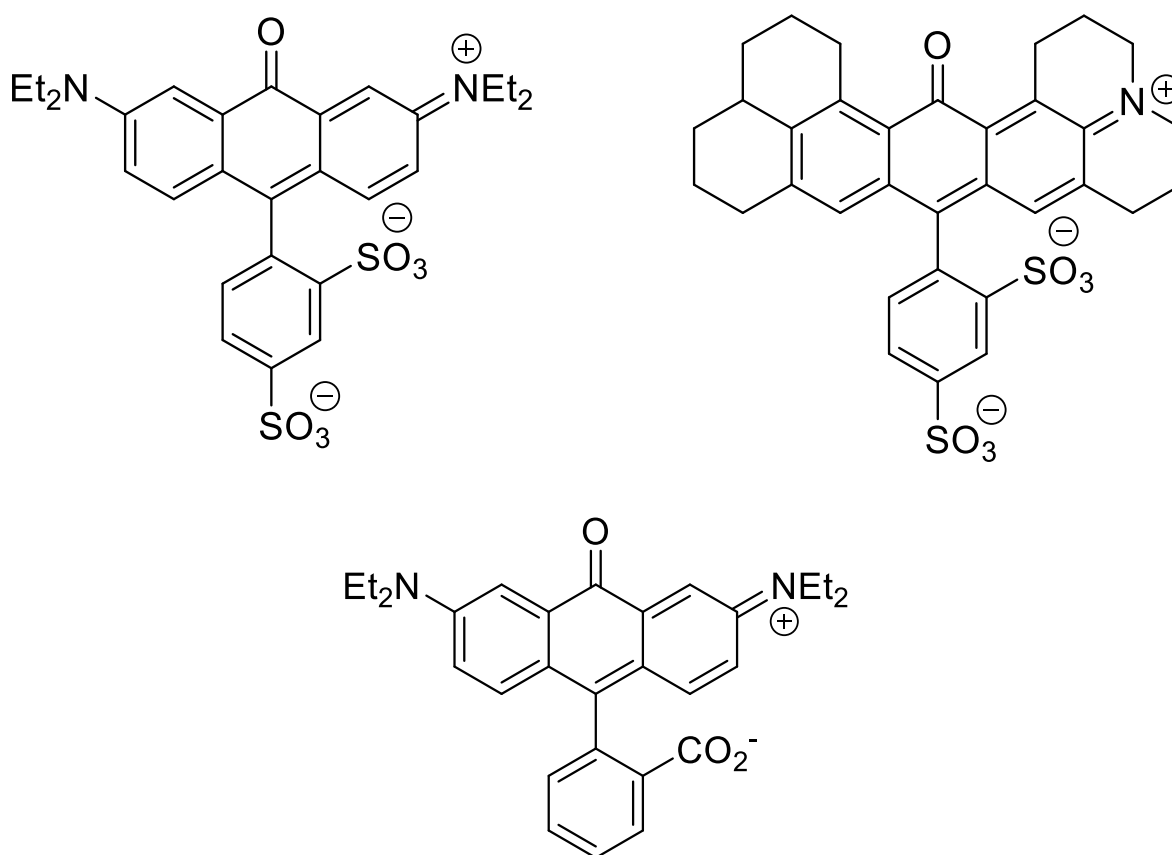


Figure 1.17 - Chemical Structures of SR, SR101, and RB.

To my knowledge, there are no published studies that employ ITC as a means to determine the binding affinity of RNA or DNA Mango aptamers to the target ligand, TO1-3PEG.

1.8 Research Objectives

The purpose of this investigation was to demonstrate how a variety of analytical instruments can be employed to characterize the same system. Specifically, in this research, SPR, ITC, and fluorescence spectroscopy were used for the biochemical characterization of three main systems – the complexes formed between TO1-3PEG and the 2a, 4a, and 6b DNA Mango aptamer sequences. Furthermore, the study aimed to bring to light discrepancies in results that can be obtained from different analytical approaches. For example, it was shown by Da Costa that binding affinities varied depending on the instrument used for measurement.^{49,92} Specifically, in 2011 Da Costa investigated the binding affinity of the malachite green RNA aptamer (MGA) to malachite green (MG) and several other derivatives, TMR, pyronin Y (PY) and crystal violet (CV) using NMR, ITC, equilibrium dialysis, and fluorescence titrations.⁴⁹ Table 1.2 summarizes the equilibrium dissociation constants determined by each analytical method.

Table 1.2 - Summary of Equilibrium Dissociation Constants Obtained from Different Analytical Approaches

Analytical Instrument	Ligand	K _D
NMR	MG	800 nM
	TMR	40 nM
	PY	225 nM
Equilibrium Dialysis	MG	0.26 μM
	PY	8.35 μM
Fluorescence Titrations	MG	2.73 μM
	TMR	0.8 μM
	CV	7.6 μM
	PY	7.6 μM
ITC	MG	0.28 μM
	TMR	0.28 μM
	PY	4.08 μM
	CV	4.45 μM

In addition to the contradictory results within Da Costa's investigation, the equilibrium dissociation constants were also not in agreement with some of the values previously reported in

literature by Baugh *et al.*, who found that the affinity of MG was 0.80 μM .⁹³ Da Costa noted that discrepancies in reported values can arise from a variety of factors, such as conformation, divalent salt concentration, pH, and the difficulty of some methodologies to differentiate between specific and nonspecific binding, such as ITC and fluorescence titrations.⁴⁹ Additionally, analytical methods that rely on a computational model to fit the experimental data, such as ITC which utilizes a model based on a well-defined number of binding sites, exposes the research to incorrect conclusions if the analyzed system does not precisely fit the model.

Based on the aforementioned considerations, SPR was employed in this research, in addition to ITC and fluorescence titrations, to investigate the binding affinities of the DNA Mango aptamer sequences 2a, 4a, and 6b to TO1-3PEG, since this instrument has the capability of differentiating between specific and nonspecific binding. The results obtained from each of the three analytical instruments are discussed and compared in the following chapters.

Chapter 2 Materials and Methods

The following section will summarize the materials, methods, and experimental procedures of this research.

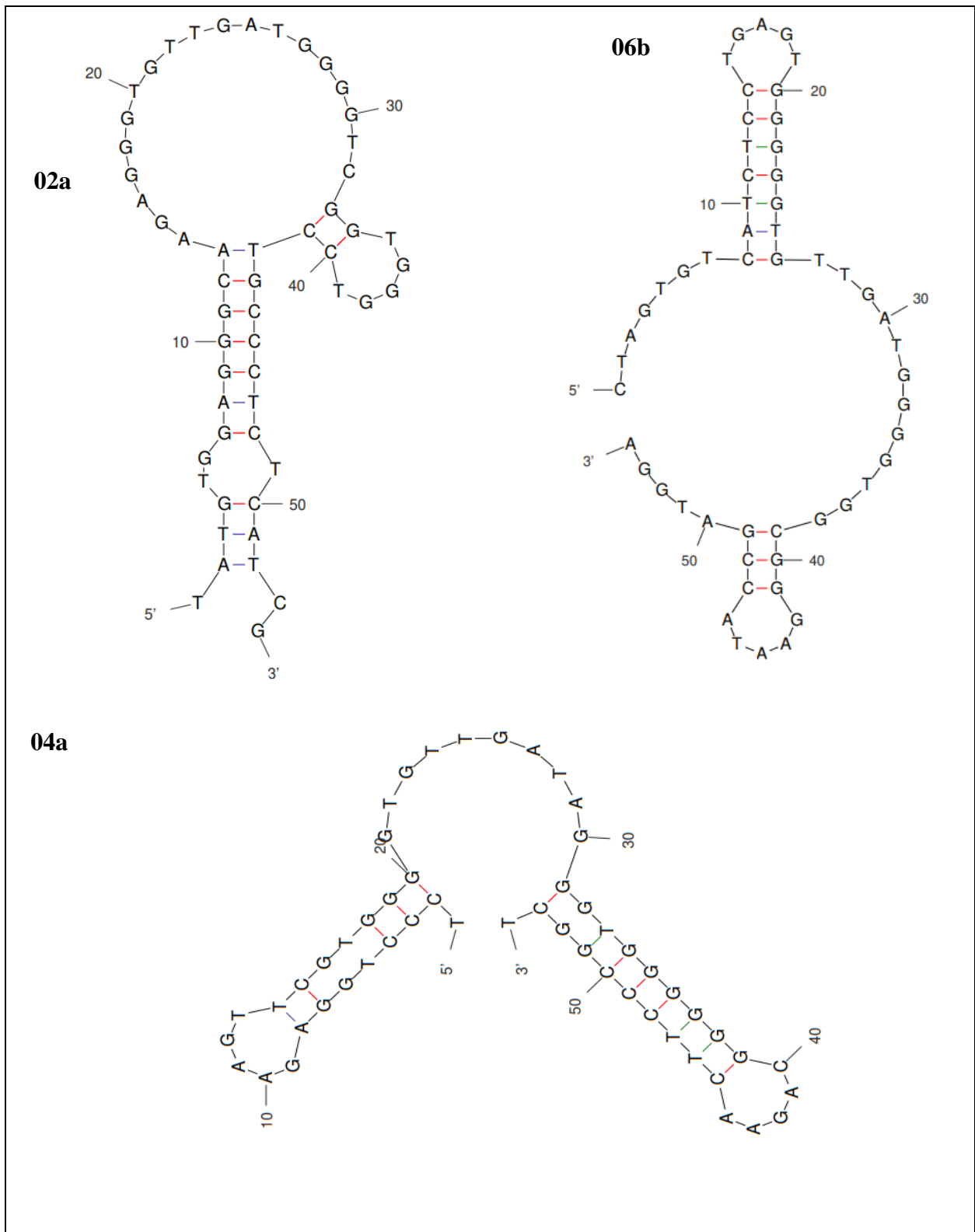
2.1 DNA Purification

For the purpose of investigating the binding kinetics of nucleic aptamers and biotinylated dyes using LSPR, various DNA sequences were purchased from Integrated DNA Technologies (IDT). DNA aptamer sequences for TO1-3PEG were previously selected for by PhD. candidate, Volition La. Sequences 2a, 4a, and 6b, were determined to be the aptamers with the highest affinity for the target ligand by fluorescence spectroscopy, and thus, were chosen for this research for further biochemical characterization. An RNA sequence was transcribed from a custom synthesized DNA template via T7 in vitro transcription. The following sequences were used in this research:

Table 2.1 - Utilized DNA and RNA Sequences

Sequence ID	Sequence
02a	5'-TAT GTG GAG GGC AAG AGG GTG TTG ATG GGG TCG GTG GGT CCT GCC CTC TCA TCG-3'
04a	5'-TCC CTG GAG AAG TTC GTG GGG TGT TGA TAG GGT GGG GGG CAG AAC TTC CCG GCT-3'
06b	5'-CTA GTG TCA TCT CCT GAG TGG GGG TGT TGA TGG GGT GGC GGG AAT ACC GAT GGA-3'
RNA	5'-GGC ACG UAC GAA GGA GAG GAG AGG AAG AGG AGA GUA CGU GA-3'
Hoechst 1-bt	5'-GCG CAA TTC CGG-3'
Hoechst 2	5'- CCG GAA TTG CGC-3'
Hoechst 2 Hairpin	5'-CAT GCA TGG TTA CAT GCA TGC CGG AAT TGC GC-3'

Figure 2.1 shows the secondary structures for the aforementioned DNA sequences. The structures were generated by *UNAFold*.



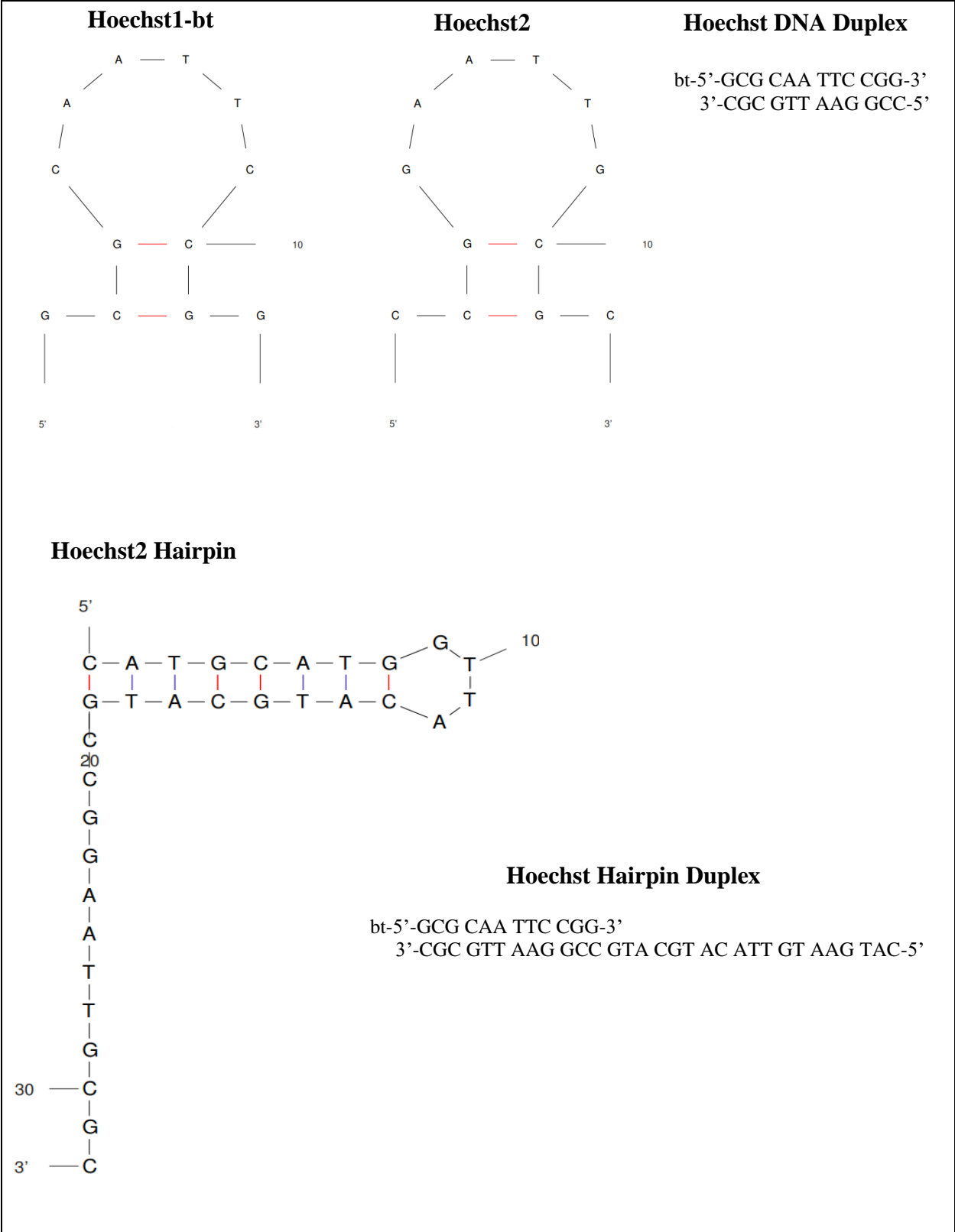


Figure 2.1 - Structures of Utilized DNA Sequences

The DNA sequences were custom synthesized, desalted and deprotected by IDT. Once received, a procedure to purify the sequences was performed for each sequence. To begin the purification, denaturing polyacrylamide gel electrophoresis (PAGE) was run. PAGE is a purification technique widely used in biological fields of study that separates macromolecules (proteins, nucleic acids, etc.) according to their electrophoretic mobility. The percent of acrylamide in the PAGE solution is what aids in the separation of the macromolecules in the sample. The percent needed for optimal separation is outlined in *Molecular Cloning. A Laboratory Manual*, whose requirements are summarized in Table 2.2.⁹⁴

Table 2.2 - Required Acrylamide Content in PAGE for Optimal Separation

Acrylamide (%)	Size of Oligonucleotides (in Bases)
20-30	2-8
15-20	8-25
13-15	15-35
10-13	35-45
8-10	45-70
6-8	70-300

For the DNA sequences, containing 54 bases, a 10% gel was run. For the Hoechst sequences, which contains 32 bases, a 15% gel was run.⁹⁴ The size of the gel to run (small, intermediate, large) is dependent on the synthesis size of the sequence. Typically, for a 250 nanomole synthesis, an intermediate gel is the appropriate size for PAGE.⁹⁴ The PAGE solution required for a 10% intermediate gel is summarized below in Table 2.3:

Table 2.3 - Contents of a 10% PAGE Solution

Solution	Volume (mL)
25% 19:1 Acrylamide Bis 6.667 M Urea	16
6.667 M Urea	20
10X TBE	4

Once the solution with the appropriate acrylamide concentration was made, TEMED and APS were added to initiate the gel. The solution was then poured in the PAGE apparatus and was allowed to solidify. Once solidified, the gel was “pre-run” for approximately 45 minutes at a constant voltage (~250 V), or until the glass plates of the apparatus were warm to the touch. The wells of the gel were then flushed with 1X TBE. The oligonucleotide solution was then made up (3.33 M Urea in water with approximately 20 μ L bromophenol blue). Bromophenol blue was included in the mixture as it allowed for the position of the oligonucleotide to be estimated by tracking the position of the dye.⁹⁴ The amount of bromophenol blue required for visual estimations depends on the percent of polyacrylamide, which was determined to be >15 microliters for a 10% gel.⁹⁴ The solution was then vortexed and loaded evenly into the wells of the gel, and the gel was run for approximately 4 hours at 250 V. The macromolecules of the DNA sample were considered successfully separated once the sample had migrated approximately 4/5 of the length of the gel. The gel was then removed from the experimental apparatus and transferred to a TLC plate with fluorophores with a Saran Wrap protective covering. The DNA was visualized by UV shadowing – the DNA contained in the gel absorbs UV radiation; thus, against a uniform background, the DNA appears dark blue, therefore allowing for ease of visualization and recovery.⁹⁴ The desired DNA band was then excised from the gel using a clean razor blade. It should be noted that the desired band is identified as the slowest-migrating band, otherwise identified as the band closest to the top of the gel.

The gel pieces were then transferred with tweezers to clean, dry, 15 mL conical centrifuge tubes. The gel pieces were soaked in 300 mM NaCl and taped to a rotator overnight (~36 hours) to extract the nucleic acid.⁹⁴ The eluent was filter syringed the next day into 50 mL centrifuge tubes, to which ethanol was added in a 1:2 ratio (NaCl:EtOH). The sodium chloride wash was

repeated a second time in order to ensure proper extraction of all nucleic acid content from the gel pieces. The solution of sodium chloride and ethanol was then stored at -20°C for at least one hour to allow the nucleic acid to precipitate.⁹⁴ After precipitating for approximately one hour, the centrifuge tubes were balanced with ethanol on an analytical balance and centrifuged at 13200 g for 45 minutes at 4°C. Using the Sorvall Legend RT+ (ThermoFisher Scientific, Waltham, MA). The supernatant was then decanted, and the centrifuge tubes were lyophilized at -50°C for approximately half an hour in order to isolate the solid DNA.

2.1.1 Anion Exchange Chromatography

The nucleic acid was then resuspended in 1 mL of Milli-Q water (or the minimum volume required for dissolving) in order to run the sample through anion exchange chromatography (AEC). Anion exchange chromatography is one form of ion-exchange chromatography, the other being cation-exchange chromatography. The first successful separation of oligonucleotides by AEC was reported in the 1970s, and since then, this method has become standard protocol for oligonucleotide purification. The basis of AEC is that separation of impurities can be completed based on chemical moieties. Several intermolecular interactions are possible that allow for separation, including hydrophobic or hydrophilic interactions, or electrostatic interactions.⁹⁵ For the purpose of separating oligonucleotides, a positively charged stationary phase is used because single-stranded RNA or DNA oligonucleotides are highly negatively charged. This allows for the competitive exchange of oligonucleotides with anions from the mobile phase.⁹⁵ In this separation method, the retention of certain impurities or elements of the sample are a function of the charge – retention increases proportionally to the number of charges on the analyte.⁹⁵ In this investigation, to run anion exchange chromatography, a Fast Protein Liquid Chromatography (FPLC) instrument was used with a HiPrep 16/10 diethylaminomethyl (DEAE) FF anion-exchange column from

Cytiva Life Sciences attached. Two buffers, a low salt buffer (50 mM PO₄, 150 mM NaCl, pH 6.5) and a high salt buffer (50 mM PO₄, 2M NaCl, pH 6.5), were used. Two inlets (labeled A inlets) were placed in the low salt buffer, and two inlets (labeled B inlets) were placed in the high salt buffer. The instrument was commanded to pump wash the buffers separately. After the pump wash was completed, the sample was drawn up in a 1 mL syringe to a volume of 875 uL and injected into the sample loop via the injection port. As the separation occurs, the liquid dispenses from an outlet tube. Once the sample begins dispensing, the chromatogram shows an increase in both conductivity and UV readings. This is the point at which the sample collection began. To collect the sample, a 50 mL centrifuge tube was placed under the outlet. Sample collection ended once the conductivity and UV readings returned to baseline. After the anion exchange column, another ethanol precipitation was completed: ethanol was added in a 1:2 ratio nucleic acid:ethanol, the precipitation was carried out at -20°C for approximately one hour, the sample was centrifuged for 45 minutes at 13200 g for 45 minutes, and the supernatant was decanted. Again, the centrifuge tubes were then lyophilized at -50°C for approximately 30 minutes. The sample was once again resuspended in 1 mL of Milli-Q water (or the minimum volume required for dissolving the sample) in order to run the sample through size exclusion chromatography (SEC).

2.1.2 Size Exclusion Chromatography

Similarly to anion exchange chromatography, size exclusion chromatography works to separate molecules, but rather than separating by electrostatic interactions with the stationary phase, SEC separates molecules based on the molecular hydrodynamic volume or size.⁹⁶ In SEC, the mobile phase is typically the same solvent used to dissolve the sample. As the sample is introduced to the column, molecules that are too large to penetrate the pores of the packed column will elute from the column.⁹⁶ Molecules with the right size or molecular weight will have access

to the pores of the packed column, and thus, will elute at a later time than the larger molecules. This is due to the available interaction that smaller molecules have with the pores – small molecules can freely move in and out of the pores, thus taking longer to elute.⁹⁶ For size exclusion chromatography implemented in this research, the FPLC was used with two tandem HiPrep 5 mL Desalting columns (GE Healthcare, Uppsala, Sweden) attached. All inlets (both A and B) were placed in Milli-Q water. The instrument was commanded to pump wash the inlets. The sample was drawn up in a 1 mL syringe to 875 uL and injected into the sample loop via the injection port. The appropriate program was selected and run. The sample was collected when the conductivity and UV readings indicated the presence of the desired nucleic acid. Again, the sample was collected in a 50 mL conical tube. The sample was then stored in a -80 °C freezer until frozen, after which it was lyophilized for up 24 hours. The nucleic acid was then considered purified. The Nanodrop 2000 (ThermoFisher Scientific, Waltham, MA) was then used to determine the final concentration of the purified nucleic acid.

2.2 RNA Transcription

The following custom synthesized DNA template sequence was ordered from IDT and an in vitro transcription was performed with a T7 promoter strand and home-made T7 polymerase:

5'-GCA CGT ACT CTC CTC TTC CTC TCC TCT CCT TCG TAC GTG CCT ATA GTG AGT
CGT ATT A-3'

2.3 Buffer Preparation

Buffers implemented in this research are summarized in Table 2.4.

Table 2.4 - Utilized Buffers

Buffer	Concentration
A	10 mM Na ₂ HPO ₄ /NaH ₂ PO ₄ (pH 7.2), 140 mM KCl, 1 mM MgCl ₂
B	10 mM Na ₂ HPO ₄ /NaH ₂ PO ₄ (pH 7.2), 600 mM NaCl
C	10 mM Na ₂ HPO ₄ /NaH ₂ PO ₄ (pH 7.2), 600 mM KCl, 1mM MgCl ₂
D	10 mM Na ₂ HPO ₄ /NaH ₂ PO ₄ (pH 7.2), 140 mM KCl, 1mM MgCl ₂ , 0.5% Tween
E	10 mM Na ₂ HPO ₄ /NaH ₂ PO ₄ (pH 7.2), 140 mM KCl, 1mM MgCl ₂ , 0.1% BSA
F	10 mM Na ₂ HPO ₄ /NaH ₂ PO ₄ (pH 7.2), 140 mM KCl, 1mM MgCl ₂ , 0.5% HSA
G	10 mM Na ₂ HPO ₄ /NaH ₂ PO ₄ (pH 6.5), 140 mM KCl, 1 mM MgCl ₂
H	10 mM HEPES (pH 7.4), 300 mM NaCl
I	10 mM HEPES (pH 7.4), 300 mM NaCl, 0.5% BSA
J	10 mM Na ₂ HPO ₄ /NaH ₂ PO ₄ (pH 7.2), 140 mM KCl
K	10 mM Na ₂ HPO ₄ /NaH ₂ PO ₄ (pH 7.2), 140 mM KCl, 0.5% BSA

2.4 Streptavidin Sensor Preparation for SPR

Prior to installing a new streptavidin sensor, The OpenSPR system was first primed with the appropriate running buffer for approximately 20 minutes at 150 μ L/min with a blank chip installed. Streptavidin sensors, purchased from Nicoya (Kitchener, Ontario), have streptavidin on the surface of the sensor to make use of the avidin-biotin interaction for ligand immobilization. The sensors were prepared by rinsing with deionized water (DI) followed by 80% isopropyl alcohol (IPA). The sensors were then dried using compressed air and loaded into the sensor holder of the OpenSPR instrument. The flow cell was wiped with a lint-free Kimwipe soaked in IPA and allowed to dry. The sensor was then sealed into place, and the flow cell was filled with running buffer. 150 μ L of IPA was then injected into both channels, as a precaution to remove air bubbles present in the microfluidic system. 3 injections of IPA were followed by 3 injections of 10 mM glycine HCl (pH 2.3) in both channels, each 200 μ L, to remove any contaminants present on the sensor surface, as well as to stabilize the baseline. Lastly, a streptavidin aliquot, provided by Nicoya, was made up to 200 μ L using running buffer, and was then injected into both channels at 150 μ L/min and bound to the gold nanoparticle (AuNP) sensor surface.

2.5 SPR Sample Preparation

The biotinylated ligand and the DNA samples were made up to a final concentration of 5 μM in 1X buffer. The biotinylated ligand, a thiazole orange derivative (TO1-3PEG-Biotin Fluorophore) was purchased from Applied Biological Materials Incorporation (ABM Inc.). The initial concentration was 0.5 mg/mL in dimethylformamide (DMF) with a molecular weight of 749.315 g/mol. To achieve a final ligand concentration of 5 μM , 7.49 μL was lyophilized and diluted to a final volume of 500 μL in running buffer. Similarly, DNA samples were diluted to a final concentration of 5 μM with the appropriate running buffer and MQ water.

2.6 SPR Validation Protocol

The validation experiment employed a Protein A -IgG system. All reagents required for experimentation were provided by Nicoya.

A carboxyl sensor was utilized, and similarly to the sensor preparation described in Section 2.4, was prepared by rinsing with DI water, IPA, and dried with compressed air before loading into the OpenSPR. The SPR instrument was primed with RB (PBS-T: a phosphate-buffered saline solution containing a low-concentration of detergent such as Tween), and then Glycine HCl (pH 1.5-3) was injected to clean the sensor surface. To prepare the sensor surface for ligand immobilization, a 100 μL 1-ethyl-3-(3-dimethylaminopropyl)carbodiimide (EDC) aliquot in water was mixed with a 100 μL N-Hydroxysuccinimide (NHS) aliquot in water and was injected into both channels.

For ligand immobilization, Protein A was dissolved in 200 μL “immobilization buffer”. Large ligands, such as proteins, are immobilized to carboxyl sensors via a method known as pre-concentration, which utilizes electrostatic interactions to increase the local concentration of the ligand at the sensor surface. This is accomplished by diluting the protein in a buffer >0.5 pH units

below the isoelectric point (pI) of the ligand. This results in a net positive charge on the ligand. After dilution in the immobilization buffer, Ligand A (20 $\mu\text{g/mL}$) was injected into channel 2. The OpenSPR software then performed an evaluation to confirm that the ligand had been successfully immobilized.

Prior to the analyte injection, to reduce, if not eliminate entirely, the potential for NSB of the analyte to the sensor surface, a blocking solution was injected into both channels. The blocking solution serves to bind to the remaining sites of the prepared sensor surface to ensure that the subsequent analyte injection results in specific binding of the analyte to the immobilized ligand.

Finally, the three analyte (Human IgG) samples were prepared in RB (PBS-T) with final concentrations of 11 nM, 33nM, and 100 nM. The samples were then injected from lowest to highest concentration of IgG. Between each analyte injection, glycine HCl was injected to regenerate the sensor by removing bound IgG from the Protein A.

2.7 ITC Sample Preparation

DNA samples were annealed by heating to 90 $^{\circ}\text{C}$ and allowing to cool to room temperature. Final DNA concentrations for all ITC experiments were 15 μM . TTO1-3PEG was diluted in ~4 mL MQ water, frozen at -80 $^{\circ}\text{C}$, and then lyophilized for DMF removal. The lyophilized TO1-3PEG was diluted to a final concentration of 250 μM .

2.8 Native PAGE

In order to confirm the presence of secondary structures, native PAGE experiments were conducted. A native PAGE is similar to the PAGES procedure outlined in 2.1.1; however, no urea is used in order to observe non-denatured nucleic acids. From a native gel, one can use a fluorescence imaging system to visualize the DNA conformations with the use of a comparative

DNA ladder identifying base pairs. For this research a Low Molecular Weight (LMW) DNA Ladder was used from New England Biolabs. The DNA ladder included a purple gel loading dye at a concentration of 500 $\mu\text{g}/\text{mL}$ and is an adequate ladder for 25 to 766 base pairs.

The first native PAGE experiment examined the difference in DNA aptamer conformations between unannealed and annealed samples. Annealing is the process of heating and cooling the DNA, allowing the stands to return to their natural biological state. This process can be done in order to obtain the same starting conformation for all DNA samples. The following procedure was followed. Firstly, a native gel was made by mixing Solution A (25% 19:1 acrylamide bis 6.667 M Urea), Solution C (10 X TBE) and MQ water. 40 μL APS and 10 μL TEMED was added to polymerize the solution, creating the native gel to which the DNA samples would be loaded and run for fluorescence imaging. Next, the 4a DNA Mango aptamer samples were made. Solutions were made up to 10 μL in PCR tubes, which included 1.1 μg DNA (1.40 μL DNA), 5 μL glycerol to help weigh the DNA gel down the gel, and the rest of the volume made up with MQW. The samples then underwent an annealing process, in which the PCR tubes were heated to 90 $^{\circ}\text{C}$ and cooled to 4 $^{\circ}\text{C}$ on a programmable heating block. The following table summarizes the tested conditions.

Table 2.5 – Well Contents of Native PAGE

Well	Contents
1	8 uL LMW DNA Ladder
2	DNA Control (Not Annealed): 1.40 uL 4a DNA + 5.00 uL glycerol + 3.60 uL MQW
3	DNA Control (Annealed): 1.40 uL 4a DNA + 5.00 uL glycerol + 3.60 uL MQW
4	Dye Control: 0.98 uL dye + 5.00 uL glycerol + 3.60 uL MQW
5	DNA and Dye (Not Annealed): 1.40 uL 4a DNA + 0.98 uL dye + 5.00 uL glycerol + 2.62 uL MQW
6	DNA and Dye (Annealed): 1.40 uL 4a DNA + 0.98 uL dye + 5.00 uL glycerol + 2.62 uL MQW

The samples were then loaded evenly into the wells of the 10% PAGE, and the gel was run for approximately 25 minutes at 250 V. The gel was immediately transferred to the FluorChem FC2 Imaging System (Alpha Innotech, San Leandro, CA), and was excited by an ultra-violet (UV) light with a green filter at 527 nm. This filter was chosen given the proximity of the wavelength to the excitation wavelength of the aptamer-bound ligand (514 nm).

Chapter 3

Fluorescence Spectroscopy Titrations

In this chapter, previously conducted fluorescence titrations of the 2a, 4a, and 6b DNA Mango aptamer will be summarized to provide a direct comparison to the fluorescence titration experiments conducted in this research. Additionally, single-read fluorescence experiments were conducted for proof-of-concept.

3.1 Previous Fluorescence Research

PhD. candidate, Volition La, conducted fluorescence titration experiments on several DNA Mango aptamers for which he selected to bind to TO1-3PEG. DNA concentrations ranged from 50 nM – 5 μ M in sodium phosphate buffer (pH 7.4), with a constant ligand concentration of 50 nM across all samples. Samples were prepared without the ligand and annealed by heating to 90 °C. Samples were then incubated with the ligand before subjecting to fluorescence spectroscopy using a Molecular Devices SpectraMax M5 microplate reader (Molecular Devices, San Jose, CA). The binding affinities found by La for the aptamers of interest are summarized in Table 3.1.

Table 3.1 - Determined Binding Affinities of DNA Mango Aptamers to TO1-3PEG by Fluorescence Spectroscopy

DNA Mango Aptamer	Reported K_D (nM)
2a	172.7
4a	366.4
6b	570.0

It was concluded from this investigation that each of the aptamers displayed a strong binding affinity for the target ligand, with the strongest binding aptamer being the 2a sequence.

3.2 Fluorescence Titration Investigation

The results of La's research were severely contrasting to the binding affinities produced in this investigation by ITC and SPR, as discussed in Chapters 4 and 6, respectively. Thus, the

fluorescence titration experiments were repeated in order to determine the repeatability and reliability of La's reported binding affinities. The aforementioned sample preparation procedure was followed precisely. Fluorescence enhancement was observed for the 4a sequence, from which a titration curve was generated and a K_D was measured using GraphPad Prism 9, a binding analysis software. Figure 3.1 illustrates the titration curve of the 4a sequence, from which a K_D of 161 nM was determined.

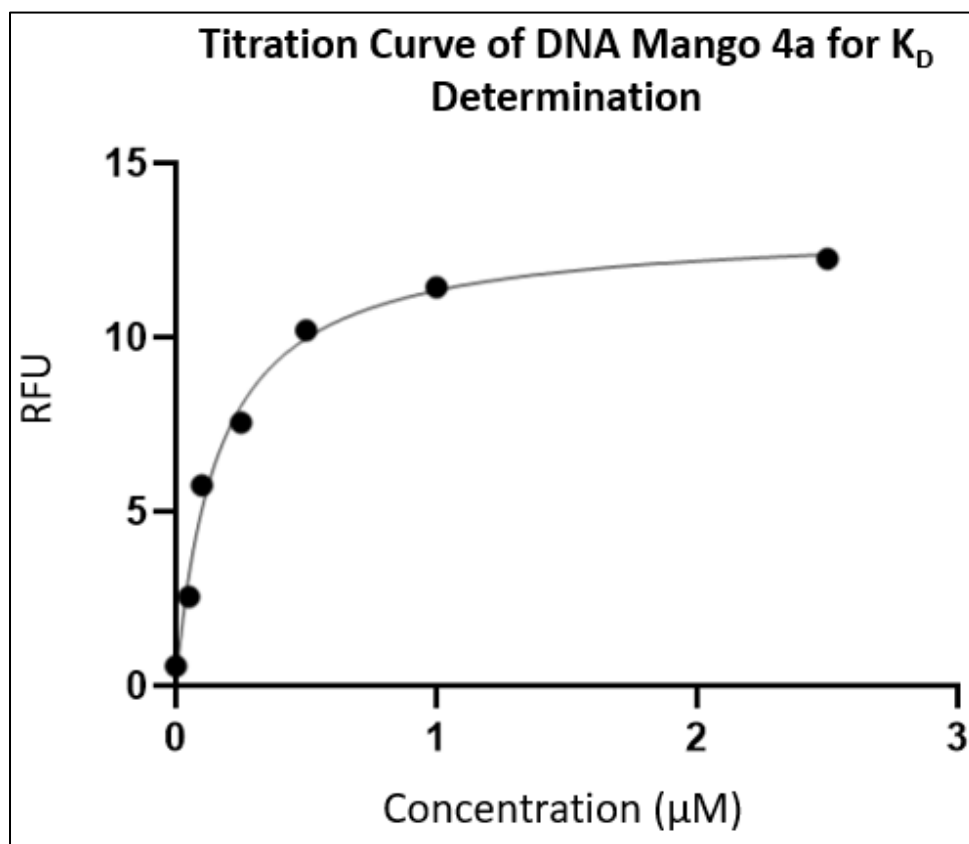


Figure 3.1 - Fluorescence Titration Curve Pertaining to DNA Mango 4a for K_D Determination

While an equilibrium dissociation constant in the nanomolar range, specifically 161 nM, was determined from this experiment, the fluorescence intensity for each of the DNA-containing samples was lower than previously observed – while free TO1-3PEG has little to no fluorescence, DNA-bound TO1-3PEG should yield an ~100-fold increase in fluorescence intensity. Figure 3.1 shows a much lower enhancement which could be attributed to quenching; however, further

fluorescence spectroscopy investigations would be required for definitive conclusions regarding the reliability of this measurement, as well as to explore other aptamer sequences.

Considering that fluorescence spectroscopy provided evidence of binding between the 4a DNA Mango aptamer sequence and TO1-3PEG, isothermal titration calorimetry, native PAGE, and surface plasmon resonance were then investigated as methods by which these systems could be biochemically characterized.

Chapter 4

Isothermal Titration Calorimetry

As previously mentioned, ITC is an analytical method that can be used to determine the thermodynamic properties of binding interactions in solution, such as ΔH , ΔS , ΔG , η , K_A , and K_D . Unlike SPR, however, the on and off rates, k_{on} and k_{off} , respectively, cannot be easily determined. The following chapter will discuss ITC experiments performed on DNA aptamer sequences 4a, 6b, and 2a, and will extract the binding affinities of each sequence to the target ligand. Additionally, the chapter will discuss fluorescence experiments and native PAGE gels that were investigated given the hypotheses derived from ITC results.

4.1 ITC Investigation on 4a DNA Mango Aptamer Sequence

Previous research in the Dieckmann laboratory successfully measured the equilibrium dissociation constant for the 4a DNA Mango aptamer to the target ligand, TO1-3PEG, using ITC. The following description highlights the parameters and conditions of the experiment. 300 μL of the 4a DNA Mango sequence in HEPES buffer (10 mM HEPES, 5 mM MgCl_2 , 100 mM KCl, pH 7.4) was loaded into the cell of the ITC at a concentration of 15 μM . The ligand, also in HEPES buffer, was loaded into the syringe at a concentration of 250 μM to be titrated into the cell. From this experiment, an exothermic reaction was observed yielding an equilibrium dissociation constant, K_D , of 14.27 μM , indicative of a very weak binding affinity ($K_D > \text{nM}$). When the experiment was repeated for this research, the only alteration was the implemented buffer. In the repeated experiment, Buffer A (10 mM $\text{Na}_2\text{HPO}_4/\text{NaH}_2\text{PO}_4$, 140 mM KCl, 1 mM MgCl_2 , pH 7.2), the buffer previously selected for by PhD. candidate, Volition La, was used, instead of the aforementioned HEPES buffer. Figure 4.1 illustrates the normalized injection heats for the repeated ITC experiment with the 4a DNA Mango aptamer.

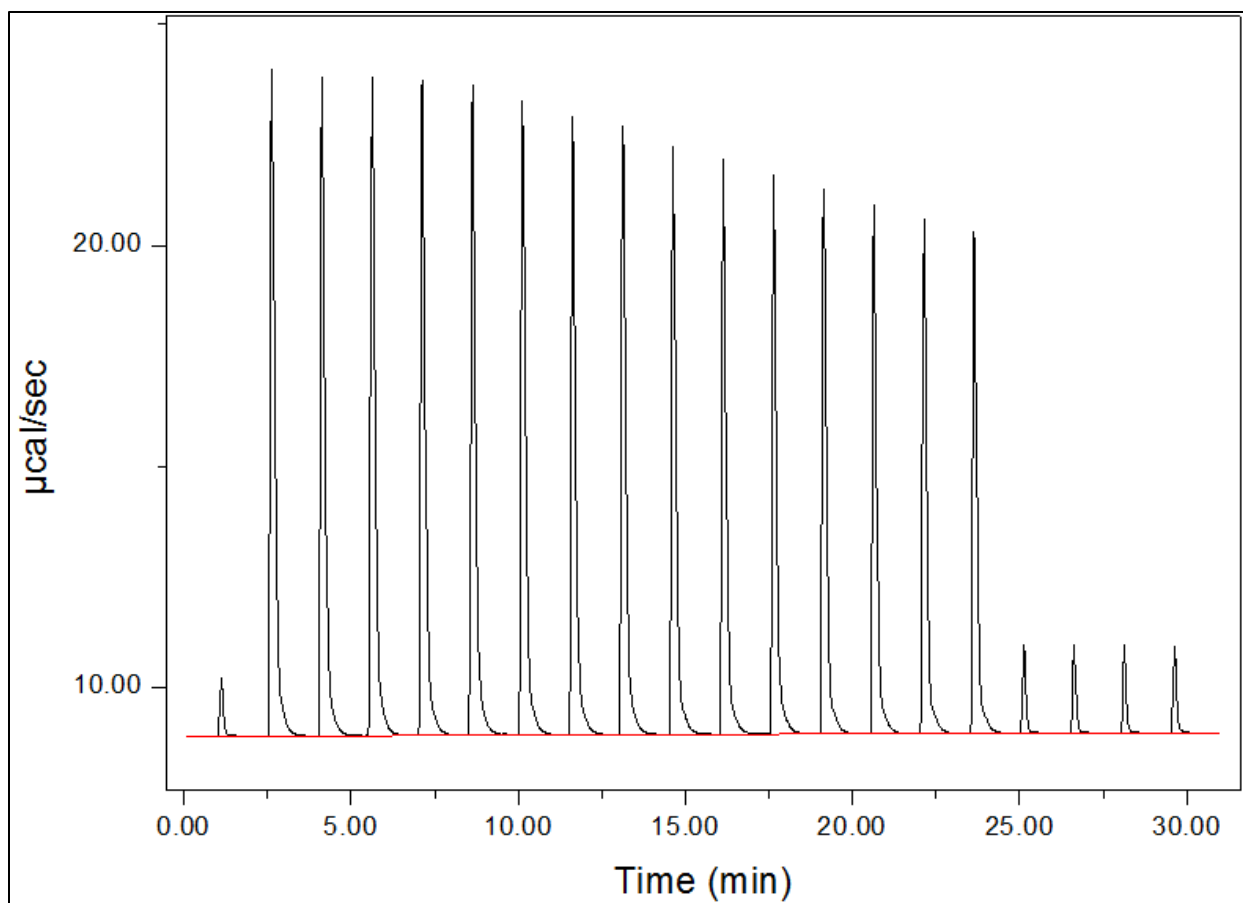


Figure 4.1 - Normalized Injection Heats from ITC Experiment with 4a DNA Mango Aptamer. Individual, normalized injection heats pertaining to the injections of the ligand, TO1-3PEG (250 μ M) into the 4a DNA Mango aptamer (15 μ M).

In contrast to the exothermic response seen in the original experiment, this repeated experiment exhibited a strong, endothermic (positive) reaction, from which a decreasing trend in intensity was observed in the second to fifteenth peak. The unanticipated endothermic signal was attributed to the occurrence of a reaction that produced a strong enough endothermic signal, such that the true exothermic signal pertaining to the binding interaction of the ligand and aptamer was masked. After the fifteenth peak, a drastic decrease in intensity was noted. This response was highly unexpected and did not indicate the end of the titration, but rather, indicated the result of an artifact, an instrument malfunction, or a contamination in the sample cell. To process the raw data

and obtain the equilibrium dissociation constant, the last 4 injections were removed. Figure 4.2 illustrates the processed data.

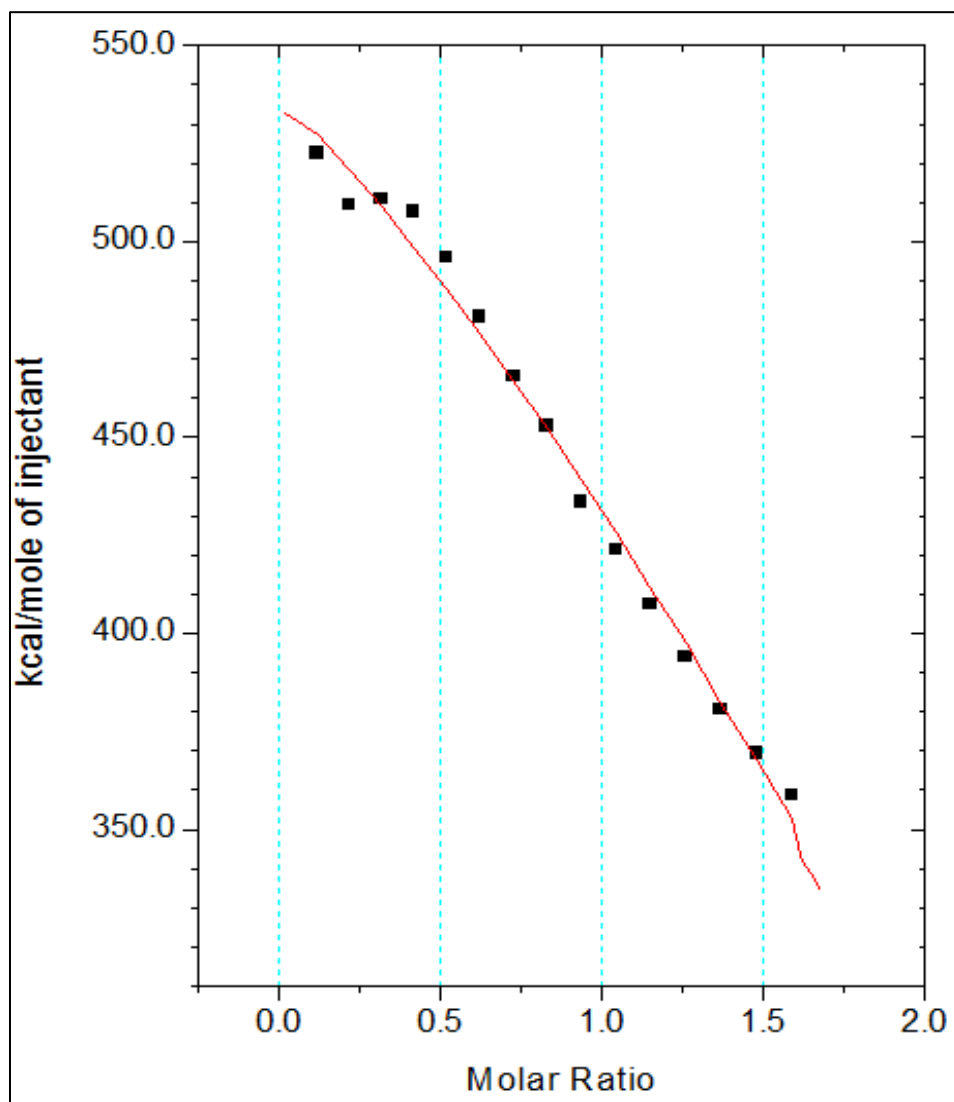


Figure 4.2 – Isotherm of 4a DNA Mango-TO1-3PEG in Sodium Phosphate Buffer. The generated isotherm pertaining to the 4a DNA Mango ITC titration experiment in which 250 μM of TO1-3PEG was titrated into 15 μM 4a DNA Mango aptamer.

Despite the endothermic signal, the processed data yielded a comparable equilibrium dissociation constant to that previously determined. Specifically, from this experiment, the equilibrium dissociation constant was obtained by employing a single binding site model for fitting the data.

The K_D was found to be 9.71 μM , only a 4.56 μM difference to that established by the previous

undergraduate researcher. Equation 4.1 demonstrates how the K_D was obtained from the association constant generated by the ITC software.

$$K_D = \frac{1}{K_A} \quad (\text{Equation 4.1})$$

The K_A from this experiment was found to be 104000 M^{-1} with an error of 32700 M^{-1} , yielding a K_D of $9.71 \text{ }\mu\text{M} \pm 3.05 \text{ }\mu\text{M}$.

In spite of what was considered a successfully repeated experiment, it was hypothesized that one of the reasons for the stark contrast between experimental responses and binding signatures could be the presence of dimethylformamide (DMF) in the ligand solution. DMF is the solvent in which TO1-3PEG was dissolved, and at high concentrations, can be harmful to the ITC, and is also known to denature DNA above 50% v/v. Given the low concentration of DMF in the final solution used in the experiment, however, the DMF was initially deemed a non-issue. To confirm that the DMF content was not interfering with the binding interactions of the 4a DNA Mango aptamer and the TO1-3PEG, the thermal signature of DMF was evaluated in an ITC experiment, in which sodium phosphate Buffer A containing DMF was titrated into Buffer A. The normalized injection heats can be seen below in Figure 4.3.

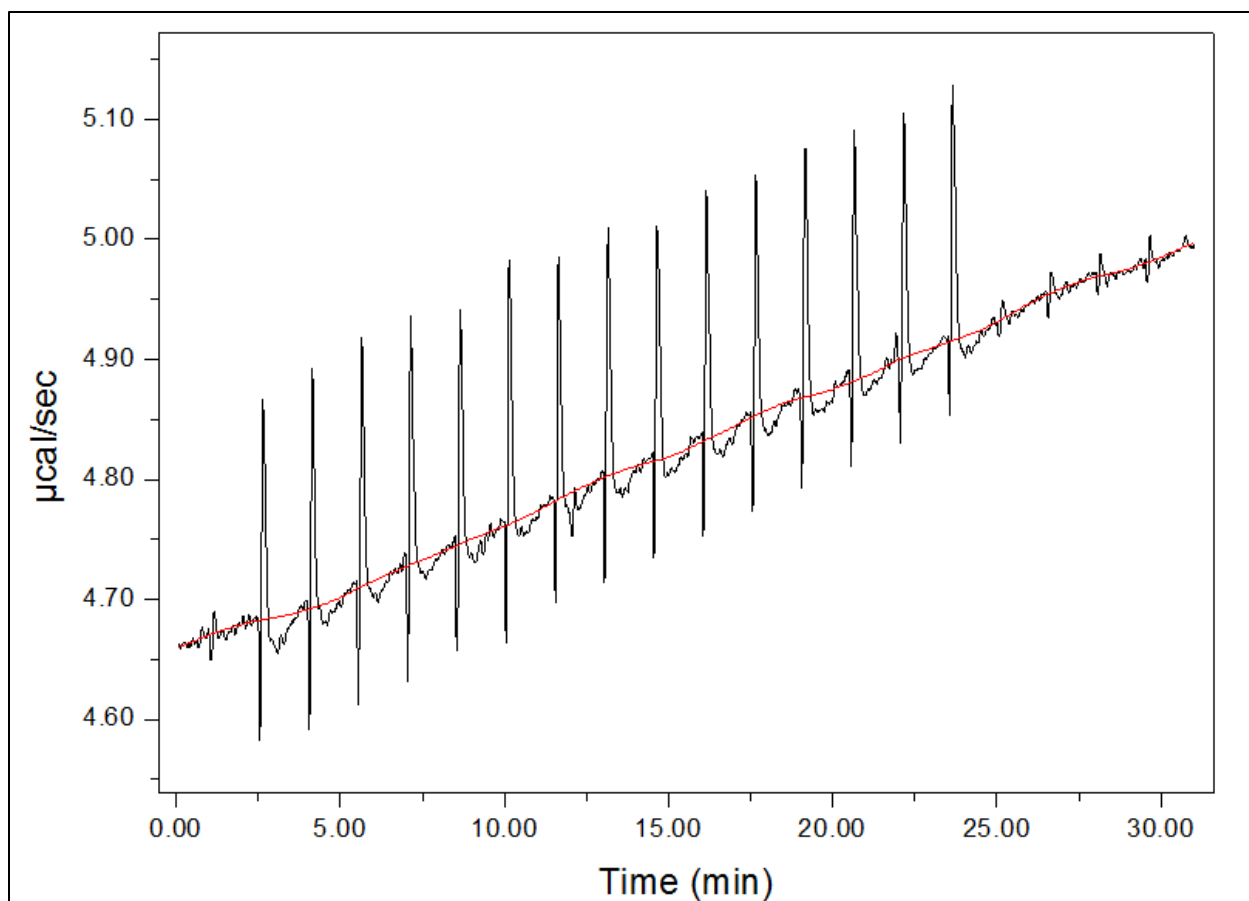


Figure 4.3 - Normalized Injection Heats of DMF Titration. The normalized injection heats resulting from the titration of DMF-containing buffer (22.48% DMF) into buffer to determine if the presence of DMF contributed to an endothermic heat signature.

Illustrated in the experimental data are endothermic peaks with an upward baseline drift. The endothermic peaks were attributed to either an endothermic heat of dilution arising from the DMF or a mismatch in buffer concentrations.

4.1.1 Fluorescence Investigation on the Effect of DMF on Binding Interactions

To further investigate the effect of DMF on the binding interactions between the ligand and aptamer, a fluorescence scan was performed. Four samples were analyzed:

Table 4.1 - Samples Analyzed in Fluorescence Titration Investigation of Effect of DMF

Sample	Contents
1	Buffer A, Ligand (5 μ M)
2	Buffer A, Ligand (5 μ M), DMF
3	Buffer A, Ligand (5 μ M), 4a DNA Mango aptamer (15 μ M)
4	Buffer A, Ligand (5 μ M), DMF, 4a DNA Mango aptamer (15 μ M)

It should be noted that in samples containing DMF, the percent of DMF replicated the 22.48 % v/v of DMF contained in previous ITC experiments. Figure 4.4 shows a direct comparison of the fluorescence intensity spectra of the samples.

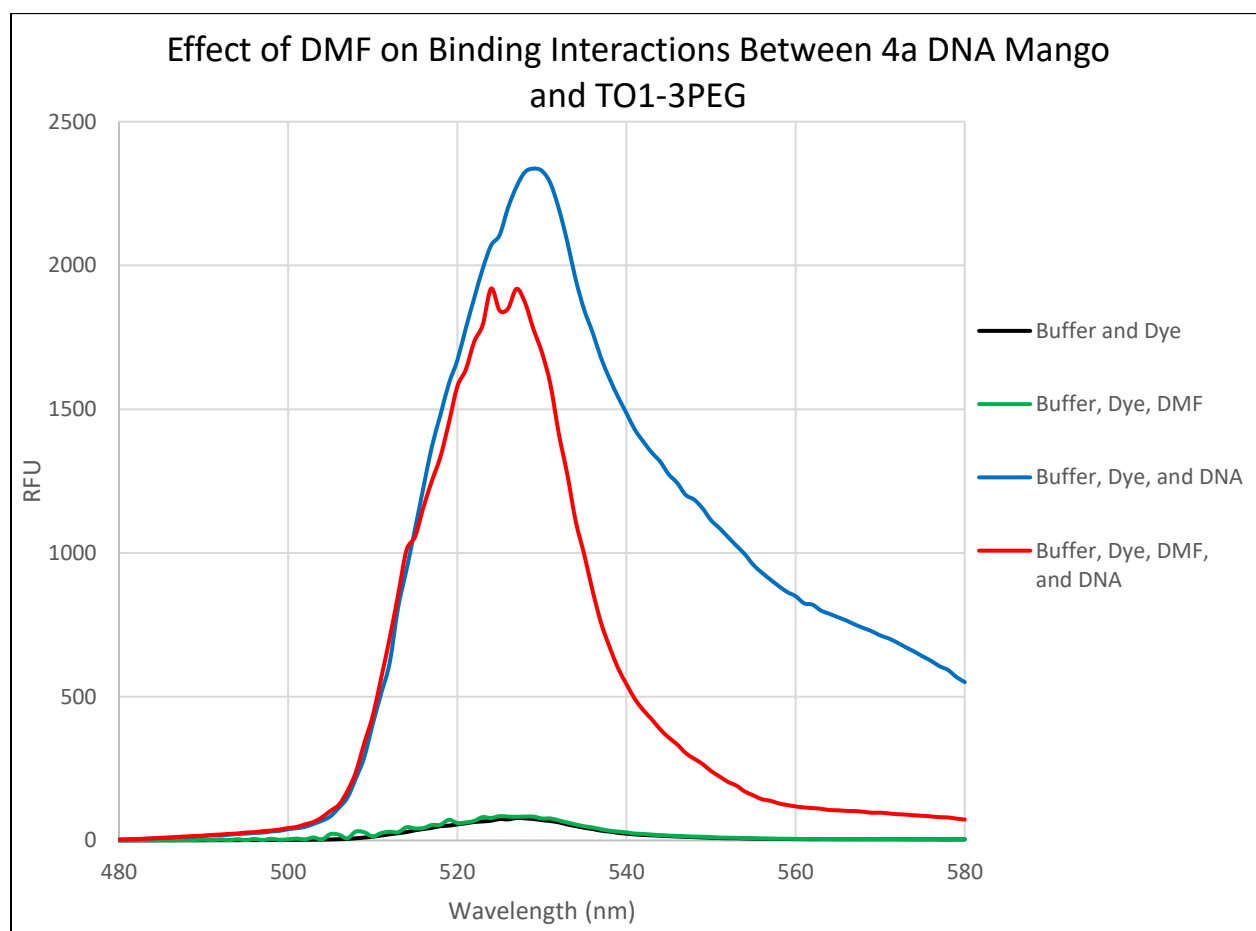


Figure 4.4 - Fluorescence Investigation to Determine the Effect of DMF on Binding Interactions Between 4a DNA Mango and TO1-3PEG. The intensity of fluorescence in the absence and presence of DMF was investigated to determine the effect of DMF on the binding affinity between the 4a DNA Mango aptamer and the ligand.

It was concluded from Figure 3.4 that the presence of DMF does, in fact, directly impact the ability of the aptamer to specifically bind to the ligand. At the fluorescent maximum, a significant difference in the intensity (~500 RFUs) was observed between the sample that did not contain DMF and the DMF-containing sample. Furthermore, the difference in fluorescent intensity became increasingly substantial along the shoulder of the curves (>535 nm). Given the suppressed fluorescence of the DMF-containing sample across the spectrum, it was concluded that binding between the aptamer and the ligand is affected by the presence of DMF. Specifically, the decreased fluorescent intensity in the presence of DMF indicated weaker binding between the aptamer and ligand, possibly due to the ligand orientation, given its sensitivity to environmental changes. Thus, the DMF content of the ligand solution was removed by lyophilization in proceeding experiments in order to ensure that the characteristics of the ligand, such as its fluorescence and ability to bind to aptamers, was not disrupted.

4.1.2 Implementation of HEPES Buffer

The endothermic peaks obtained from the ITC experiment were then attributed to the sodium phosphate buffer. A sodium phosphate buffer was implemented primarily because it was the one in which the DNA Mango aptamers were initially selected, but also because the capability of a ligand binding to aptamers has known dependence on the presence of divalent counter-ions to stabilize the aptamer's negatively charged backbone. Another imperative consideration was that sodium phosphate buffers are commonly used in structural characterization investigations employing Nuclear Magnetic Resonance (NMR) spectroscopy, and thus, the conditions are often replicated in biochemical characterization research to ensure that the investigated system behaves as expected under NMR conditions. Despite these considerations, a HEPES buffer was used in subsequent ITC experiments in order precisely replicate the previously successful conditions. The

raw, untreated data from which 250 μM TO1-3PEG ligand in 1 X HEPES buffer was titrated into 15 μM 4a DNA Mango aptamer supported the findings of the first experiment by again producing endothermic peaks. Figure 4.5 contains the processed binding curve for the experiment, from which the equilibrium dissociation constant was determined.

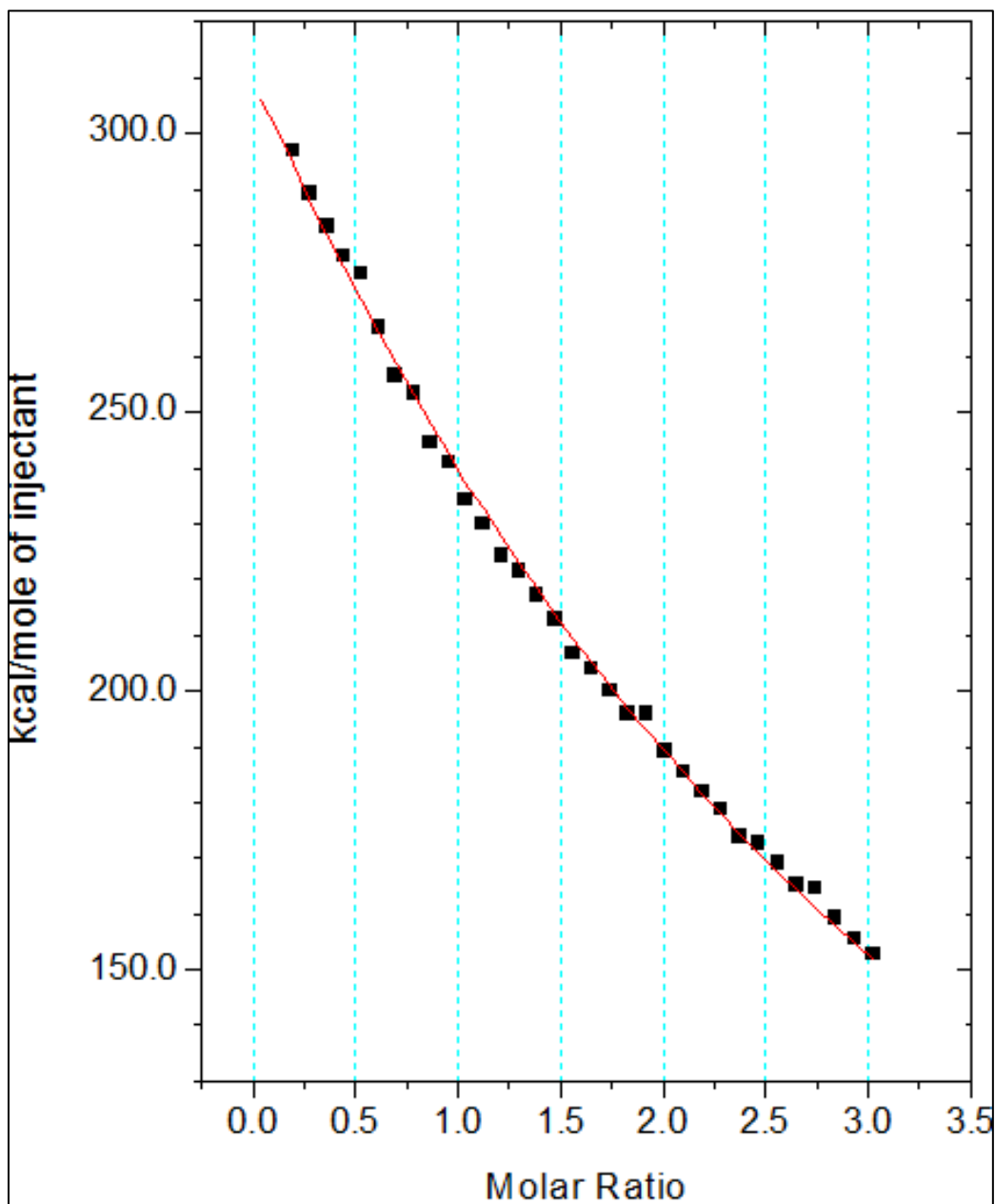


Figure 4.5 - ITC Isotherm of 4a DNA Mango-TO1-3PEG in HEPES Buffer. The generated isotherm pertaining to the 4a DNA Mango ITC titration experiment in which 250 μM TO1-3PEG was titrated into 15 μM 4a DNA Mango aptamer.

From this binding curve, the K_A value was determined to be $5910 \text{ M}^{-1} \pm 1940 \text{ M}^{-1}$, yielding an equilibrium dissociation constant, K_D , of 0.183 mM . The error within the K_A and the large K_D indicated that the one site binding model failed for this system under these conditions. The ITC experiment was repeated in order to introduce reliability in the results. Figure 4.6 displays the processed data for the experiment

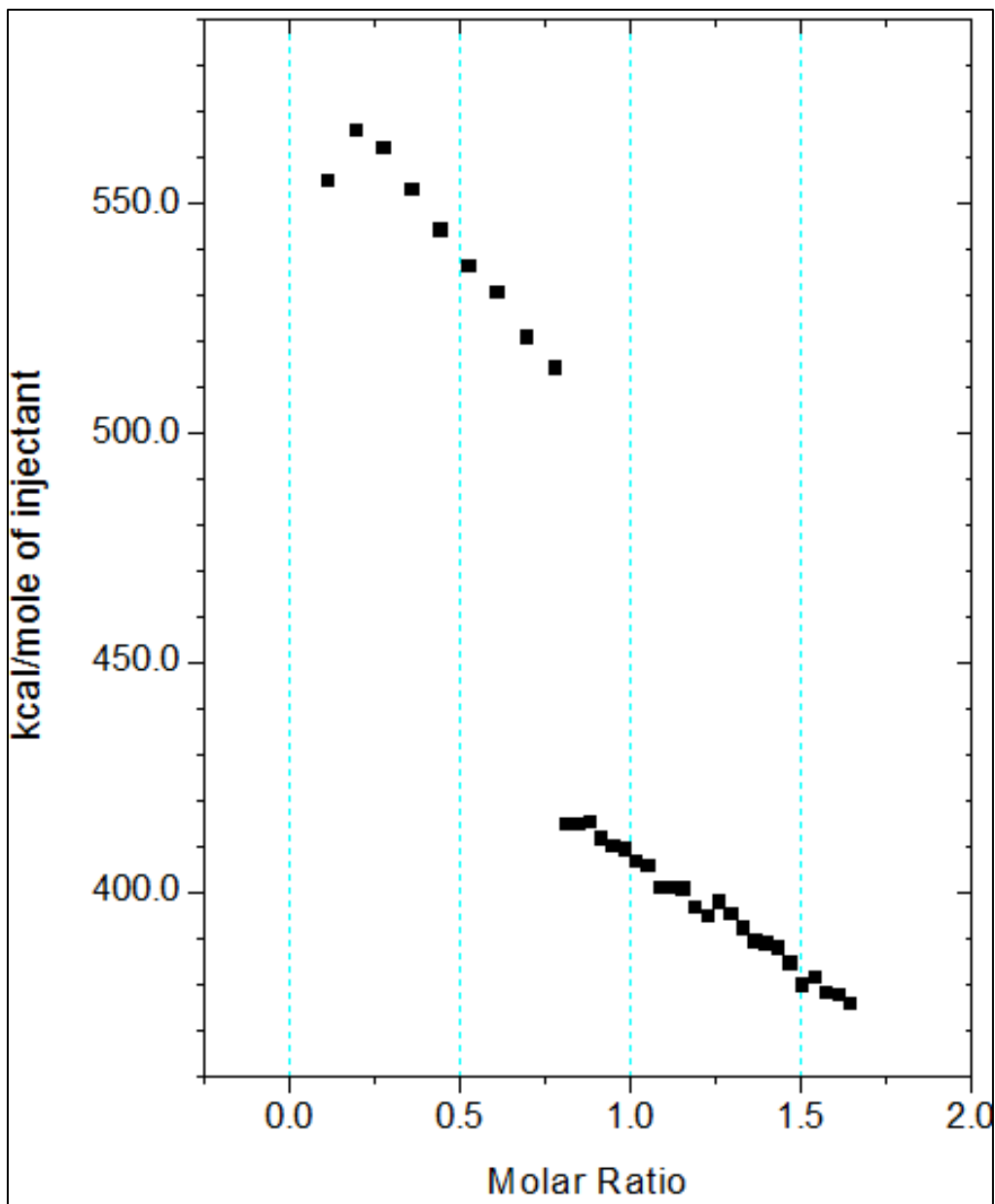


Figure 4.6 - Isotherm of Repeated 4a DNA Mango-TO1-3PEG in HEPES Buffer. The generated isotherm pertaining to the repeated 4a DNA Mango ITC titration experiment in which $250 \mu\text{M}$ TO1-3PEG was titrated into $15 \mu\text{M}$ 4a DNA Mango aptamer.

While the equilibrium dissociation constant for this experiment was found to be 0.100 mM, a comparable K_D to the previously conducted experiment, the presented isotherm illustrated a highly unexpected response, which made conclusive statements unreliable. The typical shape of an ITC isotherm was shown in Section 1.3 and illustrated a continuous response with “S-like” curvature. As illustrated above, there was an abrupt break in the titration data; therefore indicating a possible structural change. Considering the large errors and resulting equilibrium dissociation constants of these measurements, the ITC data was fitted to various other binding models; however, the fits failed on all accounts. It was hypothesized that the origin of the error lay in the structural heterogeneity of the DNA sequences, supported by the aforementioned disjointed ITC data. The hypothesis of structural heterogeneity was investigated by Native PAGE experiments, summarized in Chapter 5.

The endothermic peaks shown in Figure 4.1 were further investigated and it was considered that they were a result of an impurity in the TO1-3PEG, given a >95% purity by HPLC. Considering this can also be interpreted as <5% impurity, it was deemed possible that an impurity was not sublimed by the lyophilizer and had an endothermic heat of dilution larger than the exothermic heat of dilution of the aptamer-ligand binding interaction. To investigate this theory, a buffer-buffer experimental run was conducted, in which 100 μ M of the TO1-3PEG, diluted in HEPES buffer, was titrated into HEPES buffer. The goal of this experiment was to determine if an endothermic heat of dilution could be visualized via ITC – since it was previously concluded that the DMF content in solution did not impact the binding affinity of the ligand, an endothermic heat of dilution in this experiment would strongly suggest the presence of an impurity in the ligand solution. Inconsistent, however, with the aforementioned hypothesis was the following raw data, from which exothermic peaks can be observed in Figure 4.7.

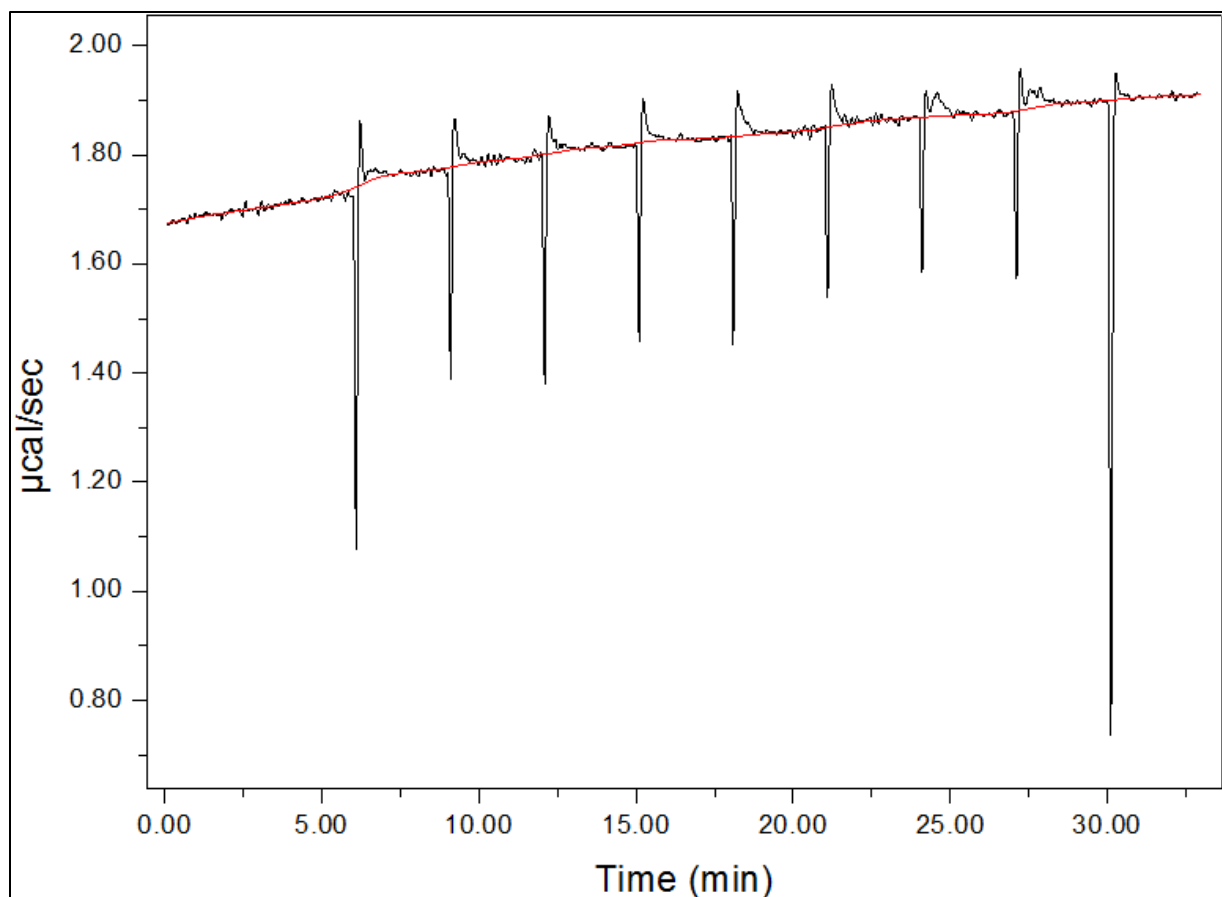


Figure 4.7 - Normalized Injection Heats of TO1-3PEG ITC Titration. The normalized injection heats pertaining to the titration of ligand (250 μM) into HEPES buffer.

Therefore, it was again concluded that the endothermic signal could not be attributed to the ligand. With three repeat experiments acting as evidence in support of a truly endothermic signal with a weak binding affinity, this was the accepted conclusion for this aptamer-ligand pair.

4.2 ITC Investigation on 6b DNA Mango Aptamer Sequence

The binding affinity of the 6b DNA Mango aptamer sequence to TO1-3PEG was investigated, similarly to that described in Section 3.1 for the 4a DNA aptamer. 300 μL of the 6b DNA Mango sequence in HEPES buffer (10 mM HEPES, 5 mM MgCl_2 , 100 mM KCl) was loaded into the sample cell of the ITC at a concentration of 15 μM . The ligand, also in HEPES buffer, was

loaded into the syringe at a concentration of 250 μM to be titrated into the cell. Figure 4.8 illustrates the normalized data pertaining to the aforementioned titration.

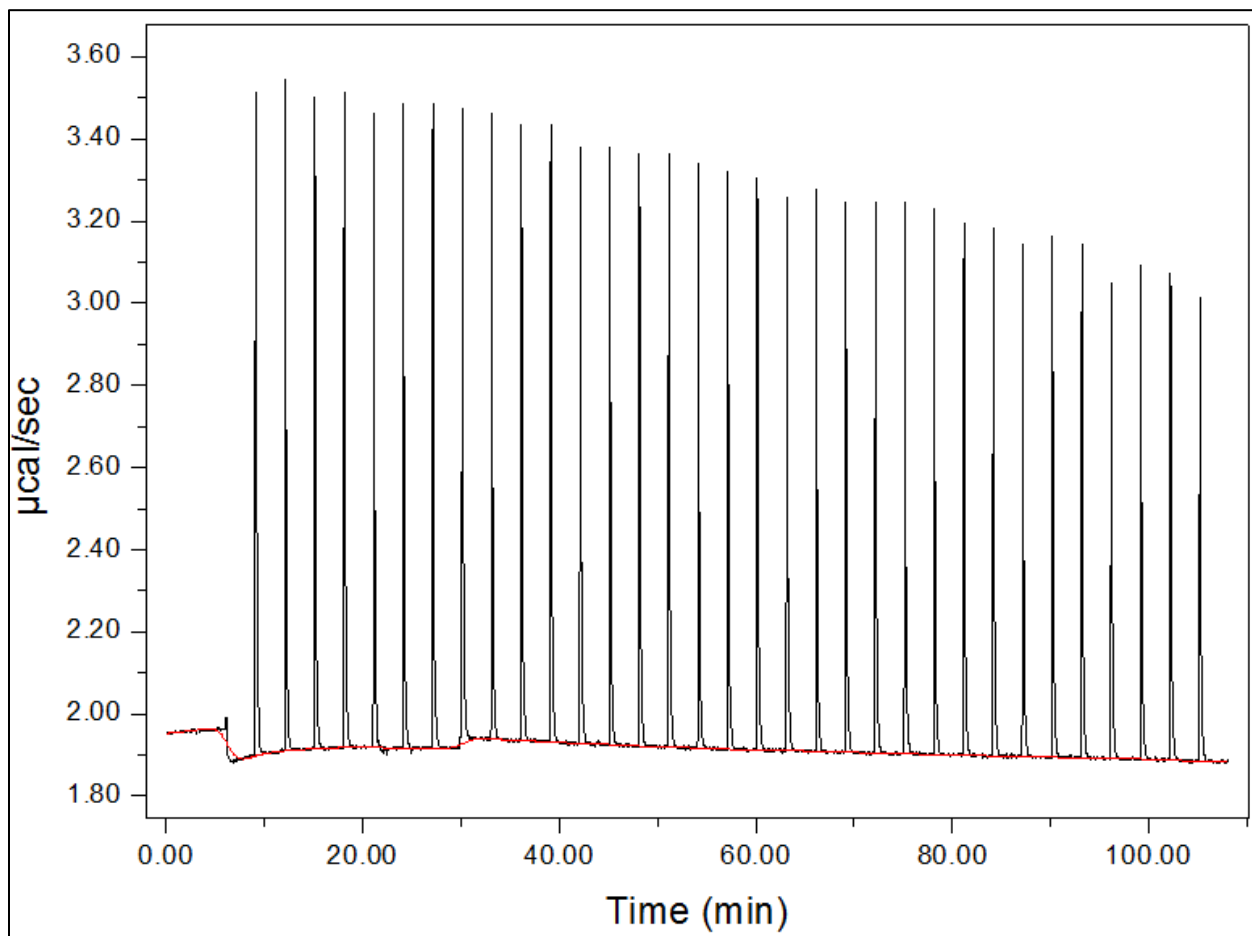


Figure 4.8 - Normalized Injection Heats of 6b DNA Mango Titration. The normalized injection heats resulting from the titration of TO1-3PEG (250 μM) into the 6b DNA Mango aptamer (15 μM).

Consistent with the data obtained for the 4a DNA Mango aptamer sequence were endothermic peaks. Also similar to the 4a sequence in HEPES buffer was the failure of the ITC to provide a reliable fit for the 6b DNA sequence under these conditions.

Despite the lack of evidence in the ITC data, the existence of multimeric conformations was considered. In order to determine whether the 6b DNA Mango aptamer sequence exists as a mixture of monomeric and multimeric conformations, a Native PAGE investigation was conducted, the results of which are discussed in Chapter 5.

4.3 ITC Investigation on 2a DNA Mango Aptamer Sequence

The binding affinity of the 2a DNA Mango aptamer sequence to TO1-3PEG was investigated, utilizing the same procedure as described for the 4a and 6b aptamers. Figure 4.9 illustrates the normalized injection heats for the 2a DNA Mango titration.

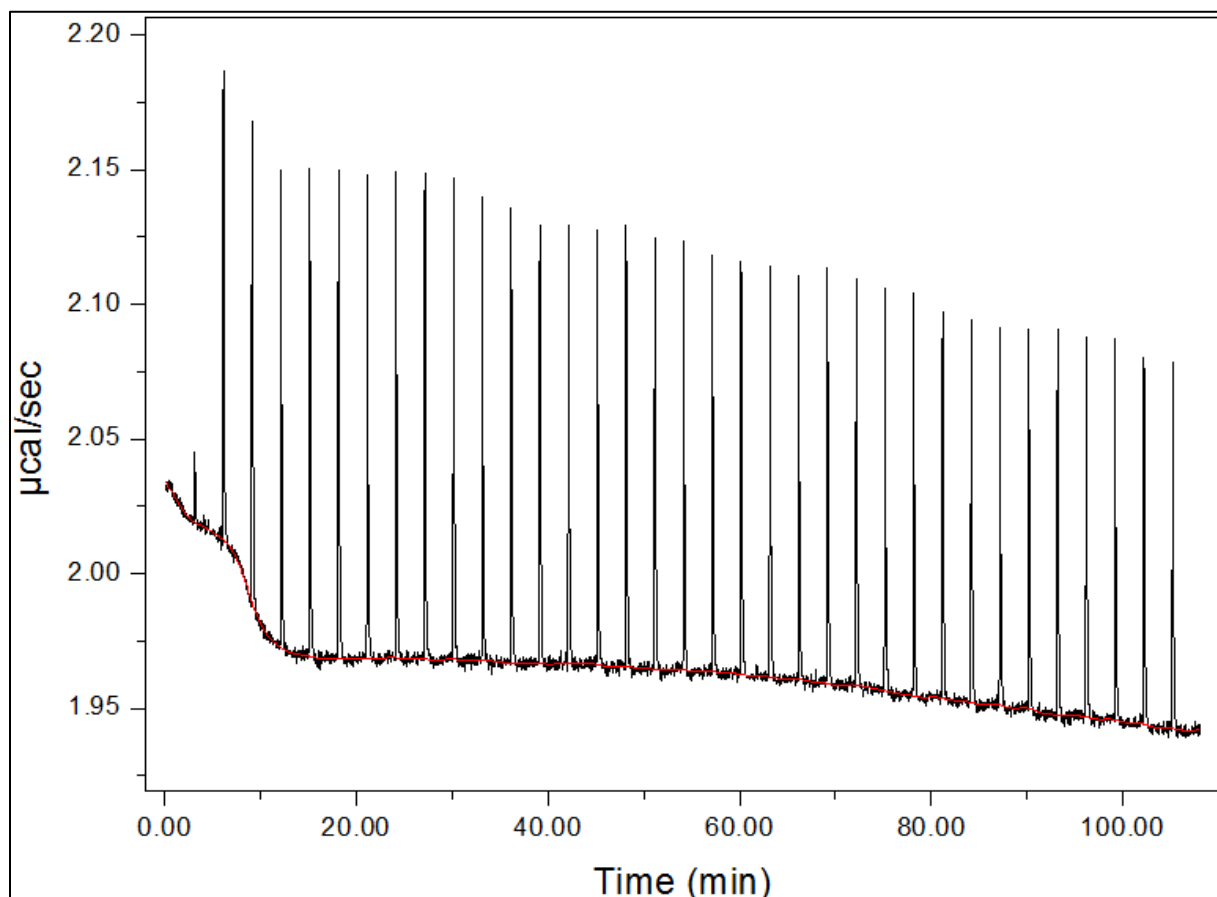


Figure 4.9 - Normalized Injection Heats of 2a DNA Mango Titration. Normalized injection heats resulting from titrating TO1-3EG (250 μM) into the 2a DNA Mango aptamer (15 μM).

As seen with both the 4a and 6b DNA aptamers, an endothermic heat signature was produced during the 2a DNA Mango titration.

As noted with the 6b DNA Mango aptamer sequence in HEPES buffer, the ITC failed to provide a reliable fit for the 2a sequence. To confirm these results, the experiment was repeated. The repeated data further supported the conclusion that the one site binding model by ITC was insufficient for 2a DNA Mango aptamer sequence under the proposed conditions. It was therefore concluded that ITC cannot be employed as an analytical method to measure binding between the aforementioned aptamer sequences and TO1-3PEG. It should be noted that this conclusion was in direct contradiction with the findings of fluorescence spectroscopy by Volition La. In La's investigation, he reported that the 2a DNA Mango aptamer was the highest binding affinity aptamer, with a documented K_D of 0.173 μM under fluorescence spectroscopy conditions. The disparity in the equilibrium dissociation constants made conclusions regarding the aptamer unreliable, but further supported da Costa's conclusions regarding the discrepancies in values obtained by different analytical approaches. Further investigation of the 2a aptamer would be required for more concrete conclusions.

4.4 ITC Conclusions

The binding affinity of 3 DNA Mango aptamers, 2a, 4a, and 6b, to TO1-3PEG was investigated via ITC. Table 4.2 summarizes the findings of this research.

Table 4.2 - ITC-Determined Equilibrium Dissociation Constants and Parameters

DNA Mango Sequence	K_A (M^{-1})	Error (M^{-1})	N (# Binding Sites)	K_D
4a (Sodium Phosphate Buffer)	1.04×10^5	3.27×10^4	2.57 +/- 0.161	9.71 μM
4a (HEPES buffer)	5.91×10^3	1.94×10^3	0.158 +/- 1.63	183 μM
6b (HEPES buffer)	1.97×10^3	5.41×10^3	0.353 +/- 24.1	N.D.
2a (HEPES buffer)	15.9	6.05×10^5	348 +/- 1.26×10^7	N.D.

The tightest-binding aptamer was determined to be the 4a DNA Mango aptamer in a sodium phosphate buffer. Despite this observation, the determined K_D of 9.71 μM was nonetheless indicative of very weak binding. The reported K_A and wide error margins pertaining to the 2a and 6b DNA Mango aptamers in HEPES buffer concluded that the ITC one-site binding model failed to fit the data; therefore, no equilibrium dissociation constant was evaluated.

It was also demonstrated in Table 4.2 that binding between the aptamers and the target ligand had a strong buffer dependence. Specifically, the sodium phosphate buffer provided an improved environment for binding under ITC conditions.

Chapter 5

Native PAGE

As outlined in Section 4.1.2, in order to confirm the presence of secondary structures, native PAGE experiments were conducted. A native PAGE is similar to the PAGE procedure outlined in 2.1.1; however, no urea is used in order to observe non-denatured nucleic acids. From a native gel, one can use a fluorescence imaging system to visualize the DNA conformations with the use of a comparative DNA ladder identifying base pairs. For this research a Low Molecular Weight (LMW) DNA Ladder was used from New England Biolabs. The DNA ladder included a loading dye at a concentration of 500 $\mu\text{g}/\text{mL}$ and is an adequate ladder for 25 to 766 base pairs.

5.1 4a DNA Mango Aptamer Investigation

The imaging system detected no fluorescence in the unstained Native PAGE, indicating that the dye did not comigrate down the gel with the DNA. The absence of a fluorescence further supported a very weak binding affinity of the aptamer to the ligand.

The gel was then placed in a container and stained with a 10 000 X SYBR Safe DNA gel stain (Invitrogen, Waltham, MA) diluted to a 1 X stain solution by diluting in a tris-borate-EDTA buffer. The container was covered with tinfoil and incubated in the SYBR safe solution at room temperature on a bench-top shaker at approximately 50 rpm. The gel was then visualized on the FluorChem FC2 Imaging System using the aforementioned green filter at 527 nm, and a blue filter on the DRC III Fiber Optic Light Source Illuminator (Schott, Mainz, Germany). Figure 5.1 shows the obtained image.

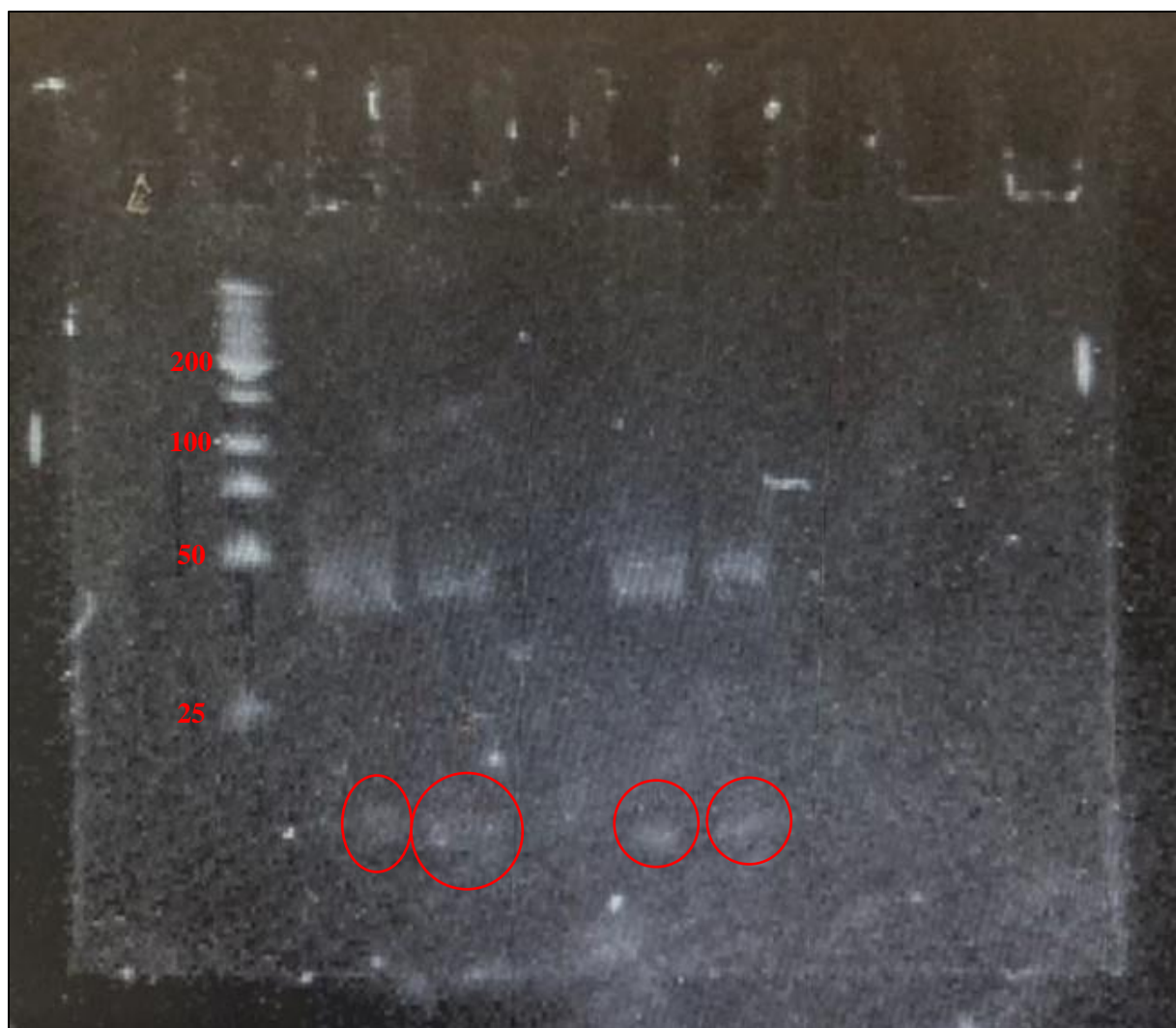


Figure 5.1 - SYBR Stained Native PAGE for 4a DNA Mango Visualization. 4a DNA Mango visualization obtained via the FluorChem Imaging System to determine the effect of annealing aptamer samples.

The native gel confirmed the presence of multiple conformations, given the existence of two bands per lane – one band slightly below the 50 base pairs (bp) marker indicated by the DNA ladder, and another faint band below 25 bp. Another observation was the presence of multiple multiplex structures, made most evident by the smearing in wells 2 and 5. The wells in which the DNA was annealed seemed to minimize smearing, indicating that the number of multiplex conformations had been reduced. Thus, it was concluded that all DNA samples should be annealed, and different methods by which the DNA samples could be annealed were explored.

5.1.1 Exploration of Annealing Methods

To determine the best annealing method for the 4a DNA Mango aptamer sequence, the annealing conditions outlined in Table 5.1 were explored with a native PAGE experiment.

Table 5.1- Well Contents of Native PAGE for Optimal Annealing Method Determination

Well	Conditions
1	DNA Ladder
2	DNA Not Annealed
3	DNA heated to 90 °C and cooled to 4°C on Eppendorf Vapo.Protect heating block
4	DNA heated to 90 °C on Eppendorf Vapo.Protect heating block and cooled to 25 °C
5	DNA heated to 90 °C on Eppendorf Vapo.Protect heating block and flash frozen in an ice bath
6	DNA heated to 90 °C in a water bath and cooled to 25 °C over 2 hours

Figure 5.2 was retrieved on the FluorChem FC2 Imaging System using a green filter (527 nm) and a blue filter on the DRC III Fiber Optic Light Source Illuminator (Schott, Mainz, Germany).

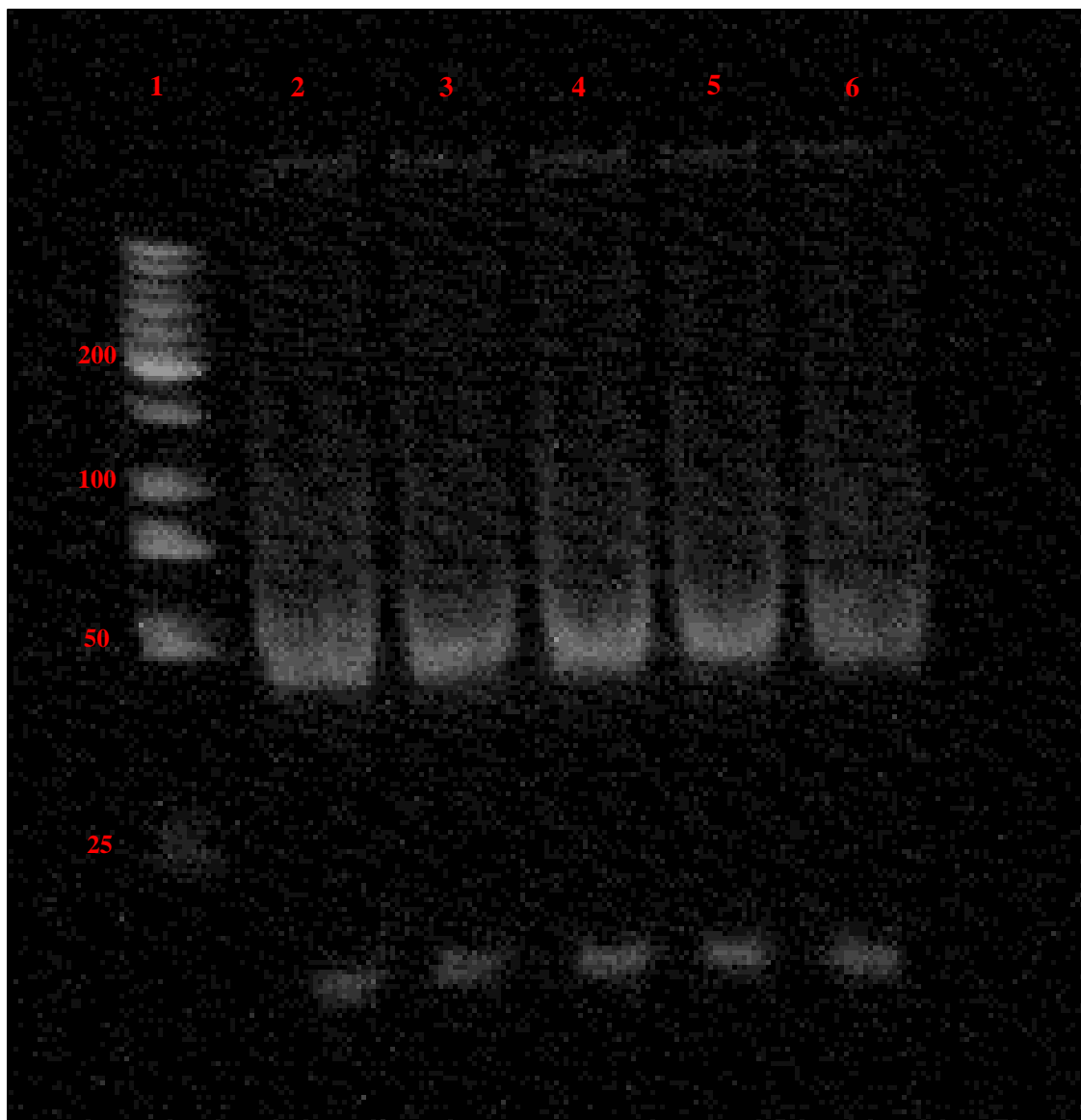


Figure 5.2 – SYBR Safe Stained Native PAGE for 4a DNA Mango Visualization. Aptamer visualization achieved via the FluorChem Imaging System to determine the optimal annealing method for aptamer samples.

The native PAGE experiment supported the two findings of the ITC experiments summarized in Chapter 4. More specifically, it was indisputably concluded that the 4a DNA Mango aptamer sequence existed in multiple conformations – a monomeric structure, indicated by the bottom bands of the native PAGE, and a multiplex, likely a duplex, indicated by the larger, smeared bands. It was also noted that the DNA ran as a single band on the denaturing gel, therefore

supporting the hypothesis of multiple conformations of the multimeric structure. This finding could act as evidence for the disjointed, incohesive ITC data obtained for this sequence in Section 4.1.2, supporting the hypothesis that the multiplex conformations inhibit preferential binding of the ligand to the monomeric structure. Furthermore, the 4a DNA Mango aptamer was the only aptamer evaluated by ITC that the one-site binding could characterize, and it was the only aptamer investigated by native PAGE with a monomeric structure. The 6b aptamer illustrated no presence of a monomeric structure via native PAGE and was uncharacterizable by the one-site binding model of the ITC. Considering the aforementioned observations, it was hypothesized that there is a necessity of a monomeric structure in order to reliably and accurately employ the one-site binding model of the ITC. Furthermore, this native PAGE experiment re-illustrated the reduction of multiple duplex conformations through annealing (wells 3 – 6); therefore reinforcing the need for annealing.

In addition to supporting the findings of Section 4.1.2., the native PAGE experiment also aided in confirming the most optimal annealing method. By comparing the wells in which DNA samples were annealed, it was observed that wells 3 – 5 exhibited brighter, more defined bands, indicating a higher concentration of a single conformation, as opposed to well 6, in which the band was dull and displayed increased smearing, indicating lower concentrations of multiple conformations. Therefore, it was concluded that a faster cooling process was a more favorable approach to annealing to obtain increasingly defined DNA conformations.

5.2 6b DNA Mango Aptamer Investigation

A native PAGE experiment was conducted on the 6b DNA Mango aptamer sequence, following the procedure described in Section 2.8. Figure 5.3 illustrates the SYBR stained native gel retrieved from the FluorChem FC2 Imaging System.

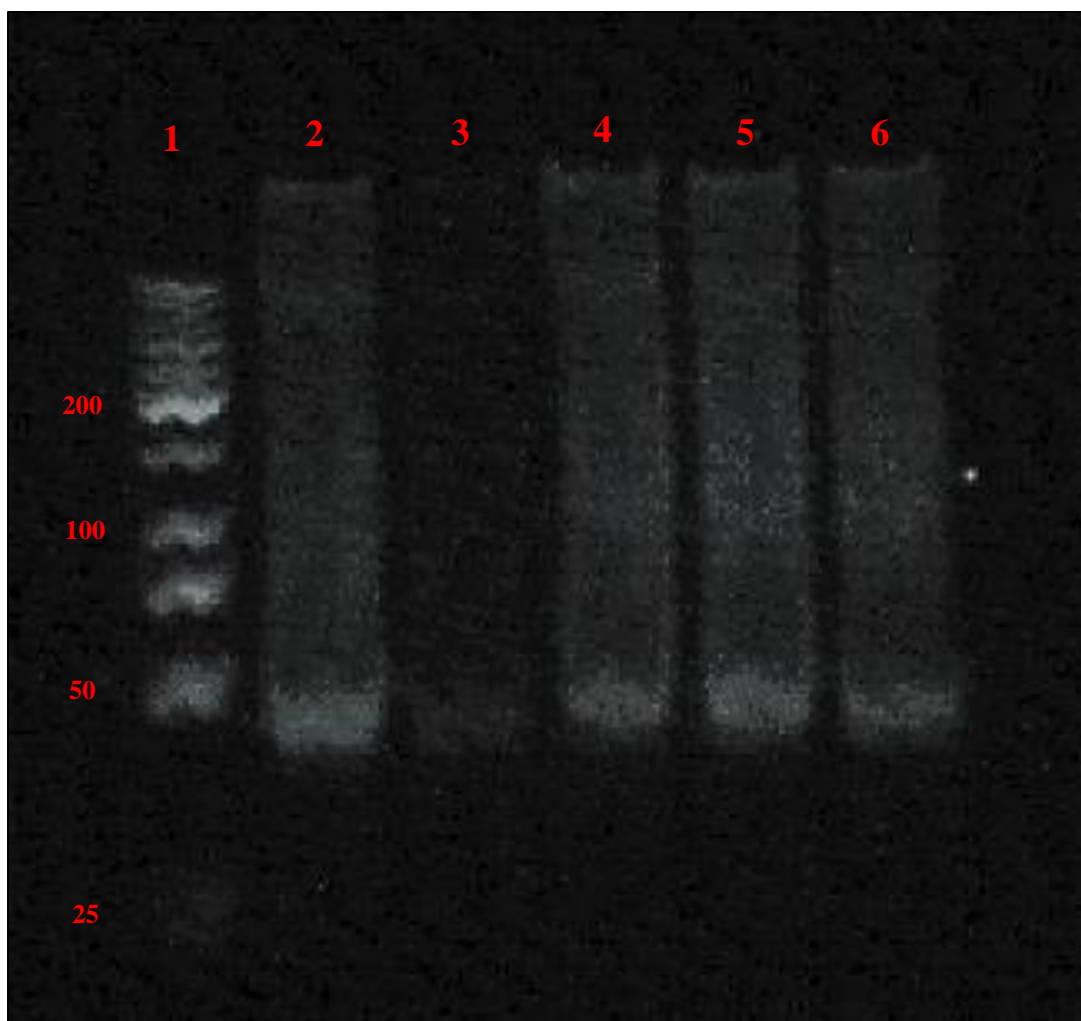


Figure 5.3 – SYBR Safe Stained Native PAGE for 6b DNA Mango Visualization. SYBR Safe Stained Native PAGE to determine the optimal annealing method for the 6b DNA Mango aptamer.

In contrast to the native PAGE experiment pertaining to the 4a DNA Mango aptamer sequence, the 6b native PAGE lacked any indication of multiple conformations. More specifically, while the migration of DNA through a native PAGE is largely dependent on structural properties, the image suggested the existence of the DNA sequence in a single conformation, considering the single band present at the 50 bp DNA ladder marker. Moreover, comparing the size of the band, as well as the smearing, to that seen in the 4a sequence native PAGE, it was concluded that the band was indicative of duplex conformations with multiple oligomer associations. This conclusion supported the weak binding affinity findings of the ITC experiments detailed in Section 4.2.

5.3 Native PAGE Conclusions

In Chapter 5, different methods of annealing were investigated to determine the optimal annealing method to reduce structural variation of the DNA aptamer sequences. The unstained native PAGE of the 4a investigation illustrated that the ligand did not bind to the aptamer, therefore migrating off the gel and undetectable by the FluorChem FC2 Imaging System. The stained native PAGE containing the 4a sequence indicated that a fast-cooling method was the most optimal annealing method. Specifically, wells 4, 5, and 6, in which the DNA was heated to 90 °C and then cooled quickly to various temperatures yielded the highest concentrations of the DNA aptamer in a single conformation (as indicated by the bright, condensed bands). Wells 1 and 6, in which the DNA was not annealed or cooled slowly, respectively, demonstrated increased smearing and dull bands, indicative of structural heterogeneity. Annealing, despite improving the existence of configurational heterogeneity, did not eliminate it entirely.

Additionally, it was determined via the 4a native PAGE investigation that the aptamer existed in multiple conformations, indicated by the presence of bands of different molecular weights. The small bands at the bottom of the gel pertained to a monomeric structure of the sequence, while the smeared bands indicated a secondary structure, likely a duplex with structural heterogeneity, and therefore acted as supporting evidence for the discontinuous ITC data summarized in Section 4.1.2.

Lastly, the 6b native PAGE investigation also acted as supporting evidence to the ITC findings for the aptamer. Specifically, the significant smearing of the 6b DNA aptamer, despite annealing, was indicative of duplex conformations with structural heterogeneity, a structural factor that would influence weaker binding between the aptamer and the target ligand. Furthermore, as previously mentioned, the native PAGE pertaining to the 6b aptamer showed no indication of a monomeric structure. Since this aptamer was uncharacterizable by the one-site binding model of

the ITC, it was hypothesized that there is a necessity for a monomeric structure in order to employ this analytical instrumentation method.

Considering the aforementioned hypothesis, it could be further evaluated that the ITC investigation was limited by the experimental parameters of the instrumentation methods. Specifically, in order to conduct ITC experiments, the concentrations of the contents of sample cell and reference cell must be accurately determined. In considering that monomeric structures might be required for the reliable employment of the one-site binding model, the presence of multimeric structures in both the 4a and 6b sequences brought into question the determined concentration – the calculated concentration pertained to the total concentration of the aptamer in all conformations (monomeric and multimeric), suggesting that the concentration of the monomeric conformation of the 4a aptamer was significantly lower; therefore acting as a source of error for the ITC investigation.

Chapter 6

Surface Plasmon Resonance

Localized Surface Plasmon Resonance (LSPR) is a form of SPR that also measures the shift in resonance angle upon the binding of an analyte to the sensor surface or immobilized target molecule; however, it has advantageous properties in comparison to SPR, such as a decreased cost of operation and less complex hardware. The following chapter will discuss the use of LSPR, used in Nicoya's OpenSPR system, as an analytical instrument to determine the equilibrium dissociation constant between the target ligand, TO1-3PEG biotin fluorophore, immobilized on the sensor surface, and DNA Mango aptamers, 4a and 6b. The system will also be used to investigate the binding of Hoechst DNA sequences to form a duplex, as well as the RNA Mango aptamer, the aptamer that was originally selected for the thiazole orange derivative ligand. Materials and methods utilized in this Chapter were summarized in Section 2.1-2.5.

6.1 Non-specific Binding Experiments

Non-specific binding is the binding of the analyte to molecules on the sensor surface other than the target molecule. NSB occurs between the analyte and sensor surface and is caused by molecular forces such as electrostatic interactions, hydrogen bonding, hydrophobic interactions, or Van der Waals interactions⁹⁶. The occurrence of NSB can be attributed to several factors, such as a conformational alteration of the ligand during immobilization, or biomolecular coating on the surface of the sensor. The effect of NSB is a "false positive contribution to the signal in a sensorgram".⁹⁶ NSB can be reduced, or eliminated entirely, by changing the pH of the buffer, or by implementing surfactants or blocking proteins in the experimental conditions. In order to better understand the interactions that occur during a binding experiment using the OpenSPR system, various sequences and buffer conditions were explored. In this investigation, 6b and the Hoechst

DNA sequences were examined, and alternative buffers were investigated to determine the conditions most optimal for reducing NSB and providing a distinct binding signature to the immobilized target. Buffers C-K, as described in Section 2.2.2, were used.

A high salt content buffer was investigated in this research, as high salt is known to decrease electrostatic interactions. Specifically, salt ions reduce, but not eliminate entirely, electrostatic effects in charged systems by generating a “shielding effect” on the analyte.⁹⁶ In this research, the electrostatic interactions to which we aimed to reduce occur between the positively charged biotin-avidin complex and the negatively charged DNA. The initial selection buffer (Buffer A) contained a total salt content of 250 mM, which was increased to 610 mM by increasing the concentration of potassium chloride to 600 mM (Buffer C). Alternatively, the potassium chloride was entirely replaced by sodium chloride, another monovalent salt, to a final concentration of 610 mM (Buffer B). In addition to the monovalent salts, magnesium chloride, a divalent salt, has also been explored as a necessary salt in buffer for DNA/RNA-ligand binding systems.

Buffer D contained 0.5% Tween 20. Tween 20 is a non-ionic surfactant that disrupts hydrophobic interactions that can occur between the analyte and the sensor surface. The detergent can also prevent the binding of the analyte to the tubing of the instrument.⁹⁶ This condition, implemented by Dolgosheina *et al.* in their investigation of RNA Mango for fluorescent labeling at 0.05%, seemed appealing for utilization in this research.^{59,96}

Buffer E contained 0.1% bovine serum albumin (BSA), a protein blocker. BSA can act as a shield for the analyte to protect it from non-specific interactions such as protein-protein, charged surfaces, and glass and plastic surfaces.⁹⁶ Similarly, human serum albumin (HSA) was also investigated as a protein blocker to reduce NSB, in a 0.5% w/v. The last buffer condition to

examine was an alternative pH, specifically, a slightly acidic pH. Buffer G was adjusted to pH 6.5 using HCl.

In addition to adjusting the conditions of the sodium phosphate buffers, two HEPES buffers were explored – a HEPES buffer with 300 mM KCl (Buffer H) and a HEPES buffer with 300 mM KCl and 0.5% BSA (Buffer I). By comparing the data obtained from the HEPES buffers with the data obtained from phosphate buffers, the most optimal buffer, the nonspecific interactions occurring during binding could be identified; therefore allowing for the most optimal buffer to be exploited in further research.

6.1.1 6b DNA Mango Nonspecific Binding Experiment

The first NSB investigation utilized sequence 6b, and explored buffers A and C–G. A streptavidin sensor was prepared as described in Section 2.1.2, and the instrument was primed with Buffer A (the RB). The system was then washed with injections of IPA and glycine HCl. A streptavidin aliquot was injected to create the biotin-streptavidin sensor surface required binding experiments. Figure 6.1 was created in TraceDrawer, a SPR software for processing the real-time experimental data, and shows the response signal that was generated upon the injection.

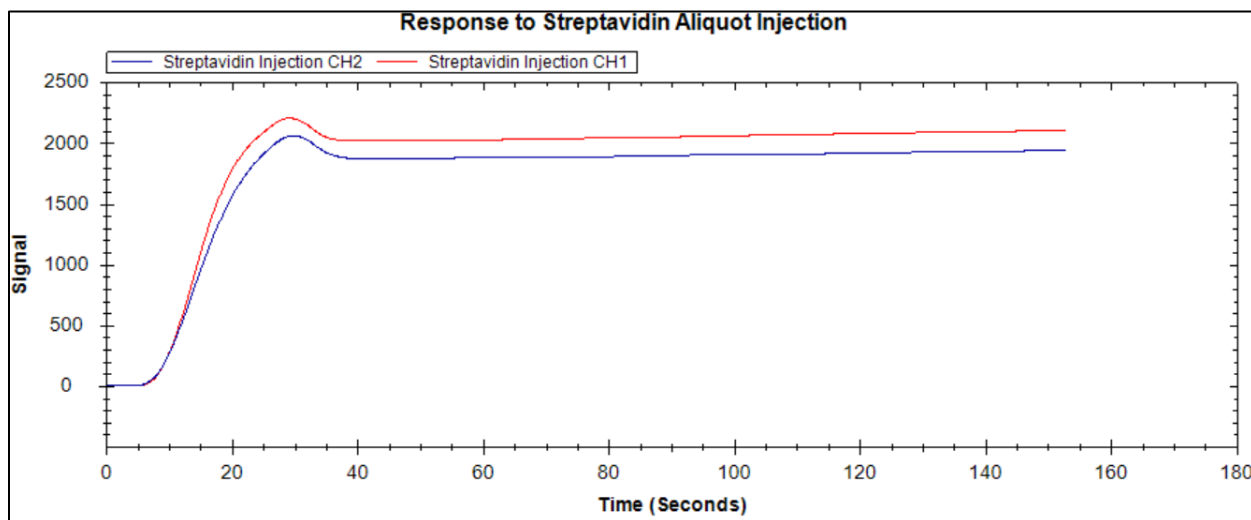
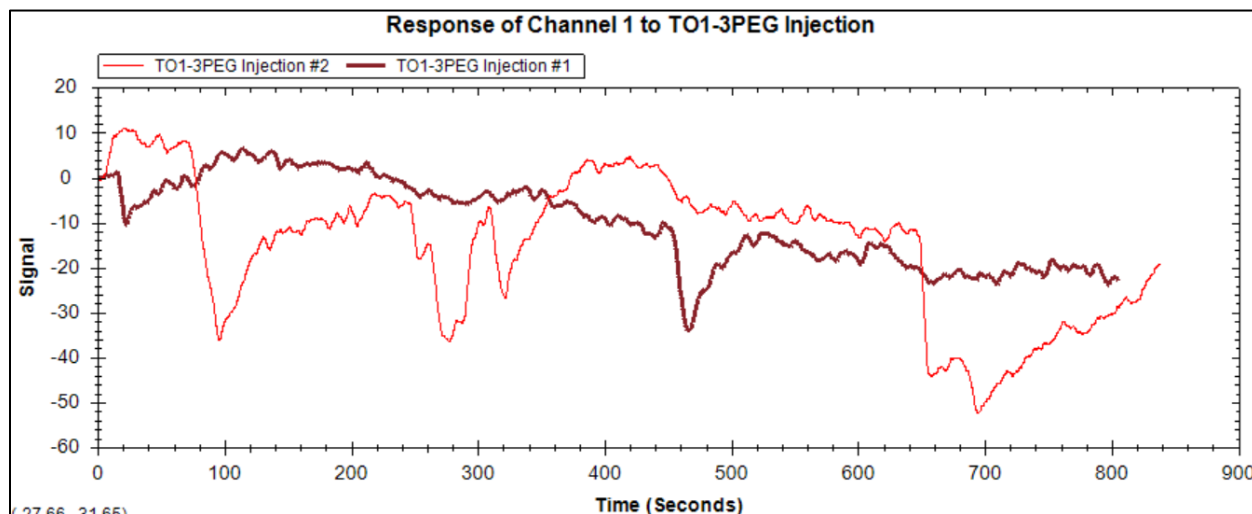


Figure 6.1 - Response to Streptavidin Aliquot Injection. To prepare the biotin-streptavidin sensor surface, a streptavidin aliquot is injected through the microfluidic channel. The increase in

response (~2200 R.U.), along with the newly achieved baseline, is indicative of a successfully prepared sensor surface.

The large positive response signal observed in both channels indicated that the streptavidin had been successfully immobilized on the surface of the biotin sensor chip. Channel 1 was then closed, so subsequent injections only flowed through Channel 2. 200 μL of the TO1-3PEG-Biotin Fluorophore was injected (5 μM) into Channel 2 at a flow rate of 150 $\mu\text{L}/\text{min}$. This is known as the control channel – channel 1 contained the bare sensor surface with only avidin, and channel 2 contained the immobilized biotinylated dye; therefore allowing for the observation of non-specific binding to the sensor surface, or specific binding to the ligand, respectively. Figure 5.2 displays the response of both channels to this injection – 6.2a illustrates the response from channel 1, while 6.2b illustrates the response from channel 2.



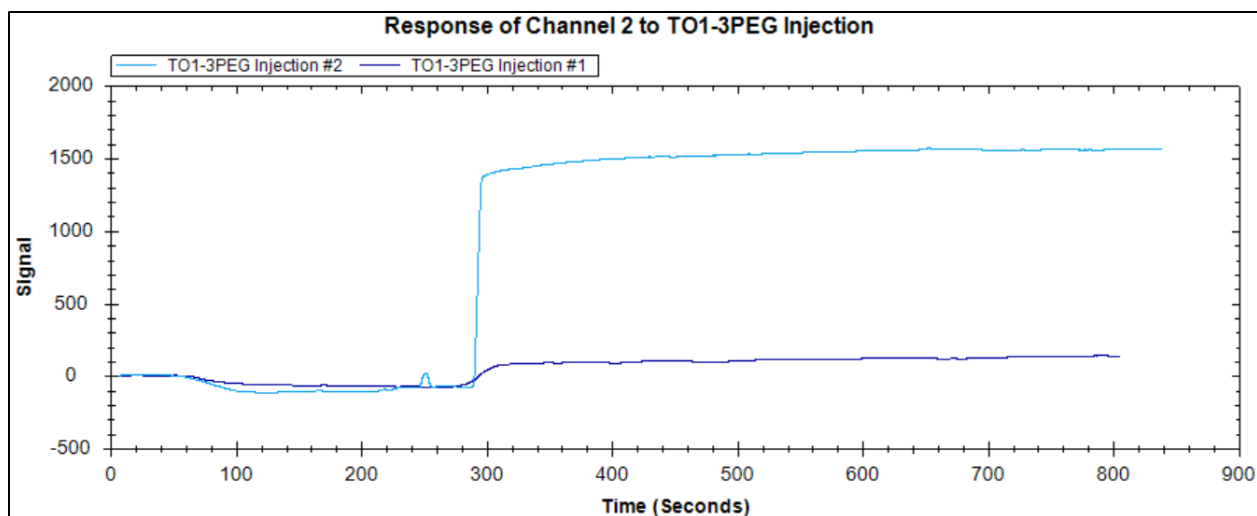
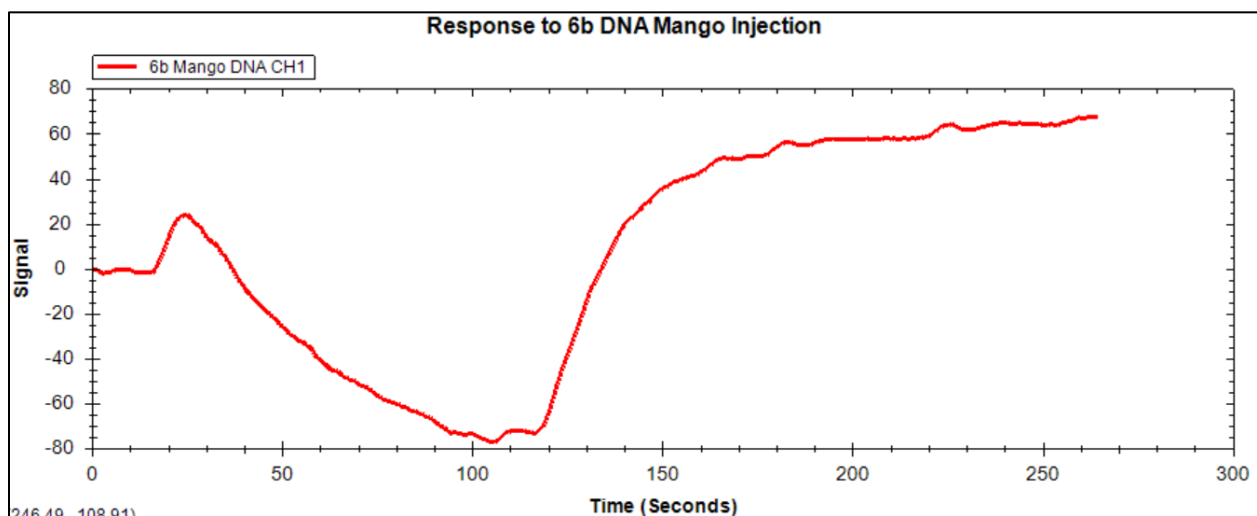


Figure 6.2 - Response of Channel 1 and Channel 2 to TO1-3PEG Injections. To ensure that the control channel successfully generated, the response from each channel of the OpenSPR system is monitored. Channel 1 shows no response indicative of binding, while channel 2 shows an increase in the response (~1500 R.U.) after the second ligand injection.

Evident from Figure 5.2, was the successful ligand binding in Channel 2 only. Once the ligand was successfully immobilized, channel 1 was re-opened. The flowrate was decreased to 40 $\mu\text{L}/\text{min}$, and the baseline was allowed to stabilize. An injection of DNA sequence 6b was then completed in Buffer A, and the response in both channels was monitored (Figure 6.3) – a response in Channel 1 indicated NSB to the sensor surface, whereas a response in Channel 2 demonstrated specific binding to the immobilized target ligand.



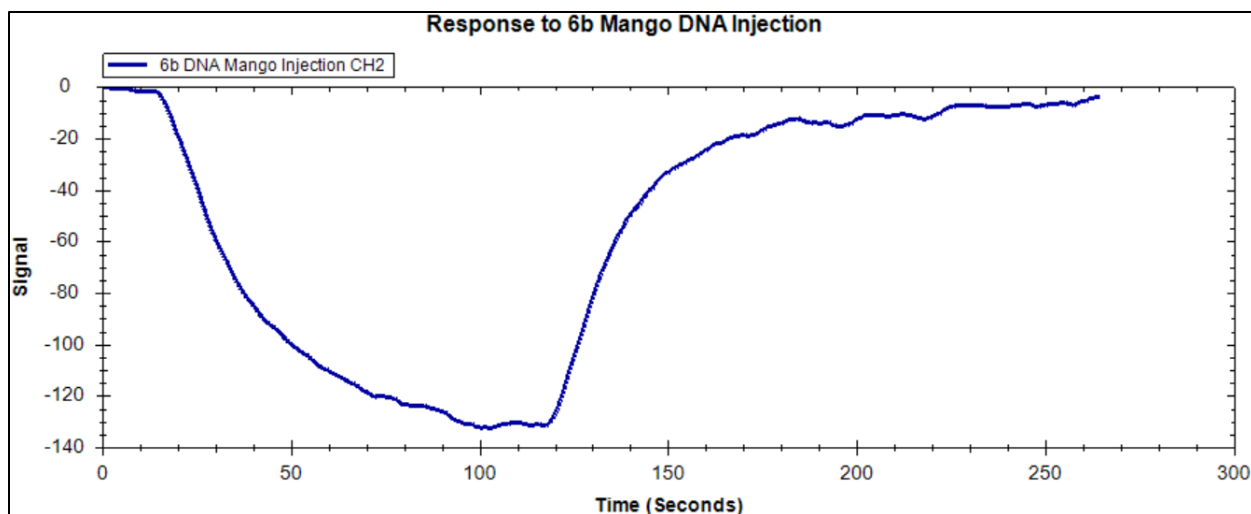


Figure 6.3 - Response of Channel 1 and Channel 2 to 6b DNA Mango Injection. The response signal produced in Channel 1 (red) and Channel 2 (blue) to the 6b DNA Mango aptamer injection.

The decrease in signal observed in both channels brought into question the optical properties of the fluorophore. Specifically, the SPR is extremely sensitive to changes in refractive indices, which can result in negative signals. Figure 5.3 revealed an inverted binding signal, which indicated that the refractive index had been altered or disrupted in some capacity, resulting in the negative signal upon binding between the aptamer and ligand. One proposed hypothesis for this inverted signal was the interference of the ligand with the operational wavelengths of the SPR. Specifically, the ligand system absorbs and emits in the operational wavelength of the SPR, and therefore could have induced alterations to the refractive index such that binding between the aptamer and the target ligand was inverted. Alternatively, TO1-3PEG is highly sensitive to environmental effects, such that perhaps the immobilized ligand behaves differently than in solution. Specifically, it can be hypothesized that steric issues were induced upon immobilization to the streptavidin sensor, such that the ligand conformation was adjusted, in turn interfering with the interaction with the DNA aptamer. Despite the aforementioned considerations, the corrected signal for the injection of the DNA aptamer was obtained (Figure 6.4) – the response from Channel

1 was subtracted from the response in Channel 2, thus eliminating the response pertaining to NSB, and revealing the binding response, if any, of the DNA-ligand interaction.

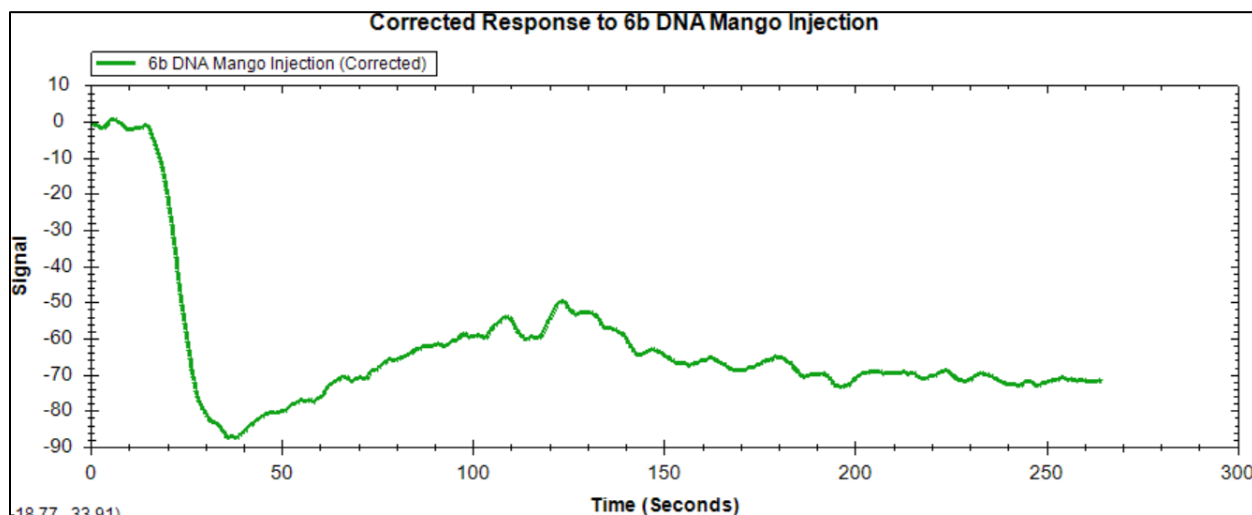


Figure 6.4 - Corrected Response to 6b DNA Mango Injection. The corrected response is obtained by subtracting the response of channel 1 (NSB) from channel 2 (specific binding), to obtain the true signal of the binding interaction.

Evident from the corrected signal was the appearance of an inverted association curve, which indicated that while a typical binding curve was not achieved, some interaction had occurred upon the injection of the aptamer.

Once the injection was completed, the system was switched to Buffer C, a high salt buffer. Injections of 10 mM glycine HCl (pH 2.3) were then performed until a stable baseline was achieved, indicating a successful sensor regeneration. A 6b DNA Mango aptamer sample in the corresponding buffer was injected into Channel 1 and 2. The response of the channels to the DNA injection are depicted in Figure 6.5.

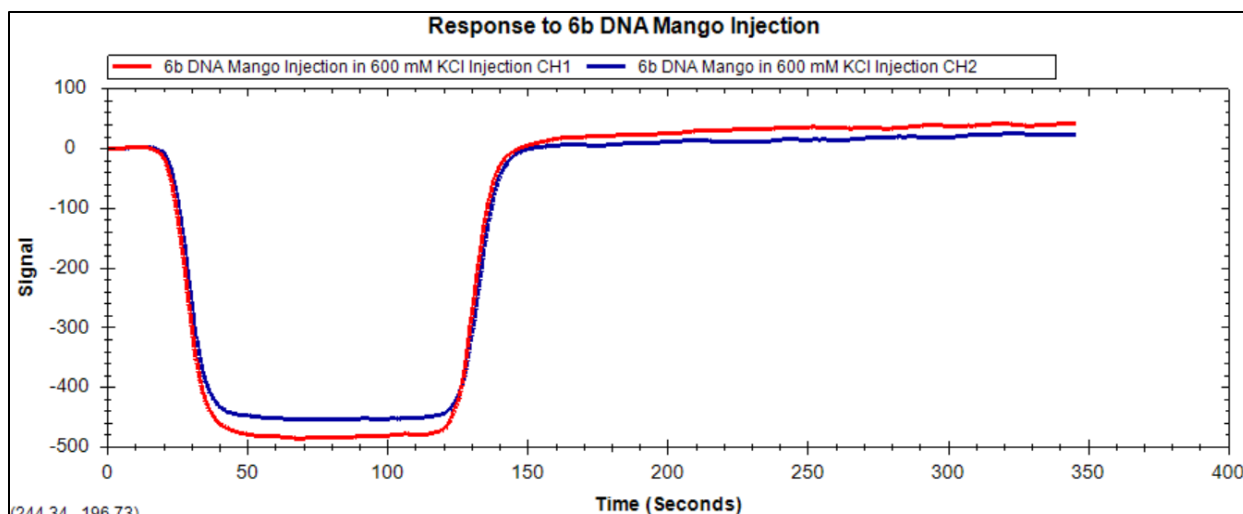


Figure 6.5 - Response of Channel 1 and Channel 2 to 6b DNA Mango Injection in High Salt Buffer. The direct comparison of the response of channel 1 (red) and channel 2 (blue) to the 6b DNA Mango injection in high salt (600 mM KCl) is demonstrated to determine if specific binding of the aptamer to the ligand occurred.

The response observed in both channels was deemed a bulk shift. A bulk shift occurs due to a difference in the refractive index between the analyte buffer and the running buffer and is made evident from the square-like shape of the response curve. The occurrence of bulk shifts made for difficulty with data interpretation for optimal buffer conditions; therefore, the effect of the high salt buffer on the binding capability of the system was inconclusive.

The process of switching buffers and injecting the DNA samples was continued until all buffers had been tested. Buffers D, F, and G were explored during this SPR experiment, the responses to which are summarized in Figures 6.6a, 6.6b and 6.6c, respectively.

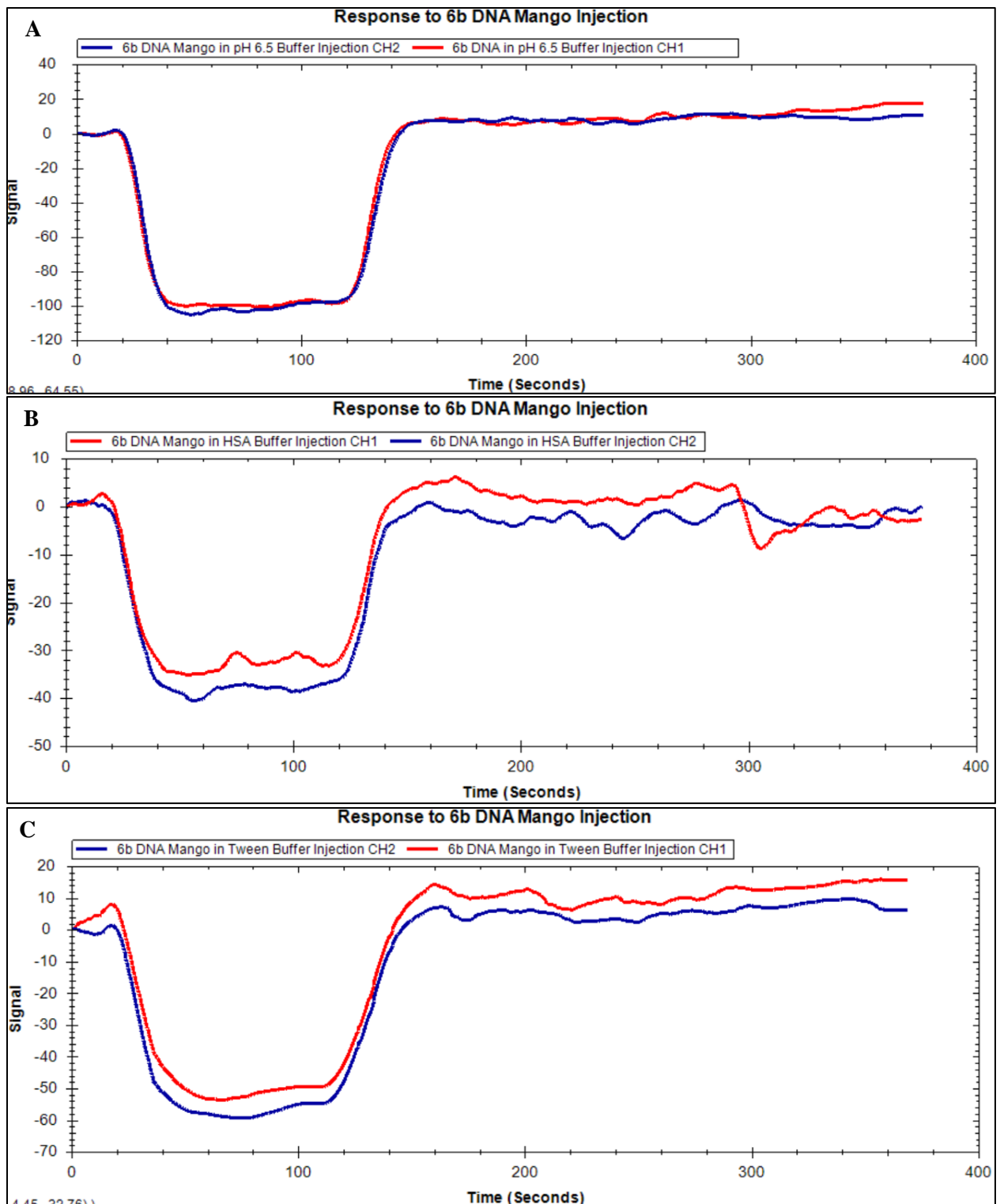


Figure 6.6 - Response of Channel 1 and Channel 2 to Various 6b DNA Mango Injections. The direct comparison of the response in channel 1 (red) and channel 2 (blue) to the 6b DNA Mango injections in various buffers (A: pH 6.5; B: 0.5% HSA; C: 0.5% Tween) is demonstrated to determine if the buffer conditions improve specific binding of the aptamer to the ligand.

The injection of the 6b DNA Mango aptamer in pH 6.5 buffer (Buffer G) showed identical responses in both channels, both of which had a curvature indicative of a bulk shift. Again, while bulk shifts make data interpretation difficult, it was nonetheless concluded that this buffer was not optimal for this system, given the absence of a reduced signal response in Channel 1. Similarly, the response to the injection of the 6b DNA Mango in an HSA-containing buffer (Buffer F) was also expressed a bulk shift-like signature, so the same conclusion was drawn. Lastly, although the injection of DNA in a tween-containing buffer (Buffer D) illustrated a semi-square like curve characteristic of a bulk shift, it was the only other explored condition that perhaps had a minor resemblance to a binding curve.

Despite the challenging data interpretation, it was observed that the Tween-containing buffer and the HSA-containing buffer provided a positive effect at reducing NSB that might have been present, although masked by the bulk shift. Specifically, the scale of the y-axis pertaining to the two surfactant-containing buffers was significantly decreased in comparison to the high salt concentration buffer. Furthermore, the response of channel 1 to the DNA aptamer injection under either of these conditions was lower than the response observed in channel 2, indicating that nonspecific binding between the aptamer and the sensor surface had been reduced.

It was therefore concluded that the two-surfactant containing buffers did, in fact, provide a positive effect at reducing NSB; however, further investigation is required to confirm this conclusion. Unfortunately, reduced pH buffer and the high salt concentration buffer did not optimize binding between the 6b DNA Mango aptamer and the TO1-3PEG biotin fluorophore.

6.1.2 Hoechst DNA

The NSB experiments were then continued with the Hoechst DNA sequences. The purpose of this research was to employ a double stranded DNA system that contained the binding site for

its target ligand as a test case for proof of concept of detectable binding via SPR. Additionally, this research aimed to identify whether the NSB was a result of hydrophobic or electrostatic interactions. Initially, the binding between a biotinylated Hoechst DNA strand and a non-biotinylated complementary Hoechst DNA strand to form double-stranded DNA was investigated as a test case for proof-of-concept. The Hoechst1-bt sequence was immobilized on the streptavidin-prepared sensor surface, followed by injections of the Hoechst2 sequence; however, based on experimental results, it was hypothesized that the orientation of binding between the two sequences was not detectable by the OpenSPR given the dimension of binding. Specifically, when the phenomenon of surface plasmons occur upon binding, as described in Section 1.5, a plasmonic wave is generated on the surface of the gold nanoparticles of the sensor chip. The electric field of the plasmonic wave extends hundreds of nanometers into the solution flowing through the microfluidic system above the surface of the sensor. The reflected light will have a significant decrease in intensity at a certain angle, which is measured at the detector. While the immobilization of the Hoechst1-bt strand to the streptavidin-prepared surface would create surface plasmons, and subsequently plasmonic waves extending into the analyte solution flowing above the microfluidic system which can be detected by the OpenSPR system, the second Hoechst strand, Hoechst2, would not further contribute to surface plasmons. Specifically, the Hoechst 2 strand is of equivalent base pairs to the biotinylated Hoechst strand and would therefore not further extend the plasmonic wave into the solution flowing through the microfluidic system. Figure 6.7 illustrates the response observed in both channels to the injection of the DNA strands, as well as corrected response.

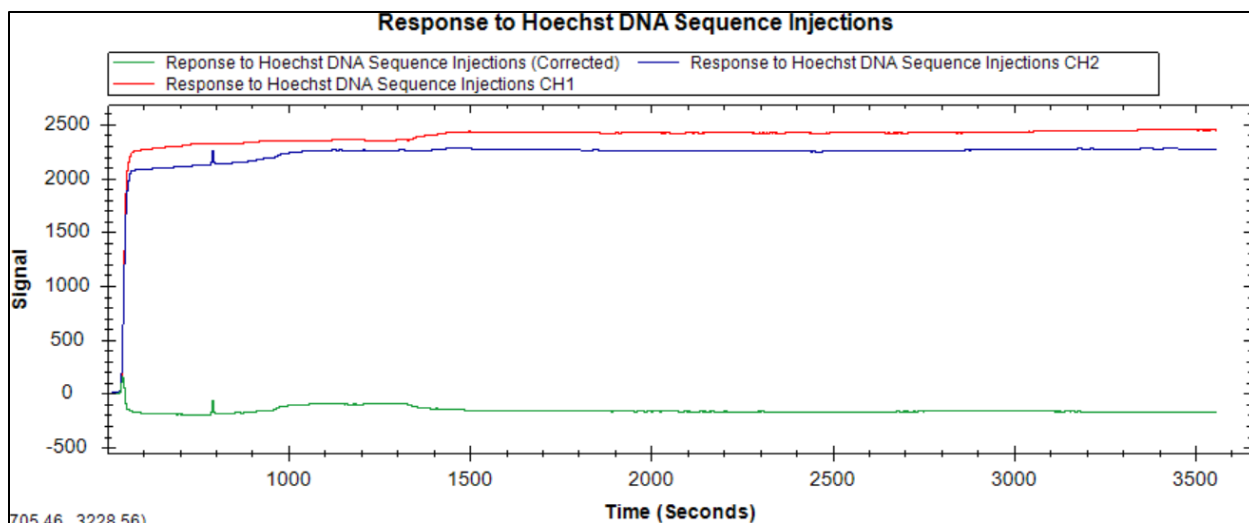


Figure 6.7 - Channel 1, Channel 2, and Corrected Signal for Hoechst DNA Injections. The channel 1 (red), channel 2 (blue) and corrected (green) response to the injection of the Hoechst DNA sequence.

The injection of the biotinylated Hoechst DNA strand occurred at 833.44 s. The corrected signal shows a response to this injection. The duplex strand, however, was injected at 1300.0 s, for which no response was observed in the corrected signal, indicating that the binding of the second strand was not detected by the SPR.

In order to investigate the hypothesis that the directionality of binding was not sufficient for detection by the SPR, a Hoechst DNA hairpin sequence was employed to bind to the immobilized biotinylated strand, as this should have increased the size of the complex, which should have resulted in detectable binding. The response to the biotinylated sequence injections and the hairpin sequence injections are depicted in Figure 6.8.

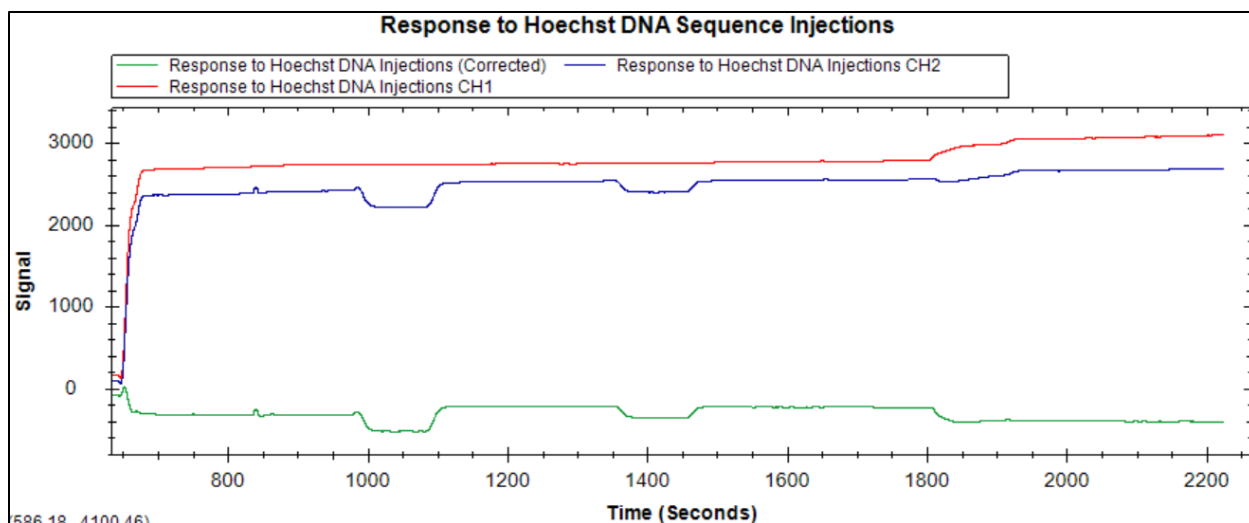


Figure 6.8 - Response to Biotinylated Hoechst DNA and Hoechst Hairpin DNA Injections. The channel 1 (red), channel 2 (blue) and corrected (green) response to the biotinylated and hairpin Hoechst DNA sequence injections.

The biotinylated sequence was injected twice during this investigation in order to maximize its immobilization (959.50 s, 1330.51 s). While the standard depiction of successful binding was not evident for the aforementioned injections, an increase in the baseline after each injection was noted; therefore indicating that the biotinylated strand had been immobilized to some degree. The hairpin sequence was injected at 1787.68 s, to which both channels responded. The corrected signal illustrated what appeared to be the association of the hairpin sequence; however, a dissociation was not observed. This likely indicated that the hairpin sequence successfully bound to the biotinylated Hoechst DNA strand with such strength that a dissociation had not occurred in the allotted time. Alternatively, the response to the hairpin sequence injection was not indicative of binding. Given the known strength of binding between the Hoechst DNA strands, the response visualized in the sensorgram was severely lacking in evidence to support the use of SPR for determination of binding parameters.

6.1.3 RNA Mango Aptamer

With the Hoechst DNA system failing to produce concrete results, an aptamer-ligand pair known to bind was subjected to SPR analysis. Specifically, the RNA Mango aptamer, the aptamer originally selected for the TO1-3PEG target, was employed for SPR experimentation. This was done in order to confirm that the OpenSPR system could be used for biochemical characterization of fluorophore-binding nucleic acids, but also to fully grasp the effects of the investigated buffer conditions. To first demonstrate proof of concept, successful binding of the aptamer to the immobilized ligand was confirmed (Figure 6.9).

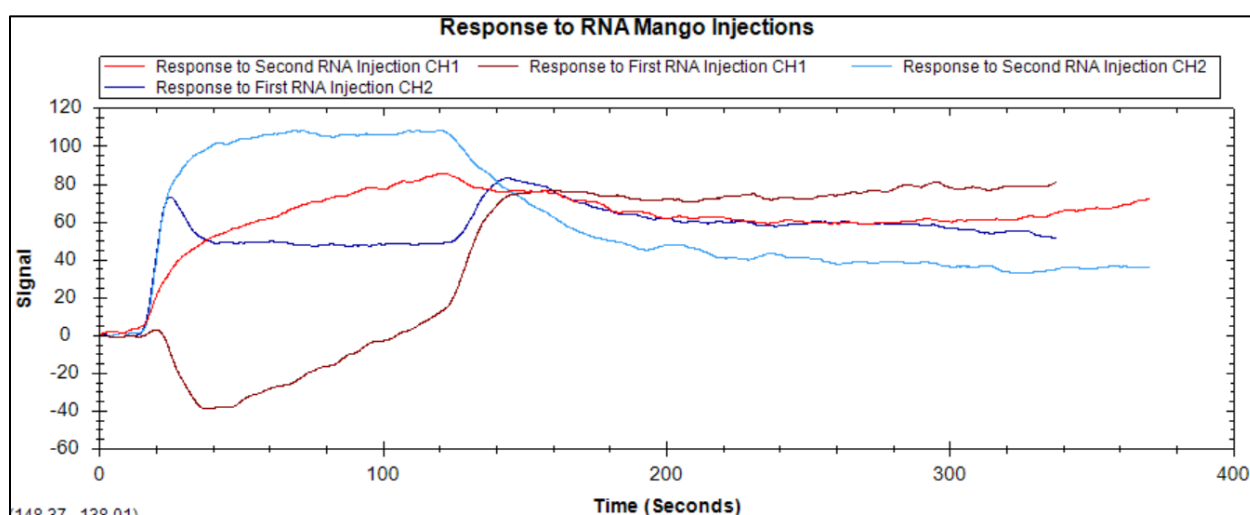


Figure 6.9 - Responses of Channel 1 and Channel 2 to RNA Mango Injections. The direct comparison of the response of channel 1 (red) and channel 2 (blue) to two RNA Mango injections. It was noted that a binding curve was not generated for the first injection of the RNA Mango aptamer; however, the second injection of the aptamer yielded binding curves in both channel 1 and channel 2, with the most distinct evidence of binding occurring to the target ligand in channel 2 (light blue curve). With evidence of binding, the investigation to determine the optimal buffer conditions was continued, with the same conditions explored as with the 6b DNA Mango aptamer, except for Buffer G (pH 6.5). Figure 6.10 summarizes the responses – Figure 6.10a: response to RNA injection in a high salt buffer (600 mM KCl); Figure 6.10b: response to RNA injection in Tween-containing buffer; Figure 6.10c: response to RNA injection in HSA-containing buffer.

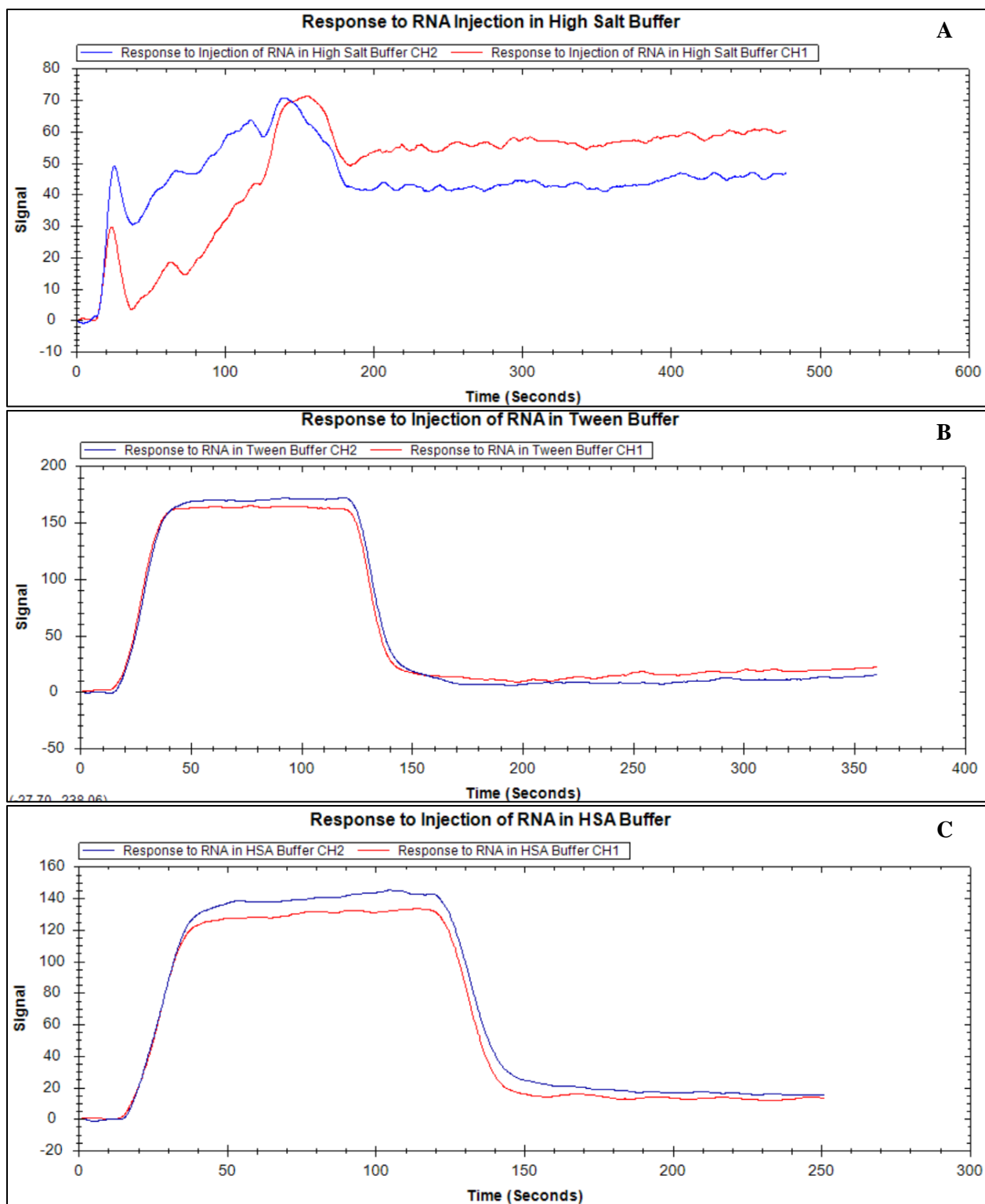


Figure 6.10 - Responses of Channel 1 and Channel 2 to Various RNA Mango Injections. The direct comparison of the response of channel 1 (red) and channel 2 (blue) to RNA Mango injections in various buffers (A: 600 mM KCl; B: 0.5% Tween; C: 0.5% HSA) to determine if the buffer conditions improved specific binding of the aptamer to the ligand.

Evidently, the buffers containing Tween and HSA resulted in bulk shifts, and therefore, conclusions regarding the effect of these buffers were unsupported. Additionally, while the response to the RNA injection in high salt buffer resulted in an increased baseline post-injection, a binding curve from which data could be extracted was not present, and the response was unstable. Therefore, this investigation was inconclusive.

6.2 Concentration Dependence Investigation

It was hypothesized that the explanation for the lack of binding evidence was due weaker binding to the immobilized ligand than anticipated. Specifically, while PhD. candidate, Volition La, determined nanomolar binding affinities for the aptamers to TO1-3PEG via fluorescence spectroscopy, it was possible that the ligand behaved differently under SPR conditions, such that immobilization of the ligand to the sensor surface interfered with the binding interactions. To probe this proposition, various concentrations of the 4a DNA Mango aptamer, the 6b DNA Mango aptamer, and the RNA Mango aptamer were investigated. The following section will summarize the findings of this research.

6.2.1 4a DNA Mango Concentration Dependence

The dependence of successful binding on concentration was first investigated with the 4a DNA Mango aptamer. Final concentrations of 4a DNA Mango samples were made up to be: 450 nM, 900 nM, 1.2 μ M, 1.88 μ M, 3.76 μ M, and 7.57 μ M, and were injected in order of increasing concentration. Figure 6.11 directly compares the corrected response signal for each of the DNA injections.

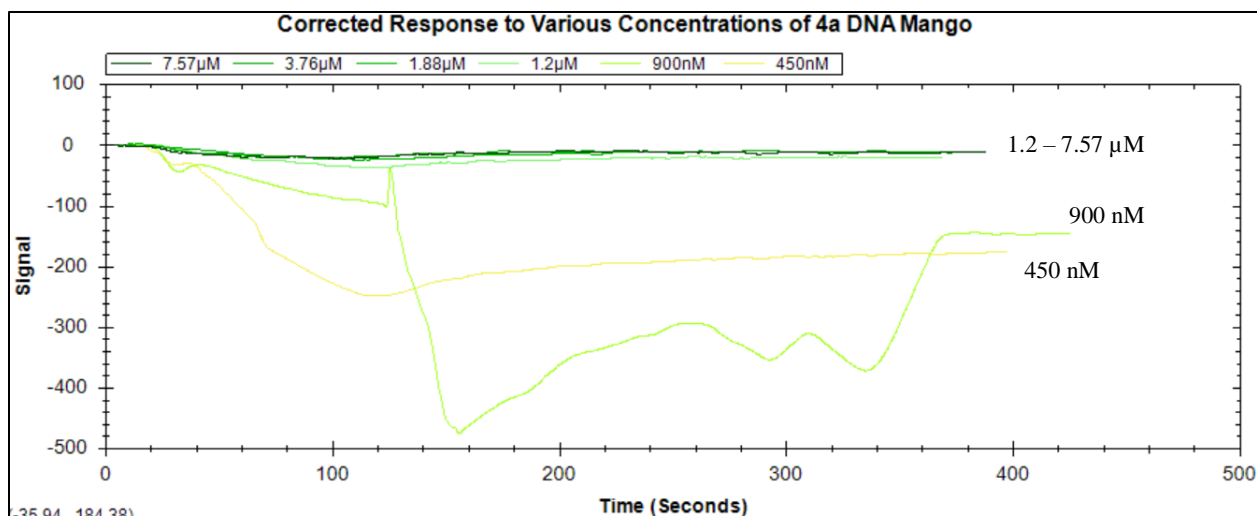


Figure 6.11 - Corrected Response to Various Concentrations of 4a DNA Mango. The direct comparison of the corrected responses to injections of varying concentrations of the 4a DNA Mango aptamer are depicted in order to determine the optimal aptamer concentration for complex formation.

Interestingly, from this data set, larger concentrations of the 4a DNA Mango aptamer (1.20 μM , 1.88 μM , 3.76 μM , and 7.57 μM) resulted in the least significant responses, with no visual evidence of binding. DNA concentrations of 450 nM and 900 nM, however, provided signals of quite large magnitudes. Despite this, the only concentration of the aptamer that seemed to vaguely represent a standard binding curve was the 900 nM injection. It was proposed that the implemented concentration range was not broad enough, and that the concentrations were still not sufficient to be detected by the SPR; therefore, higher concentrations of DNA were explored.

6.2.2 6b DNA Mango Concentration Dependence

To further probe at the need for higher aptamer concentrations to visualize binding between the aptamer and target ligand, the 6b DNA Mango aptamer was utilized, and concentrations ranging from 5 μM – 80 μM were tested. Figure 6.12a illustrates the corrected response for 5 – 20 μM concentration injections. Figure 6.12b exhibits the corrected response for 10 – 80 μM concentration injections.

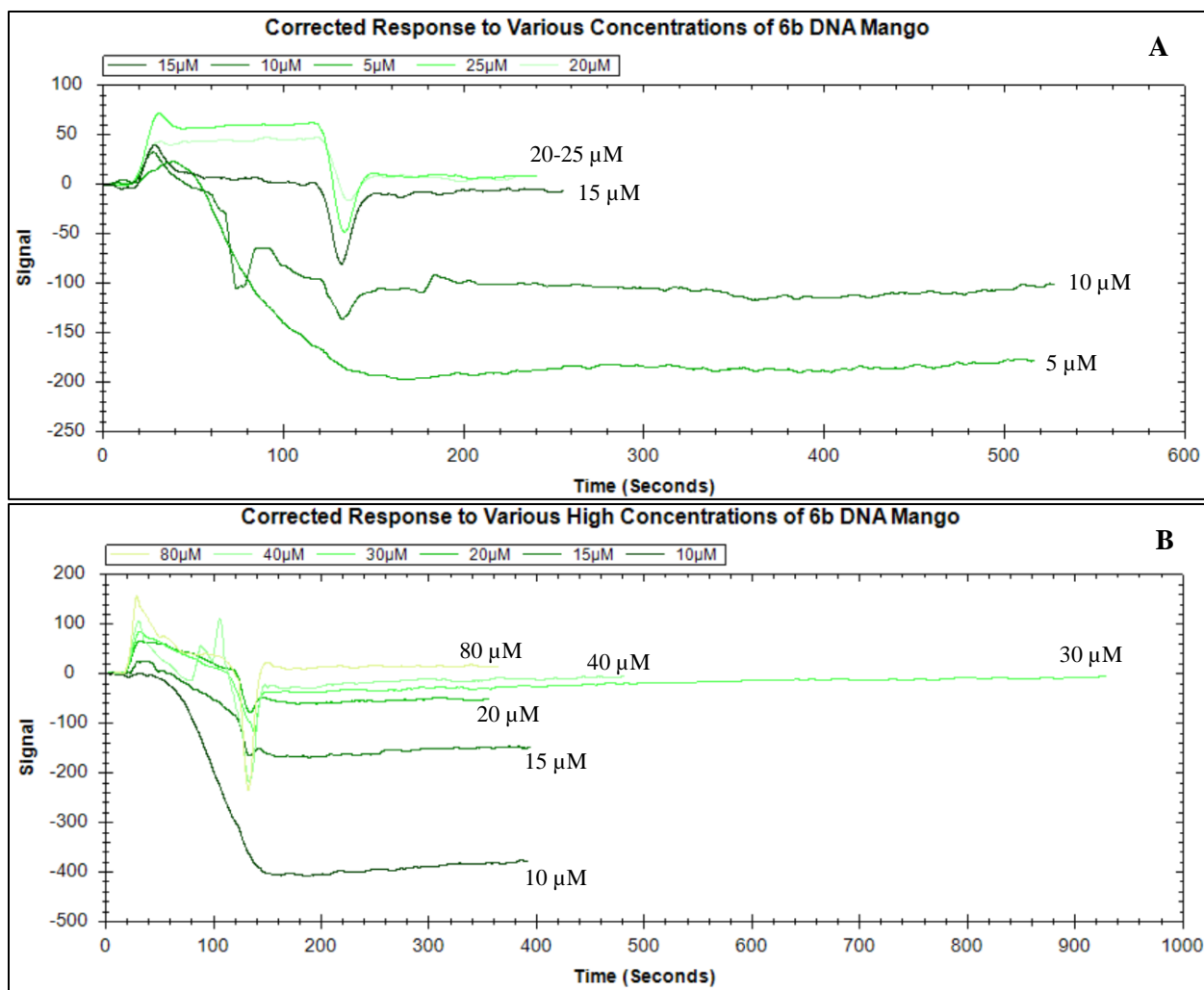


Figure 6.12 - Corrected Response to Ranging Concentrations of 6b DNA Mango. The direct comparison of the corrected responses to injections of varying concentrations of the 6b DNA Mango aptamer are depicted in order to determine the optimal aptamer concentration for complex formation.

Interestingly, the responses obtained in this investigation were similar to those obtained in section 6.2.1 – inverted curves somewhat representative of binding curves. Furthermore, it was observed in both experiments that the magnitude of the response signal did not demonstrate a proportionality to the concentration of aptamer, thus indicating much weaker binding interactions under SPR conditions than anticipated by fluorescence spectroscopy.

6.2.3 RNA Mango Concentration Dependence

In order to unquestionably determine if a concentration dependence can be detected by SPR, the well-described RNA Mango-TO1-3PEG binding system was exploited. Concentrations implemented in this investigation range from 5 μM to 25 μM , seeing as no evidence was provided in the aforementioned 6b DNA Mango experiment to suggest the requirement for higher concentrations. Figure 5.13 summarizes the corrected responses for each injection.

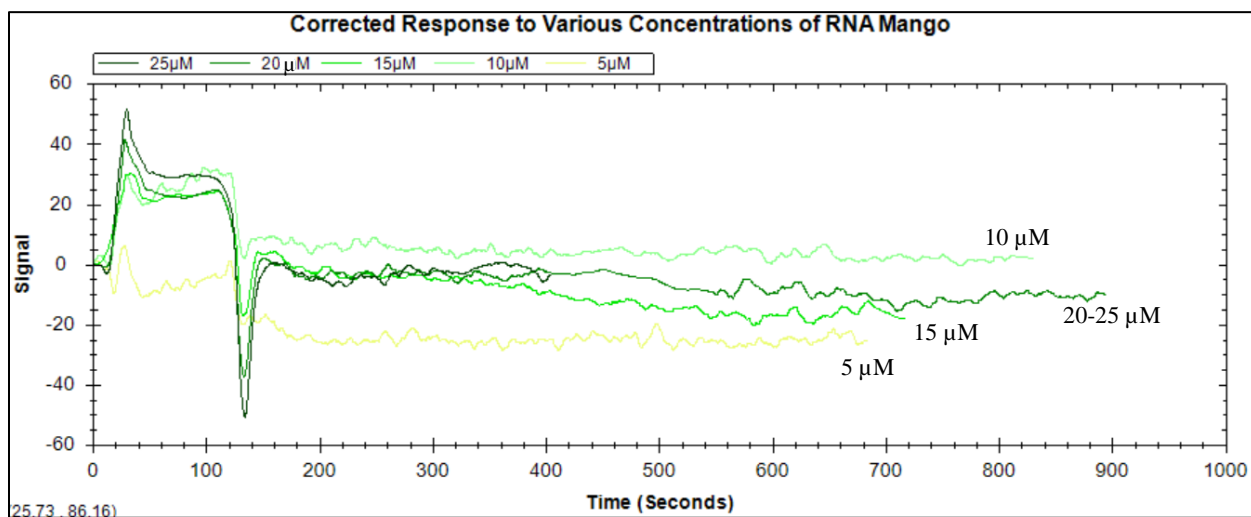


Figure 6.13 - Corrected Response to Various Concentrations of RNA Mango. The direct comparison of the corrected responses to varying concentrations of the RNA Mango aptamer to validate the concentration-dependence hypothesis and to determine the most optimal concentration for aptamer-ligand binding.

Consistent with the findings from the 4a and 6b DNA Mango concentration investigation, was the inability to extract any valuable information or data from this corrected sensorgram. Specifically, the expected response to an aptamer-ligand interaction was not observed. Not only was the magnitude of the response quite small, which made for noisy data, but none of the injected concentrations demonstrated any indication of successful binding or concentration dependence. More specifically, the lack of successful binding made conclusive remarks regarding concentration dependence unsubstantiated.

Based on the presented data, it was therefore determined that the DNA aptamers had weaker binding affinities to the target ligand than those previously determined by fluorescence spectroscopy. It was hypothesized that the immobilization of the ligand generated steric effects or environmental effects that interfered with the ability of the aptamers to bind to the ligand. Alternatively, the analyzed system was not a reliable system for detection via SPR.

6.3 SPR Conclusions

The nonspecific binding experiments conducted with the 6b DNA Mango aptamer and the RNA Mango aptamer were generally inconclusive – while the HSA-containing buffer and the Tween-containing buffer were seen to provide a positive effect at reducing nonspecific binding in the 6b DNA aptamer investigation, this was not further supported in the NSB experiment with the RNA aptamer. All other explored buffers were not seen to improve the binding conditions. Specifically, the raw signals for each buffer illustrated bulk shifts and lacked any indication of successful specific binding. Additionally, the response of the OpenSPR to any of the aforementioned DNA injections was not as expected - despite exploring a wide range of concentrations (450 nM – 80 μ M) across various aptamers (4a, 6b, and RNA Mango), the results lacked indications of binding curves from which kinetic information could be extracted and lacked concentration dependence. Based on these findings, it was concluded that the SPR was not suitable for characterizing the interactions between these aptamer sequences (4a DNA Mango, 6b DNA Mango) and the target ligand, TO1-3PEG, using the tested conditions and avidin type-sensors. Specifically, under the explored SPR conditions, binding between TO1-3PEG and two of the DNA Mango aptamer sequences, 4a and 6b, was not observed. While this was originally attributed to insufficient SPR conditions for observable binding, the concentrations and equilibrium dissociation constants used in and determined by ITC now bring to light the conclusion that the

binding between these systems was too weak to be detected by SPR. In conjunction with the equilibrium dissociation constants measured by ITC, the surface concentrations during SPR experimentation were not reliably known, therefore further exposing the potentially insufficient range of explored aptamer concentrations. For example, given the K_D of the 4a sequence of 9.71 μM in sodium phosphate buffer under ITC conditions, it would be expected that half of the DNA would bind to the immobilized target ligand at this aptamer concentration under SPR conditions. As discussed in Chapter 6, however, the concentration dependence investigation utilizing the 4a sequence only explored concentrations of this aptamer up to 7.57 μM . At this maximum concentration, it would be expected that less than half of the DNA would bind to the immobilized TO1-3PEG. Given the detection limits of SPR, this concentration of aptamer was insufficient for detections. Furthermore, as discussed in Section 5.3, if the hypothesis that the presence of a monomeric structure is required for binding is correct, not only for the employment of the one-site binding model of the ITC, but also as a means by which preferential or specific binding can be achieved, then the explored concentrations during the SPR investigations were insufficient for detection. Specifically, as previously mentioned, the explored concentrations pertained to the total concentration of the aptamer in all conformations (monomeric and multimeric). Despite annealing to reduce structural heterogeneity, the presence of a multimeric structure suggested that the concentration of the monomeric structure, potentially required for specific binding, was significantly lower than the employed concentration, such that binding between the aptamer and the target ligand would have gone undetected by the SPR. It was therefore concluded that the SPR was not a suitable method for characterizing these systems given the explored concentrations and ITC-identified equilibrium dissociation constants.

Chapter 7

Conclusions

This research aimed to determine if ITC and SPR were reliable analytical methods by which binding between DNA Mango aptamers and TO1-3PEG could be determined. It was demonstrated that ITC could only reliably detect binding for the 4a DNA Mango aptamer and the target ligand in sodium phosphate buffer and HEPES buffer. None of the computational models employed to interpret the ITC data gave an acceptable fit for the 2a or 6b DNA Mango aptamers in HEPES buffer. One hypothesis for unreliability of the ITC to detect and measure binding was aptamer structural heterogeneity, which was observed by native PAGE for the 4a and 6b sequences. Furthermore, the native PAGE investigation illustrated the presence of a monomeric structure in the 4a aptamer sequence, which was absent in the 6b native PAGE investigation. This observation acted as evidence in support of the ITC data, such that it was hypothesized that there is a necessity of a monomeric structure in order to accurately and reliably employ the one-site binding model of the ITC. Specifically, the 4a sequence was the only aptamer explored by ITC that the one-site binding model was capable of characterizing and determining an equilibrium dissociation constant. The one-site binding model of the ITC failed to fit the data pertaining to the 6b DNA aptamer, and this was the only aptamer investigated by native PAGE that did not have the presence of a monomeric structure. It was therefore hypothesized that a monomeric structure is required in order to employ the one-site binding model of the ITC.

It was concluded that SPR was an unsuitable analytical method for these systems. Despite assessing a wide range of concentrations and running buffer conditions, there was a general lack of binding evidence to support the use of SPR to biochemically characterize the explored systems.

One hypothesis for the lack of binding evidence using this instrumentation method was interference of the ligand with the operational frequencies of the OpenSPR. Specifically, the excitation and emission wavelengths of the fluorophore are 510 and 535 nm, respectively, while the operational frequency of the OpenSPR is 550 nm. Given the proximity of the fluorophore's wavelengths to the frequency of the instrument, it was not only concluded that negative associations could arise, but that interference effects may have made binding detection challenging, if not impossible. Alternatively, surface interactions between the biotinylated ligand and the avidin-prepared sensors may have interfered with potential binding – since prior research of systems with this ligand employed a ligand free in solution, such as in fluorescence spectroscopy, it was hypothesized that the behaviour of the ligand was altered upon immobilization, such that binding between the aptamer and ligand might have been weakened or absent.

Lastly, as discussed in Chapter 5 and 6, the presence of a multimeric structure in both the 4a and the 6b sequences introduced uncertainty in the explored concentrations. Specifically, as previously mentioned, the explored concentrations pertained to the total concentration of the aptamer in all conformations (monomeric and multimeric). If monomeric structures are, in fact, necessary for preferential and specific binding to the ligand, the uncertainty in this conformation's concentration imposed a problem in both the ITC and SPR investigations, such that the employed concentration was not an accurate concentration of the monomeric structure – this concentration would have been substantially lower; therefore, binding between the aptamer and the target ligand may have gone undetected by both methods. In ITC, the occurrence of structural changes during the titration could have generated the endothermic signal. Furthermore, the multimeric structures may have inhibited preferential binding of the monomeric structure to the target ligand.

Future research could explore higher concentrations of the 4a and 6b aptamers when investigating the systems via SPR in order to concretely determine which of the aforementioned factors was responsible for the outcome of the research. Specifically, higher aptamer concentrations would aid in deciphering whether the inability of the SPR to detect binding in this investigation was due to large binding affinities, as demonstrated by ITC, or problems arising from behavioural changes of the immobilized ligand. Furthermore, in addition to the 4a sequence, the 2a and 6b aptamers should be analyzed by ITC in sodium phosphate buffer to determine the buffer dependence on binding. Lastly, since a reasonable binding affinity was determined by ITC for the 4a DNA Mango aptamer in sodium phosphate buffer, structural characterization by NMR could be investigated for this system. Additionally, in order to gain insight into the structural properties of immobilized TO1-3PEG, and if and how this immobilization impacts the ability of the aptamer to bind to the target, an NMR titration could be performed during which the aptamer is titrated into TO1-3PEG immobilized on avidin covered beads. This NMR investigation would allow for structural characterization of the complex, such that the impact of ligand immobilization could be determined when compared directly to a titration in which the ligand was free in solution.

References

- (1) Lakhin, A. v; Tarantul, V. Z.; Gening, L. v. Aptamers: Problems, Solutions and Prospects. *34 / ActA nAturAe* / **2013**, 5 (19), 2013.
- (2) Zhang, Y.; Lai, B. S.; Juhas, M. Recent Advances in Aptamer Discovery and Applications. <https://doi.org/10.3390/molecules24050941>.
- (3) Harris, D. C. *Quantitative Chemical Analysis*; 2016; Vol. 9.
- (4) *Handbook of Analytical Instruments - R S Khandpur - Google Books*. https://books.google.ca/books?hl=en&lr=&id=yUp_CgAAQBAJ&oi=fnd&pg=PT33&dq=handbook+of+analytical+instruments&ots=x7bG4U_haN&sig=MiMJOBqHj8yOCOSTBzyK7eiEtzY#v=onepage&q=handbook%20of%20analytical%20instruments&f=false (accessed 2022-06-22).
- (5) Raju TN. 1999. The Nobel Chronicles - 1962: Francis Harry Compton Crick (b 1916); James Dewey Watson (b 1928); Maurice Hugh Frederick Wilkins (b 1916). *Lancet*. 354(9179):690
- (6) Watson, J.D.; Crick, F.H.C. Molecular structure of nucleic acids: A structure for deoxyribose nucleic acid, *Nature*. 171 (1953) 737–738. <https://doi.org/10.1038/171737a0>.
- (7) Franklin, R.E.; Gosling, R.G. Evidence for 2-chain Helix in crystalline structure of sodium deoxyribonucleate, *Nature*. 172 (1953) 156–157. <https://doi.org/10.1038/172156a0>.
- (8) Wilkins, M.H.F.; Stokes, A.R.; Wilson, H.R. Molecular structure of nucleic acids: Molecular structure of deoxypentose nucleic acids, *Nature*. 171 (1953) 738–740. <https://doi.org/10.1038/171738a0>
- (9) Grunberg-Manago, M.; Ochoa, S. Enzymatic synthesis and breakdown of polynucleotides; polynucleotide phosphorylase, *J. Am. Chem. Soc.* 77 (1955) 3165–3166. <https://doi.org/10.1021/ja01616a093>
- (10) Holley, R. W.; Apgar, J.; Everett, G. A.; Madison, J. T.; Marquisee, M.; Merrill, S. H.; Penswick, J. R.; Zamir, A. Structure of a Ribonucleic Acid. *Source: Science* **1965**, 147 (3664), 1462–1465
- (11) Khorana, H.G.; Büchi, H.; Ghosh, H.; Gupta, N.; Jacob, T.M.; Kössel, H.; Morgan, R.; Narang, S.A.; Ohtsuka, E.; Wells, R.D. Polynucleotide synthesis and the genetic code., *Cold Spring Harb. Symp. Quant. Biol.* 31 (1966) 39–49. <https://doi.org/10.1101/SQB.1966.031.01.010>
- (12) Bernfield, M. R.; Nirenberg, M. W. RNA Codewords and Protein Synthesis. *New Series* **1965**, 147 (3657), 479–484.
- (13) Raju TN. 1999. The Nobel chronicles - 1968: Har Khorana (b 1922); Robert Holley (1922-93); Marshall Nirenberg (b 1927). *Lancet*. 354(9173):171
- (14) Arber, W.; Dnssorx, D. Host Specificity of DNA Produced by Escherichia Coli I. Host Controlled Modification of Bacteriophage 11. *J. Mol. Biol* **1962**, 5, 18–36. [https://doi.org/10.1016/S0022-2836\(62\)80058-8](https://doi.org/10.1016/S0022-2836(62)80058-8).
- (15) Smithand, H. O.; Wilcox, K. W. A Restriction Enzyme from Hemophilus Influenzae I. Purification and General Properties. *J. MoZ. Biool* **1970**, 51, 379–391.
- (16) Danna, K.; Reviewed, D. N.; Roberts, R. J. Specific Cleavage of Simian Virus 40 DNA by Restriction Endonuclease of Hemophilus Influenzae. *Reviews in Medical Virology Rev. Med. Virol* **1999**, 9, 75–81.

- (17) Maxam, A. M.; Gilbert, W. A New Method for Sequencing DNA (DNA Chemistry/Dimethyl Sulfate Cleavage/Hydrazine/Piperidine). **1977**, *74* (2), 560–564.
- (18) Sanger, F.; Nicklen, S.; Coulson, A. R. DNA Sequencing with Chain-Terminating Inhibitors. **1977**, *74* (12), 5463–5467.
- (19) Rigby, P. W. J.; Dieckmann, T. Labeling Deoxyribonucleic Acid to High Specific Activity in Vitro by Nick Translation with DNA Polymerase I. *J. Mol. Biol* **1977**, *113*, 237–251.
- (20) Crick, F. Central Dogma of Molecular Biology. *NATURE* **1970**, 227, 1970.
- (21) Gilbert W. 1986. Origin of life: The RNA world. *Nature*. 319(6055):618
- (22) Cech, T. R. Self-Splicing and Enzymatic Activity of an Intervening Sequence RNA from Tetrahymena (Nobel Lecture). *Angewandte Chemie International Edition in English* **1990**, *29* (7), 759–768. <https://doi.org/10.1002/ANIE.199007591>.
- (23) Altman, S. Enzymatic Cleavage of RNA by RNA. **1990**.
- (24) Guerrier-Takada, C.; Gardiner, K.; Marsh, T.; Pace, N.; Altman, S. The RNA Moiety of Ribonuclease P Is the Catalytic Subunit of the Enzyme. *Cell* **1963**, *35* (2), 649–857.
- (25) Kruger, K.; Grabowski, P. J.; Zaug, A. J.; Sands, J.; Gottschling, D. E.; Cech, T. R. Self-Splicing RNA: Autoexcision and Autocyclization of the Ribosomal RNA Intervening Sequence of Tetrahymena. *Cell* **1982**, *31*, 147–157.
- (26) Tuerk, C.; Gold, L. Systematic Evolution of Ligands by Exponential Enrichment: RNA Ligands to Bacteriophage T4 DNA Polymerase. *New Series* **1990**, *249* (4968), 505–510.
- (27) Ellington, A. D.; Szostak, J. W. *In Vitro Selection of RNA Molecules That Bind Specific Ligands*; 1990.
- (28) Nonaka, Y.; Sode, K.; Ikebukuro, K. Screening and Improvement of an Anti-VEGF DNA Aptamer [www.Mdpi.Com/Journal/](http://www.mdpi.com/Journal/Molecules) Molecules. *Molecules* **2010**, *15* (1), 215–225. <https://doi.org/10.3390/molecules15010215>.
- (29) Jeon, S. H.; Kayhan, B.; Ben-Yedidia, T.; Arnon, R. A DNA Aptamer Prevents Influenza Infection by Blocking the Receptor Binding Region of the Viral Hemagglutinin. *J. Biol. Chem.* **2004**, *279* (46), 48410–48419. <https://doi.org/10.1074/jbc.M409059200>
- (30) Woodland, J. G.; Chibale, K. Quinine Fever. *Nature Chemistry* **2022**, *14* (1), 112. <https://doi.org/10.1038/s41557-021-00872-2>.
- (31) Herschel, J. F. W.; *Phil. Trans. R. Soc. Lond.* 135, 143–145 (1845).
- (32) Vira, S.; Mekhedov, E.; Humphrey, G.; Blank, P. S. Fluorescent-Labeled Antibodies: Balancing Functionality and Degree of Labeling. *Analytical Biochemistry* **2010**, *402*, 146–150. <https://doi.org/10.1016/j.ab.2010.03.036>.
- (33) Coons, A. H.; Creech, J.; Norman, R.; Berliner, E. THE DEMONSTRATION OF PNEUMOCOCCAL ANTIGEN IN TISSUES BY THE USE OF FLUORESCENT ANTIBODY
- (34) Shimomura, O.; Johnson, F. H.; Saiga, Y. Extraction, Purification and Properties of Aequorin, a Bioluminescent Protein from the Luminous Hydromedusan, Aequorea. *Journal of Cellular and Comparative Physiology* **1962**, *59* (3), 223–239. <https://doi.org/10.1002/JCP.1030590302>.

- (35) Swaminathan, S. GFP: The Green Revolution. *Nature Cell Biology* **2009**, *11*. <https://doi.org/10.1038/ncb1953>.
- (36) Prasher, D. C.; Eckenrode, V. K.; Ward, W. W.; Prendergast, F. G.; Cormier, M. J. Primary Structure of the Aequorea Victoria Green-Fluorescent Protein. *Gene* **1992**, *111* (2), 229–233. [https://doi.org/10.1016/0378-1119\(92\)90691-H](https://doi.org/10.1016/0378-1119(92)90691-H).
- (37) Chalfie, M.; Tu, Y.; Euskirchen, G.; Ward, W. W.; Prasher, D. C. Green Fluorescent Protein as a Marker for Gene Expression. *New Series* **1994**, *11* (5148), 802–805.
- (38) Cody, C. W.; Prasher, D. C.; Westler, W. M.; Prendergast, F. G.; Ward, W. W. Chemical Structure of the Hexapeptide Chromophore of the Aequorea Green-Fluorescent Protein. *Biochemistry* **1993**, *32*, 1212–1218.
- (39) Yang, F.; Moss, L. G.; Phillips, G. N. *The Molecular Structure of Green Fluorescent Protein*; 1996.
- (40) Brejc, K.; Sixma, T. K.; Kitts, P. A.; Kain, S. R.; Tsien, R. Y.; Ormö, M.; Remington, S. J. Structural Basis for Dual Excitation and Photoisomerization of the Aequorea Victoria Green Fluorescent Protein. *Proc Natl Acad Sci U S A* **1997**, *94* (6), 2306–2311. <https://doi.org/10.1073/PNAS.94.6.2306>.
- (41) Ormö, M.; Cubitt, A. B.; Kallio, K.; Gross, L. A.; Tsien, R. Y.; James Remington, S. Crystal Structure of the Aequorea Victoria Green Fluorescent Protein. *New Series* **1996**, *273* (5280), 1392–1395.
- (42) Kong, J.; Wang, Y.; Qi, W.; Huang, M.; Su, R.; He, Z. Green Fluorescent Protein Inspired Fluorophores. **2020**. <https://doi.org/10.1016/j.cis.2020.102286>.
- (43) Tsien, R. Y. The Green Fluorescent Protein. *Annual Review of Biochemistry* **1998**, *67*, 509–544. <https://doi.org/10.1146/ANNUREV.BIOCHEM.67.1.509>.
- (44) Heim, R.; Tsien, R. Y. Engineering Green Fluorescent Protein for Improved Brightness, Longer Wavelengths and Fluorescence Resonance Energy Transfer. *Current Biology* **1996**, *6* (2), 178–182. [https://doi.org/10.1016/S0960-9822\(02\)00450-5](https://doi.org/10.1016/S0960-9822(02)00450-5).
- (45) Rizzuto, R.; Brini, M.; de Giorgi, F.; Rossi, R.; Heim, R.; Tsien, R. Y.; Pozzan, T. Double Labelling of Subcellular Structures with Organelle-Targeted GFP Mutants in Vivo. *Current Biology* **1996**, *6* (2), 183–188. [https://doi.org/10.1016/S0960-9822\(02\)00451-7](https://doi.org/10.1016/S0960-9822(02)00451-7).
- (46) Sando, S.; Narita, A.; Aoyama, Y. Light-up Hoechst-DNA Aptamer Pair: Generation of an Aptamer-Selective Fluorophore from a Conventional DNA-Staining Dye. *ChemBioChem* **2007**, *8* (15), 1795–1803. <https://doi.org/10.1002/cbic.200700325>.
- (47) Sando, S.; Narita, A.; Hayami, M.; Aoyama, Y. Transcription Monitoring Using Fused RNA with a Dye-Binding Light-up Aptamer as a Tag: A Blue Fluorescent RNA. *Chem.Comm.* **2008**, No. 33, 3858–3860. <https://doi.org/10.1039/b808449a>
- (48) Autour, A.; Jeng, S. C. Y.; Iii, R. J. T.; Abdolazadeh, A.; Andreoni, A.; Cojocar, R.; Garipov, R.; Dolgosheina, E. v; Knutson, J. R.; Rycelynck, M.; Unrau, P. J.; Ferré-D'amaré, A. R. Structure and Functional Reselection of the Mango-III Fluorogenic RNA Aptamer. *Nature Chemical Biology* **2019**, *15*. <https://doi.org/10.1038/s41589-019-0267-9>.

- (49) Bernard Da Costa, J.; Dieckmann, T. Entropy and Mg²⁺ Control Ligand Affinity and Specificity in the Malachite Green Binding RNA Aptamer. *Molecular BioSystems* **2011**, 7 (7), 2156–2163. <https://doi.org/10.1039/c1mb05075c>.
- (50) Duchardt-Ferner, E.; Juen, M.; Bourgeois, B.; Madl, T.; Kreutz, C.; Ohlenschläger, O.; Ohnert, J. W. Structure of an RNA Aptamer in Complex with the Fluorophore Tetramethylrhodamine. *Nucleic Acids Research* **2019**, 48 (2), 949–961. <https://doi.org/10.1093/nar/gkz1113>.
- (51) Paige, J. S.; Wu, K. Y.; Jaffrey, S. R. RNA Mimics of Green Fluorescent Protein. *Science* (1979) **2011**, 333 (6042), 642–646. <https://doi.org/10.1126/science.1207339>.
- (52) Fernandez-Millan, P.; Autour, A.; Ennifar, E.; Westhof, E.; Ryckelynck, M. Crystal Structure and Fluorescence Properties of the ISpinach Aptamer in Complex with DFHBI. **2017**. <https://doi.org/10.1261/rna>.
- (53) Deigan Warner, K.; Chen, M. C.; Song, W.; Strack, R. L.; Thorn, A.; Jaffrey, S. R.; Ferré-D'Amaré, A. R. Structural Basis for Activity of Highly Efficient RNA Mimics of Green Fluorescent Protein. *Nature Publishing Group* **2014**. <https://doi.org/10.1038/nsmb.2865>.
- (54) Neubacher, S.; Hennig, S. RNA Structure and Cellular Applications of Fluorescent Light-Up Aptamers. *Angewandte Chemie* **2019**, 131 (5), 1278–1291. <https://doi.org/10.1002/ange.201806482>.
- (55) Filonov, G. S.; Moon, J. D.; Svensen, N.; Jaffrey, S. R. Broccoli: Rapid Selection of an RNA Mimic of Green Fluorescent Protein by Fluorescence-Based Selection and Directed Evolution. *J Am Chem Soc* **2014**. <https://doi.org/10.1021/ja508478x>.
- (56) Deigan Warner, K.; Sjekloc, L.; Song, W.; Filonov, G.; Jaffrey, S.R.; Ferré-D'Amaré, A. Homodimer Interface without Base Pairs in an Rna Mimic of Red Fluorescent Protein. *Nature Chemical Biology* **2017**, 13. <https://doi.org/10.1038/nChEMBio.2475>.
- (57) Grate, D.; Wilson, C. *Laser-Mediated, Site-Specific Inactivation of RNA Transcripts*; 1999; Vol. 96.
- (58) Babendure, J. R.; Adams, S. R.; Tsien, R. Y. Aptamers Switch on Fluorescence of Triphenylmethane Dyes. *J Am Chem Soc* **2003**, 125 (48), 14716–14717. <https://doi.org/10.1021/ja037994o>.
- (59) Stojanovic, M. N.; Kolpashchikov, D. M. Modular Aptameric Sensors. *J Am Chem Soc* **2004**, 126 (30), 9266–9270. <https://doi.org/10.1021/ja032013t>.
- (60) Dolgosheina, E. v.; Jeng, S. C. Y.; Panchapakesan, S. S. S.; Cojocar, R.; Chen, P. S. K.; Wilson, P. D.; Hawkins, N.; Wiggins, P. A.; Unrau, P. J. RNA Mango Aptamer-Fluorophore: A Bright, High-Affinity Complex for RNA Labeling and Tracking. *ACS Chemical Biology* **2014**, 9 (10), 2412–2420. <https://doi.org/10.1021/cb500499x>.
- (61) Trachman, R. J.; Abdollahzadeh, A.; Andreoni, A.; Cojocar, R.; Knutson, J. R.; Ryckelynck, M.; Unrau, P. J.; Ferré-D'Amaré, A. R. Crystal Structures of the Mango-II RNA Aptamer Reveal Heterogeneous Fluorophore Binding and Guide Engineering of Variants with Improved Selectivity and Brightness. *Biochemistry* **2018**, 57 (26), 3544–3548. <https://doi.org/10.1021/acs.biochem.8b00399>.

- (62) Tang, Y.; Zeng, X.; Liang, J. Surface Plasmon Resonance: An Introduction to a Surface Spectroscopy Technique. *Journal of Chemical Education* **2010**, *87* (7), 742–746. <https://doi.org/10.1021/ed100186y>.
- (63) *Handbook of Surface Plasmon Resonance: 2nd Edition* - Google Books. <https://books.google.ca/books?hl=en&lr=&id=cfwIDwAAQBAJ&oi=fnd&pg=PA72&dq=handbook+of+surface+plasmon+&ots=OXMpAolIjl&sig=koUa-RhSVjCIBXOfsNbDP7ZRLNk#v=onepage&q=handbook%20of%20surface%20plasmon&f=false> (accessed 2022-06-22).
- (64) *What is Surface Plasmon Resonance? - Nicoya - Improving Human Life by Helping Scientists Succeed*. <https://nicoyalife.com/nicoya-surface-plasmon-resonance-resources/what-is-spr/what-is-surface-plasmon-resonance/> (accessed 2022-06-22).
- (65) *Why SPR? - Nicoya - Improving Human Life by Helping Scientists Succeed*. <https://nicoyalife.com/nicoya-surface-plasmon-resonance-resources/what-is-spr/why-surface-plasmon-resonance/> (accessed 2022-06-22).
- (66) *How Does SPR Work? - Nicoya - Improving Human Life by Helping Scientists Succeed*. <https://nicoyalife.com/nicoya-surface-plasmon-resonance-resources/what-is-spr/how-does-surface-plasmon-resonance-work/> (accessed 2022-06-22).
- (67) Patching, S. G. Surface Plasmon Resonance Spectroscopy for Characterisation of Membrane Protein-Ligand Interactions and Its Potential for Drug Discovery. *Biochimica et Biophysica Acta - Biomembranes*. 2014, pp 43–55. <https://doi.org/10.1016/j.bbamem.2013.04.028>.
- (68) Puligedda, R. D.; Al-Saleem, F. H.; Wirblich, C.; Kattala, C. D.; Jović, M.; Geiszler, L.; Devabhaktuni, H.; Feuerstein, G. Z.; Schnell, M. J.; Sack, M.; Livornese, L. L.; Dessain, S. K. A Strategy to Detect Emerging Non-Delta Sars-Cov-2 Variants with a Monoclonal Antibody Specific for the N501 Spike Residue. *Diagnostics* **2021**, *11* (11). <https://doi.org/10.3390/diagnostics11112092>.
- (69) Shi, R.; Shan, C.; Duan, X.; Chen, Z.; Liu, P.; Song, J.; Song, T.; Bi, X.; Han, C.; Wu, L.; Gao, G.; Hu, X.; Zhang, Y.; Tong, Z.; Huang, W.; Jun Liu, W.; Wu, G.; Zhang, B.; Wang, L.; Qi, J.; Feng, H.; Wang, F.-S.; Wang, Q.; Fu Gao, G.; Yuan, Z.; Yan, J. A Human Neutralizing Antibody Targets the Receptor-Binding Site of SARS-CoV-2. | *Nature* | **2020**, *584*. <https://doi.org/10.1038/s41586-020-2381-y>.
- (70) Singh, A.; Erijman, A.; Noronha, A.; Kumar, H.; Peleg, Y.; Yarden, Y.; Shifman, J. M. Engineered Variants of the Ras Effector Protein RASSF5 (NORE1A) Promote Anticancer Activities in Lung Adenocarcinoma. *Journal of Biological Chemistry* **2021**, *297* (6). <https://doi.org/10.1016/j.jbc.2021.101353>.
- (71) Herrmann, C. Ras-Effector Interactions: After One Decade. [https://doi.org/10.1016/S0959-440X\(02\)00007-6](https://doi.org/10.1016/S0959-440X(02)00007-6).
- (72) Vetter, I. R., and Wittinghofer, A. (2001). The guanine nucleotide-binding switch in three dimensions. *Science* **294**, 1299-1304
- (73) Piccolo, K. A.; McNeil, B.; Crouse, J.; Lim, S. J.; Bickers, S. C.; Hopkins, W. S.; Dieckmann, T. Ligand Specificity and Affinity in the Sulforhodamine B Binding RNA Aptamer. *Biochemical and Biophysical Research Communications* **2020**, *529* (3), 666–671. <https://doi.org/10.1016/J.BBRC.2020.06.056>.

- (74) Procházka K. Fluorescence Studies of Polymer Containing Systems. **2016**, *16*. <https://doi.org/10.1007/978-3-319-26788-3>.
- (75) Benzaghoul, I.; Bougie, I.; Picard-Jean, F.; Bisailon, M. Energetics of RNA Binding by the West Nile Virus RNA Triphosphatase. *FEBS Letters* **2006**, *580* (3), 867–877. <https://doi.org/10.1016/J.FEBSLET.2006.01.006>.
- (76) So, P. T.; Dong, C. Y. Fluorescence Spectrophotometry.
- (77) Lakowicz, J. R. *Principles of Fluorescence Spectroscopy Third Edition*.
- (78) Menendez, M. Isothermal Titration Calorimetry: Principles and Applications. <https://doi.org/10.1002/9780470015907.a0028808>.
- (79) Freire, E.; Mayorga, O. L.; Straume, M. Isothermal Titration.
- (80) Dutta, A. K.; Rösger, J.; Rajarathnam, K. Using Isothermal Titration Calorimetry to Determine Thermodynamic Parameters of Protein-Glycosaminoglycan Interactions. *Methods in Molecular Biology* **1229**. https://doi.org/10.1007/978-1-4939-1714-3_25.
- (81) Bottari, F.; Daems, E.; de Vries, A. M.; van Wielendaele, P.; Trashin, S.; Blust, R.; Sobott, F.; Madder, A.; Martins, J. C.; de Wael, K. Do Aptamers Always Bind? The Need for a Multifaceted Analytical Approach When Demonstrating Binding Affinity between Aptamer and Low Molecular Weight Compounds. *J Am Chem Soc* **2020**, *142* (46), 19622–19630. <https://doi.org/10.1021/jacs.0c08691>.
- (82) Song, K.-M.; Jeong, E.; Jeon, W.; Cho, M.; Ban, C. Aptasensor for Ampicillin Using Gold Nanoparticle Based Dual Fluorescence-Colorimetric Methods. <https://doi.org/10.1007/s00216-011-5662-3>.
- (83) Neves, M. A. D.; Reinstein, O.; Saad, M.; Johnson, P. E. Defining the Secondary Structural Requirements of a Cocaine-Binding Aptamer by a Thermodynamic and Mutation Study. **2010**. <https://doi.org/10.1016/j.bpc.2010.09.009>.
- (84) Bishop, G.R.; Ren, J.; Polander, B. C.; Jeanfreau, B. D.; Trent, J. O.; Chaires, J. B. Energetic Basis of Molecular Recognition in a DNA Aptamer. **2006**. <https://doi.org/10.1016/j.bpc.2006.07.009>.
- (85) Steinmetzger, C.; Bessi, I.; Lenz, A.-K. Structure-Fluorescence Activation Relationships of a Large Stokes Shift Fluorogenic RNA Aptamer. *Nucleic Acids Research* **2019**, *47* (22), 11538–11550. <https://doi.org/10.1093/nar/gkz1084>.
- (86) Sjekloća, L.; Ferré-D'Amaré, A. R. Binding between G Quadruplexes at the Homodimer Interface of the Corn RNA Aptamer Strongly Activates Thioflavin T Fluorescence. *Cell Chemical Biology* **2019**, *26* (8), 1159-1168.e4. <https://doi.org/10.1016/j.chembiol.2019.04.012>.
- (87) Li, Y.; Xu, S.; Wu, X.; Xu, Q.; Zhao, Y.; Lou, X.; Yang, X. Thioflavin T as a Fluorescence Light-up Probe for Both Parallel and Antiparallel G-Quadruplexes of 29-Mer Thrombin Binding Aptamer. <https://doi.org/10.1007/s00216-016-9901-5>.
- (88) de La Faverie, A. R.; Guédin, A.; Bedrat, A.; Yatsunyk, L. A.; Mergny, J. L. Thioflavin T as a Fluorescence Light-up Probe for G4 Formation. *Nucleic Acids Research* **2014**, *42* (8). <https://doi.org/10.1093/nar/gku111>.
- (89) Mohanty, J.; Barooah, N.; Dhamodharan, V.; Harikrishna, S.; Pradeepkumar, P. I.; Bhasikuttan, A. C. Thioflavin T as an Efficient Inducer and Selective Fluorescent Sensor for the Human

- Telomeric G-Quadruplex DNA. *J Am Chem Soc* **2013**, *135* (1), 367–376. <https://doi.org/10.1021/ja309588h>.
- (90) Gabelica, V.; Maeda, R.; Fujimoto, T.; Yaku, H.; Murashima, T.; Sugimoto, N.; Miyoshi, D. Multiple and Cooperative Binding of Fluorescence Light-up Probe Thioflavin t with Human Telomere DNA G-Quadruplex. *Biochemistry* **2013**, *52* (33), 5620–5628. <https://doi.org/10.1021/bi4006072>.
- (91) Piccolo, K. A. *Studying the Structure and Kinetics of Functional Nucleic Acids*; 2021.
- (92) da Costa, J. B.; Andreiev, A. I.; Dieckmann, T. Thermodynamics and Kinetics of Adaptive Binding in the Malachite Green RNA Aptamer. *Biochemistry* **2013**, *52* (38), 6575–6583. <https://doi.org/10.1021/bi400549s>.
- (93) Baugh, C.; Ra, D. A.; Grate, A.; Wilson, C. A Crystal Structure of the Malachite Green Aptamer. **2000**. <https://doi.org/10.1006/jmbi.2000.3951>.
- (94) Sambrook, J.; Russell, D. W. *Molecular Cloning. A Laboratory Manual, Third Edit.*; Cold Spring Harbor Laboratory Press: New York, 2001. Chapter 5.26-5.28, 5.40-5.46, 5.51-5.54
- (95) Biba, M.; Foley, J. P.; Welch, C. J. Liquid Chromatographic Separation of Oligonucleotides. In *Liquid Chromatography: Applications: Second Edition*; Elsevier Inc., 2017; Vol. 2, pp 159–182. <https://doi.org/10.1016/B978-0-12-805392-8.00006-2>.
- (96) Mori S, Barth HG. *Size Exclusion Chromatography*. Springer; 1999.